

Engineering Metal Organic Frameworks for Heterogeneous Catalysis

A. Corma,* H. García, and F. X. Llabrés i Xamena

Instituto de Tecnología Química (UPV-CSIC), Universidad Politécnica de Valencia, Consejo Superior de Investigaciones Científicas, Avenida de los Naranjos s/n, 46022 Valencia, Spain

Received December 2, 2009

Contents

1. Introduction	4606
1.1. Scope and Structure of This Review	4606
1.2. Definition of Metal Organic Framework	4608
1.3. Nomenclature	4608
1.4. Synthesis of MOFs	4608
1.5. Designing MOFs for Catalysis	4609
1.5.1. Synthesis of MOFs Containing Unsaturated Metal Sites	4610
1.5.2. Synthesis of MOFs with Metal Complexes As Building Blocks	4610
1.5.3. Synthesis of MOFs Further Functionalized by a Postsynthesis Treatment	4611
1.6. Evaluating the Potential of a MOF as Catalyst	4612
1.6.1. Determining the Maximum Productivity of a MOF	4613
1.6.2. Selecting a Suitable Reaction Test and the Right Substrates	4613
2. Catalysis by MOFs	4614
2.1. Types of MOFs Used in Catalysis	4614
2.1.1. MOFs with Metal Active Sites	4614
2.1.2. MOFs with Reactive Functional Groups	4614
2.1.3. MOFs as Host Matrices or Nanometric Reaction Cavities	4614
2.2. MOFs with Metal Active Sites	4614
2.2.1. Early Studies	4614
2.2.2. Hydrogenation Reactions	4618
2.2.3. Oxidation of Organic Substrates	4620
2.2.4. CO Oxidation to CO ₂	4626
2.2.5. Photocatalysis by MOFs	4627
2.2.6. Carbonyl Cyanosilylation	4630
2.2.7. Hydrodesulfurization	4631
2.2.8. Other Reactions	4632
2.3. MOFs with Reactive Functional Groups	4634
2.4. MOFs as Host Matrices or Nanometric Reaction Cavities	4636
2.4.1. MOFs as Host Matrices to Incorporate Metal Nanoparticles	4636
2.4.2. Incorporation of Metal Oxide Nanoparticles in MOFs	4642
2.4.3. MOFs as Host Matrices to Incorporate Catalytically Active Guests	4644
2.4.4. MOFs as Nanometric Reaction Cavities	4647
3. Conclusions and Future Possibilities	4651
4. List of Acronyms and Abbreviations Used	4651

5. Acknowledgments	4652
6. References	4652

1. Introduction

1.1. Scope and Structure of This Review

The development of surface-characterization techniques, molecular modeling, and advanced synthesis methods have transformed the preparation of solid catalysts from an art into a science. In this way, catalyst preparation has evolved from trial-and-error methodologies based on chemical knowledge, accumulated experience, and common sense into a clearly multidisciplinary science that allows one to reach the molecular design of tailor-made solid catalysts. This is even more so when one refers to crystalline solid catalysts, for which the detailed structure and composition are known and can be manipulated to introduce well-defined single or multiple active sites. We have seen this to occur with various catalytic systems, and among them, it was especially relevant in the cases of zeolites, zeotypes, and well-structured mesoporous materials.^{1,2} Great fundamental and industrial advances have been made toward the ab initio design of catalysts based on the micro- and mesoporous materials named above. This has been based on the molecular mechanistic knowledge of the reactions to be catalyzed, together with the development of advanced synthesis and characterization techniques. In this way, well-defined active sites ranging from protons to Lewis acids, and even redox sites, can be introduced in the framework of zeotypes and mesoporous materials. The coordination and electronic state can be determined by spectroscopic techniques, and their interaction with reactants can be studied by means of powerful quantum chemical calculations and in situ or operando spectroscopies; in this way, the catalytic active site can be optimized.³

Finally, when combining the well-defined framework and/or extraframework active sites in the solid, with pore dimensions and topologies of the zeolites that can be selective toward different potential transition states, highly selective solid catalysts can be achieved.

However, the pore dimensions of zeolites and zeotypes were limited to the reaction of molecules with sizes below ~1.0 nm,⁴ until the discovery of zeolites with larger pores, which, in the case of the new ITQ-37,⁵ have reached the mesoporous range.

Despite the many advances made in the zeolite field, the control and modulation of the electronic properties of the framework active sites are still limited, and in any case, it is far less controlled than for transition metal complex catalysts. While some success has been achieved by combining the

* To whom correspondence should be addressed. E-mail: acorma@itq.upv.es.



Avelino Corma was born in Moncófar, Spain, in 1951. He studied Chemistry at the Universidad de Valencia (1967–1973) and received his Ph.D. at the Universidad Complutense de Madrid in 1976. He was Postdoctoral in the Department of Chemical Engineering at the Queen's University (Canada, 1977–1979). He is director of the Instituto de Tecnología Química (UPV-CSIC) at the Universidad Politécnica de Valencia since 1990. His current research field is catalysis, covering aspects of synthesis, characterization, and reactivity in acid–base and redox catalysis. Avelino Corma is co-author of more than 700 articles and 100 patents on these subjects.



Francesc X. Llabrés i Xamena received his Ph.D. in Chemistry in 2000 from the University of the Balearic Islands (Spain) working with Prof. C. Otero in the synthesis and spectroscopic characterization of zeolites. After a 2-year Postdoctoral stage at the University of Turin with Prof. A. Zecchina and one year at the University of Padua with Prof. G. Granozzi, he joined the ITQ in 2004 as a “Ramón y Cajal Research Associate”. He has recently obtained a permanent position at the ITQ as Staff Scientist of the Spanish Research Council (CSIC). His current research interests are in the preparation of metal organic framework compounds and the study of their applications, including heterogeneous catalysis.



Hermenegildo García (Herme) is full Professor and member of the Institute of Chemical Technology at the Technical University of Valencia since 1996. He has co-authored over 400 papers, has supervised over 28 Ph.D.'s, and holds 14 international patents. His main current interests are in green chemistry and catalysis as well as the use of zeolites, metal organic frameworks, and mesoporous materials in supramolecular photochemistry, photocatalysis, and nanotechnology.

well-controlled active sites of transition metal complexes and the adsorption and pore selectivity effects of zeolites or mesoporous materials by introducing the former, via “ship-in-a-bottle” or grafting techniques,⁶ the results are still limited.

In principle, it should be possible to combine organometallic and pore-selectivity functionalities by means of coordination polymers with an extended network of metal ions or clusters coordinated to multidentate organic molecules and with well-defined pore dimensions. Reports on this type of materials are known at least since 1959, when Kinoshita et al. described the crystal structure of bis(adiponitrilo)copper(I) nitrate,⁷ a material that today will be included among the family of coordination polymers or metal organic framework compounds. The structure of this compound consists of a three-dimensional network of the transition metal complex [Cu(adiponitrilo)₂] and nitrate anions. Other early reports on coordination polymers appeared in 1960,^{8,9} but the subject passed without much notice. It was not until the second part

of the 1990s that the subject was rediscovered and reborn, first from the works of Robson et al.¹⁰ and later by Yaghi et al.,¹¹ among others, especially after the preparation of the well-known MOF-5 material in 1999.¹² While the first efforts were mainly devoted to the synthesis of new materials, the search for potential applications has also been a topic of much interest, especially in the second half of this decade.

In this paper, we have traveled through the research done on metal organic frameworks (MOFs), and more specifically, we have discussed how one can engineer metal organic frameworks to build catalysts in which the active sites could be the metals at the nodes of the framework; the ligands, either directly or as components of a transition metal complex; MOFs as host matrices; and, finally, MOFs as potential multisite catalysts. We will show that, by using the different concepts of catalysts described above, MOFs already have shown activity and selectivity for a large number of reactions. The catalytic results obtained are critically reviewed, and future possibilities are outlined.

For this purpose, the review has been structured in two parts. The first part describes briefly how MOFs are formed and how they are usually characterized and classified. Then, we discuss the requirements that a MOF has to fulfill to be used in catalysis. In particular, we analyze what are the desired structural characteristics that make MOFs suitable in catalysis, how we can design or modify a MOF with a view to its application in catalysis, and what are the best methodologies for assessing its catalytic potential.

In the second part, we provide a comprehensive review of the reports describing the use of MOFs in catalysis. Special emphasis is made to present the current state of the art and to provide some hints about the logical evolution that can be anticipated in this field.

We want to anticipate that the review is not presented as a dichotomy between MOFs and zeolites—zeotypes (which are today the most successful type of solid catalyst that continuously find new applications), but to present the possibilities of MOFs as catalysts and try to give directions on the requirements to convert them into successful catalysts.

1.2. Definition of Metal Organic Framework

Coordination polymers (CPs) are solid materials formed by an extended network of metal ions (or clusters) coordinated to multidentate organic molecules. This definition encompasses a large variety of materials containing metals and organic molecules having very different characteristics, as for instance crystalline and amorphous, as well as porous and nonporous solids. The present review is dedicated to a special group of CPs referred to as metal organic frameworks (MOFs), which are crystalline and porous compounds involving strong metal–ligand interactions.¹³ Metal–ligand coordinative bonds are stronger than hydrogen bonds, and they have also more directionality than other weak interactions, such as π – π stacking, etc. Notice that hybrid organic–inorganic amorphous materials, as well as mono- and bidimensional crystalline solids and three-dimensional crystalline materials in which one or more dimensions are supported by weak interactions, such as hydrogen bonds or π – π stacking,¹⁴ are outside the scope of the present review. Therefore, according to the above definition, MOFs are a subclass of the broader CP family. The relatively recent interest in MOFs is a consequence of the simultaneous occurrence of these three important characteristics: crystallinity, porosity, and existence of strong metal–ligand interactions. This unique combination of properties renders MOFs a very special class of materials. Their microporous structures provide apparent surface areas¹⁵ of up to 5900 m² g^{−1} and specific pore volumes of up to 2 cm³ g^{−1},¹⁶ together with a large variety of pore dimensions and topologies. The very high pore volumes of MOFs have triggered an extensive investigation into their application for gas separation and storage^{16–19} and even as preconcentrators of explosive vapors and nerve agents.^{20,21} The presence of strong metal–ligand interactions can confer permanent porosity to the material, i.e., it is possible to remove completely the solvent molecules (required to liberate the inner space of the material) without structure collapse. This property has provided an additional criterion for classifying CPs into first-, second-, and third-generation materials.²² First-generation coordination polymers are materials having a porous system sustained by guest molecules, which irreversibly collapse upon removal of the guest molecules. Second-generation materials have a robust porous system, with permanent porosity after removal of the guest molecules. Finally, third-generation compounds have a flexible pore system, which changes reversibly depending on the presence of guest molecules or in response to external stimuli, such as light, temperature, or electric field. This last category is also known as “dynamic porous coordination polymers”²³ or “breathing” materials.^{24–27} According to this classification, the MOFs considered in this review belong to either the second- or third-generation coordination polymers.

An important feature of MOFs is that their pore size, shape, dimensionality, and chemical environment can be finely controlled by the judicious selection of their building blocks (metal and organic linker) and how they are connected. This allows selecting the molecules that can diffuse within the pores, acting as molecular sieves. Meanwhile, they may modulate the host–guest interactions when adsorbing molecules, and the transition states formed for reactions occurring within the pores. In other words, these coordination polymers could show molecular sieve and shape-selective properties. Finally, the possibility of modifying and functionalizing the organic ligand by conventional organic

chemistry strategies may allow tailoring the material for specific applications.

1.3. Nomenclature

Probably because of the relatively short trajectory of this family of materials, and the fact that there is not a generally accepted definition, there is not a standardized nomenclature for MOFs (such as that used for zeolites).²⁸ This lack of rationalization, together with the exponential growth of the number of new structures described each year, contributes to create a certain state of confusion that can puzzle the nonspecialized scientists.

Some researchers tend to use a descriptive name for the materials prepared in their laboratories, consisting in most cases of an acronym followed by a number, which roughly represents their chronologic order of preparation. The acronym can be indicative of (i) the type of components of the material, like in the series MOF-*n*²⁹ (metal organic framework), COF-*n*³⁰ (covalent organic framework), RPF-*n*³¹ (rare-earth polymeric framework), or MPF-*n*³² (metal peptide framework); (ii) the type of structure, like in the series ZMOF-*n*³³ (zeolite-like metal organic framework), ZIF-*n*³⁴ (zeolitic imidazolate framework), or mesoMOF-*n*³⁵ (mesoporous metal organic framework); or (iii) the laboratory in which the material was prepared, like for instance in the series MIL-*n*¹⁶ (matériaux de l’Institut Lavoisier), HKUST-*n*³⁶ (Hong-Kong University of Science and Technology), CPO-*n*³⁷ (coordination polymer of Oslo), and ITQMOF-*n*.^{38,39} (Instituto de Tecnología Química metal organic framework).

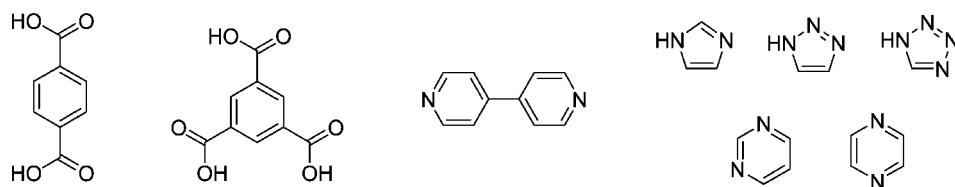
An alternative to this descriptive name consists of using the “empirical formula” of the material, i.e., expressing the metal(s), the ligand(s), and their stoichiometry in the repetitive unit, e.g., [Zn₄(O)(bdc)₃] (bdc = 1,4-benzenedicarboxylate) or [Cu(2-pymo)₂] (2-pymo = 2-hydroxypyrimidinolate).

A more systematic terminology has been proposed to rationalize the known structures, and it is based on the structure of the crystalline nets adopted by the material.^{40–42} These (3D) nets are represented by either a three-letter symbol (as in sod, rho, gis, etc.) or a three-letter symbol with an extension (such as in pcu-c or bcu-k). This method allows one to describe and classify the known structures as well as new potential MOF structures as a function of their net topology. Unfortunately, in this case, the classification term lacks any information about the chemical nature of the material.

1.4. Synthesis of MOFs

The synthesis of MOFs is usually carried out in the liquid phase, either by using a pure solvent or a suitable mixture of solvents. Formation of the crystalline framework takes place by self-assembly of the structural units forming an ordered network of metal organic coordination bonds. The synthetic method generally consists of mixing two solutions containing the metal and the organic component, either at room temperature or under (hydro) solvothermal conditions and with or without the aid of additional auxiliary molecules. A large variety of metal atoms in their stable oxidation states, i.e., alkaline, alkaline-earth, transition metals, main group metals, and rare-earth elements, have been successfully used in the synthesis of MOFs. As organic components, rigid molecules (such as conjugated aromatic systems) are usually preferred over flexible ones,^{43–45} since they favor the preparation of crystalline, porous, stable MOFs. Common

Scheme 1



choices for organic linkers are based on some of the nuclei shown in Scheme 1, including, among others, polycarboxylic aromatic molecules, bipyridines, and polyazaheterocycles (imidazoles, triazoles, tetrazoles, pyrimidines, pyrazines, etc.) and their derivatives. Both neutral and charged molecules can be used, although cationic ligands are less common in the synthesis of MOFs because of their low affinity to coordinate to metal cations.

The nature of the solvent, the ligands, or the presence of cations and other guest molecules in the synthesis of MOFs can have a dramatic effect on the crystal structure of the material obtained. Thus, a given metal–ligand combination can lead to a number of different structures (polymorphism), depending on subtle changes on the above-mentioned synthesis parameters. A clear example of the effect of these parameters is represented by the synthesis of zinc imidazolates. Tian et al.⁴⁶ have prepared up to seven different zinc imidazolate frameworks with the general formula $[\text{Zn}(\text{im})_2 \cdot x\text{G}]$ (im = imidazolate, G = guest molecule, $x = 0.2-1$), which joined the family of other already existing zinc imidazolates.^{34,47} The same metallic and organic components (Zn^{2+} and imidazolate) were used in the synthesis of all these solids, and the solvent was the only parameter that was changed during the synthesis. Thus, the solvent was considered to act as template or structure-directing agent for the resulting zinc imidazolates. The presence of ligand substituents on the imidazolate ring was also found to be important for achieving the final crystalline structure, as evidenced by Chen and co-workers.^{46,48-50} The authors were able to synthesize $[\text{Zn}(\text{bzim})_2 \cdot 5/3 \text{H}_2\text{O}]$ with benzimidazole, $[\text{Zn}(2\text{-mim})_2 \cdot 3\text{H}_2\text{O}]$ from 2-methylimidazole, and $[\text{Zn}(2\text{-eim})_2 \cdot \text{H}_2\text{O}]$ from 2-ethylimidazole, as well as a mixed ligand compound $[\text{Zn}(2\text{-eim}/2\text{-mim})_2 \cdot \text{H}_2\text{O}]$. The presence of substituents in the imidazole ring avoided the formation of dense phases and directed the topology of the resulting material. Thus, $[\text{Zn}(\text{bzim})_2 \cdot 5/3 \text{H}_2\text{O}]$ adopts a distorted zeolite-related sod topology with only 18% accessible volume to guests. $[\text{Zn}(2\text{-mim})_2 \cdot 3\text{H}_2\text{O}]$ (see Figure 1a) features a regular sod topology, with 47% of free volume composed of spherical cavities with a diameter of 12.5 Å and accessible through hexagonal windows of ca. 3.3 Å, with an apparent specific

Brunauer–Emmett–Teller (BET) surface area of 1029 $\text{m}^2 \text{g}^{-1}$. $[\text{Zn}(2\text{-eim})_2 \cdot \text{H}_2\text{O}]$ (see Figure 1b) assumes an analcime (ana) zeolite topology, while the structure of the mixed ligand compound $[\text{Zn}(2\text{-eim}/2\text{-mim})_2 \cdot \text{H}_2\text{O}]$ (see Figure 1c) has a zeolitic rho topology, with 57% free volume and truncated cuboctahedra of 18.1 Å with pore windows of 7.4 Å.

Several other examples are found in the literature in which a given binary metal–ligand system can yield different structures, depending on the particular synthesis conditions. For instance, the system zinc–terephthalate is known to produce several different structures, including MOF-2,^{29,51} MOF-3,^{29,52} MOF-5,^{12,29} $[\text{Zn}_2(\text{OH})_2(\text{bdc})_2 \cdot 2\text{def}]$ (def = diethyl formamide),⁵³ $[\text{Zn}(\text{H}_2\text{O})_2(\mu\text{-O}, \text{O}'\text{-bdc})]$,⁵⁴ zinc terephthalate hydrate,⁵⁵ sodium zinc terephthalate hydrate dmf solvate (dmf = dimethyl formamide),⁵⁶ MOCP-H, and MOCP-H'.⁴⁸

1.5. Designing MOFs for Catalysis

Crystalline inorganic molecular sieve materials such as zeolites can be synthesized within a large variety of pore dimensions. Until very recently, only microporous zeolites were prepared, with maximum pore diameters in the order of 1.2 nm (such as cloverite,⁵⁷ ECR-24,⁵⁸ or ITQ-33⁵⁹). But very recently, the first mesoporous zeolite has been synthesized (ITQ-37) with a pore diameter of ~ 2.0 nm, which is stable upon calcination at 873 K.⁵ Zeolites, owing to their well-defined system of pores and cavities, together with their thermal and hydrothermal stability and the possibility of introducing a variety of active sites in the walls, are extensively used in industry as shape-selective catalysts. Indeed, besides the preparation of zeolites with Brønsted acid sites, some metal ions can be introduced in the zeolite framework to implement the solid with Lewis acid or redox sites.⁶⁰

Taking into consideration all the above, together with the structure and pore topologies of MOFs, it could also be anticipated that coordination polymers may be designed to prepare active and selective catalysts. However, in spite of the outstanding textural properties and high metal contents of MOFs, their use in catalysis has been very limited up to

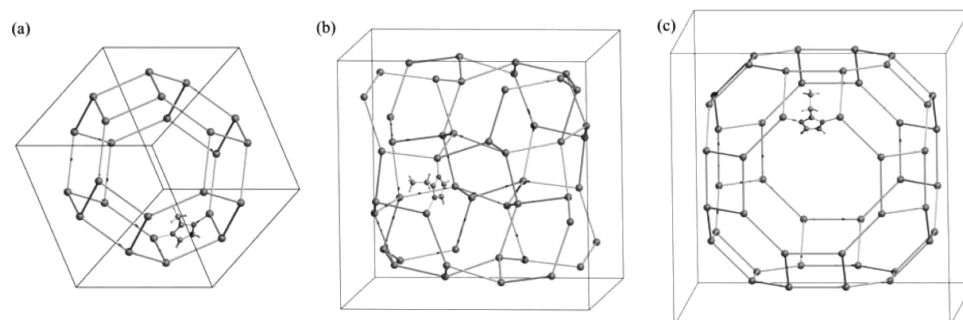
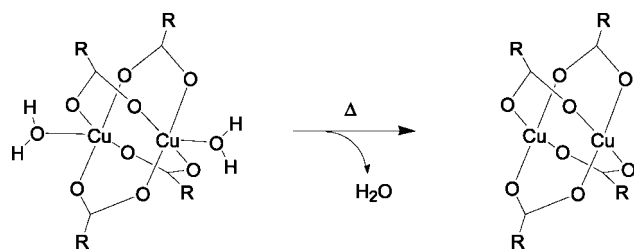


Figure 1. Crystalline network of different zinc imidazolate frameworks with zeolite topologies: (a) $[\text{Zn}(2\text{-MIM})_2 \cdot 3\text{H}_2\text{O}]$; (b) $[\text{Zn}(2\text{-EIM})_2 \cdot \text{H}_2\text{O}]$; and (c) $[\text{Zn}(2\text{-EIM}/2\text{-MIM})_2 \cdot \text{H}_2\text{O}]$. Reproduced with permission from ref 50. Copyright 2006 Royal Society of Chemistry.

Scheme 2



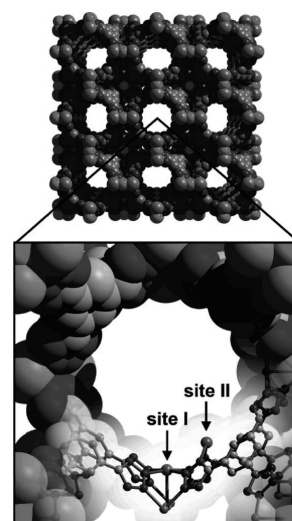
now. It is generally accepted^{61–63} that this is mainly due to the combination of two factors: (i) the stability of the materials toward temperature, moisture, and some reactants and impurities is lower as compared to inorganic crystalline porous counterparts such as zeolites, owing to the presence of organic linkers and the weakness of the metal–ligand coordinative bond compared to covalent Si–O bonds; and (ii) the fact that, in many known MOF structures, the coordination sphere around the metal ion is completely blocked by the organic linker, leaving no free positions available for substrate chemisorption. Nevertheless, in the past few years, new synthesis strategies have been developed to overcome the above drawbacks, and we will highlight some of them here.

1.5.1. Synthesis of MOFs Containing Unsaturated Metal Sites

This involves the preparation of materials in which the metal centers are not completely blocked by the organic spacers because labile ligands are introduced, which can be removed during the activation stage prior to use in catalysis. In most cases, the labile ligands are solvent molecules that, when removed, leave a free coordination position in the metal. A relevant example of this strategy corresponds to the $\text{Cu}_3(\text{btc})_2$ ($\text{btc} = 1,3,5\text{-benzenetricarboxylate}$) material HKUST-1, in which the copper sites are known to lose reversibly their coordinated apical water molecule upon thermal activation,^{63,64} thus leaving an accessible coordination vacancy on the Cu (see Scheme 2). A more complex situation is found with the material $[\text{Mn}(\text{dmf})_6]@[(\text{Mn}_4\text{Cl})_3\text{-(btt)}_8(\text{H}_2\text{O})_{12}]_2$ ($\text{btt} = 1,3,5\text{-benzenetetratrazolate}$) described by Dinca et al.,⁶⁵ in which $[\text{Mn}(\text{dmf})_6]^{2+}$ metal complexes are clathrated inside sodalite-like cages constructed by square-planar Mn_4Cl clusters and btt ligands. Upon exchanging the dmf molecules by methanol and evacuating at 423 K, the resulting material shows two types of exposed Mn sites: (a) five-coordinated sites I originated from framework Mn^{2+} ions of the Mn_4Cl clusters after losing a H_2O molecule and (b) two-coordinated sites II which correspond to Mn^{2+} ions formerly in the extraframework $[\text{Mn}(\text{dmf})_6]$ complexes, and which remain coordinated to two N atoms of adjacent tetrazole rings after removal of the dmf molecules (see Scheme 3).

The design of MOFs containing unsaturated metal centers has also been used to prepare materials with improved adsorption capacity for gas-storage applications.^{65–70} Indeed, the presence of open metal sites is of key importance for adsorption and catalysis, since it strongly favors the direct interaction between metal and substrate. Therefore, materials originally designed for adsorption may as well show good performance for the latter and vice versa, as has been demonstrated, for instance, in the case of HKUST-1.^{63,71,72}

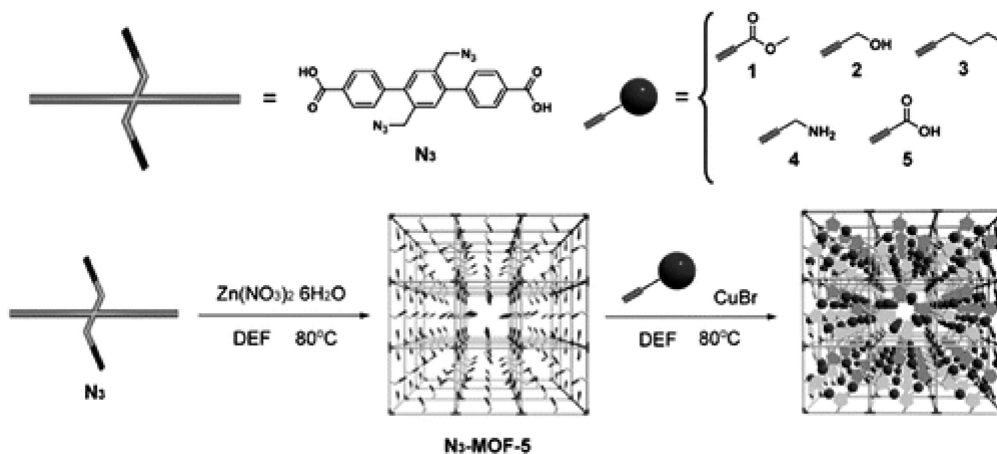
Scheme 3. Structure of the $\text{Mn}_3[(\text{Mn}_4\text{Cl})_3(\text{btt})_8(\text{CH}_3\text{OH})_{10}]_2$ MOF Showing the sod-type Topology and the Two Types of Exposed Mn^{2+} Sites (Reproduced with Permission from Ref 65; Copyright 2006 American Chemical Society)



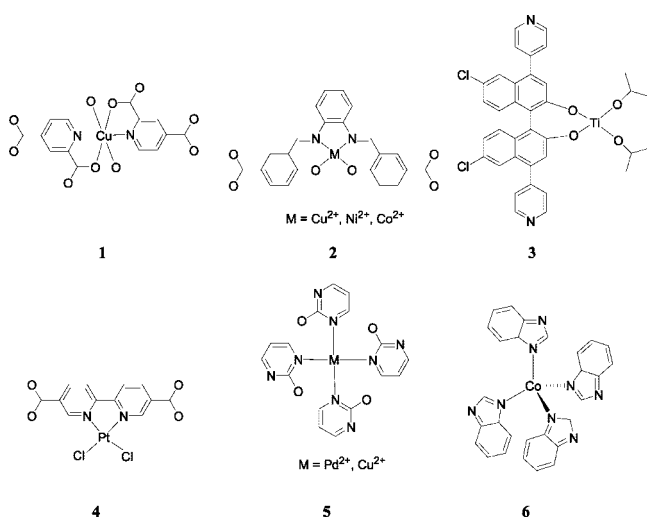
1.5.2. Synthesis of MOFs with Metal Complexes As Building Blocks

In this case, the MOF can be viewed as an ordered three-dimensional array of metal coordination complexes. This strategy has been followed in the preparation of a number of materials. Kitagawa and co-workers^{73,74} prepared a MOF by using a preassembled $\text{Cu}(2,4\text{-pydca})_2$ complex ($2,4\text{-pydca} = \text{pyridine-2,4-dicarboxylate}$) (**1**) acting as a metalloligand, which further coordinated to Zn^{2+} cations through one of the carboxylate groups to form a 3D structure. In this material, Zn^{2+} simply acted as a structural element, while Cu^{2+} ions were accessible for guest coordination. Similarly, the same group has prepared a series of materials containing metal Schiff base complexes, $\text{M}(\text{H}_2\text{salphdc})$ (**2**) ($\text{M} = \text{Cu}^{2+}$, Ni^{2+} , or Co^{2+} , $\text{salphdc} = N,N'$ -phenylenebis(salicylideneimine)dicarboxylate), with Zn^{2+} cations at the nodes.⁷⁵ Unfortunately, the authors did not investigate the catalytic activity of the materials obtained. Lin and co-workers⁷⁶ have prepared a homochiral MOF containing Cd^{2+} ions and the chiral ligand (*R*)-6,6'-dichloro-2,2'-dihydroxy-1,1'-binaphthyl-4,4'-bipyridine (**3**) as the organic building unit. The ligand coordinates to Cd^{2+} through chlorine and the pyridine nitrogen, while the two hydroxyl groups of the binaphthyl moiety remain uncoordinated and pointing to the channels. Postsynthesis modification of this material by adding titanium isopropoxide yielded a titanium containing material, with titanium di-isopropoxide grafted to the walls of the MOF through the dihydroxy groups. Szeto et al. prepared bimetallic materials containing Gd^{77} or Y^{78} ions as structural nodes, together with Pt^{2+} ions as potential catalytic sites. In both materials, Pt^{2+} ions were four-coordinated by two Cl and two N atoms of 2,2'-bipyridine-4,4'-dicarboxylate (bpydc) (**4**), thus mimicking the structure of homogeneous coordination complexes with Pt^{2+} coordinated to N-containing organic ligands by electron donation, which are known to be active in alkane activation. We have recently shown^{61,79} that the use of anionic diazaheterocycles 2-pymo and bzim ligands can yield MOFs containing single metal sites coordinated to four nitrogen atoms (**5**) and (**6**) that can be successfully used in catalysis. This was demonstrated by the preparation of $[\text{Pd}(2\text{-pymo})_2]$,⁸⁰ $[\text{Cu}(2\text{-pymo})_2]$,⁸¹ and $[\text{Co}(\text{bzim})_2]$ ³⁴ following the already reported procedures, which

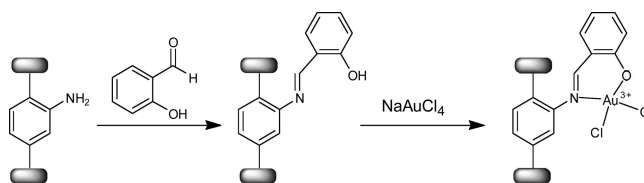
Scheme 4. Postsynthesis Modification of a MOF Bearing an Azide Ligand through Copper Catalyzed Click Reaction (Reproduced with Permission from Ref 90; Copyright 2008 American Chemical Society)



were found to be active in reactions involving the metal center and for which analogous homogeneous complexes are known to be active.⁸²



Scheme 5



the corresponding urethane) or with a carboxylic acid (to form the amide). Postsynthesis modifications of MOFs have also been applied very recently in different scenarios. Goto et al.⁹⁰ used an azide functionalized ligand that was postsynthesis reacted with organic molecules bearing a terminal alkyne (through a click reaction using CuBr as the catalyst), as shown in Scheme 4. In this way, the authors have introduced hanging groups with various functionalities: ester, alcohol, and alkyl chain. However, attempts to introduce amino and carboxylic acid groups following the same strategy caused the dissolution of the MOF. Ingleson et al.⁹¹ have described the preparation of a material containing Brønsted acid sites by postsynthesis protonation of the carboxylate ligands of a MOF with anhydrous HCl. The same authors also reported the modification of the amino groups of IRMOF-3 with salicylaldehyde to form the corresponding imine.⁹² This ligand was used to complex metal ions, as demonstrated by covalently anchoring vanadyl acetylacetonate. We have also used a similar postsynthesis strategy to prepare a metal-coordination complex covalently anchored to the organic linkers of a preexisting MOF.⁹³ First, a covalent functionalization of the available amino groups of IRMOF-3 was carried out with salicylaldehyde to form the salicylideneimine, and in a second step, Au(III) sites were coordinated to the Schiff base complex. The two-step process is shown in Scheme 5.

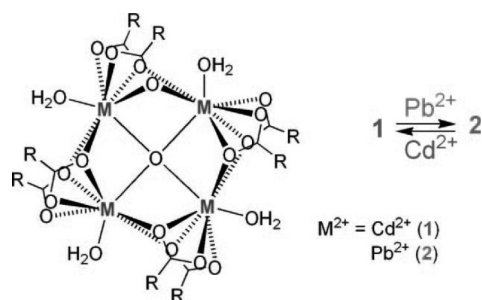
1.5.3. Synthesis of MOFs Further Functionalized by a Postsynthesis Treatment

Postsynthesis modification of MOFs has recently emerged as a highly versatile tool to prepare tailored MOFs for applications in catalysis, gas adsorption, etc. Chemical functionalization of the framework can be accomplished by either introducing covalent attachment to the organic linker or by grafting of organic molecules at metal sites coordinative vacancies created after solvent elimination.

Covalent postsynthesis modification of the organic linkers has recently received great interest after the reports by Wang et al.,^{83–86} who have recently reviewed the subject.⁸⁷ These authors used an existing MOF having suitable functional groups not directly coordinated to the metal sites, which can be transformed through a covalent reaction afterward, as opposite to the “presynthesis” strategy used so far. To demonstrate the potential of this preparative approach, the amino groups of IRMOF-3 (a material with composition $[\text{Zn}_4\text{O}(\text{ata})_3]$, ata = 2-aminoterephthalate)⁸⁸ were reacted with alkyl anhydrides^{83–85} or isocyanates.⁸⁶ This idea was later used by Sánchez Costa et al.⁸⁹ to prepare a MOF containing Gd(III) and ata ligands. The amino group of the organic ligand was postsynthesis modified with two different functionalities, by reacting either with an isocyanate (to form

An alternative to covalent modification of the organic linkers consists of anchoring to metal coordination vacancies of the MOF organic molecules containing heteroatoms with lone electron pairs. This idea was first introduced by Hwang et al.,⁹⁴ who described the grafting of an amine pendant group to the chromium sites of the chromium terephthalate MIL-101, using ethylenediamine. More recently, Banerjee et al. have described the use of a similar strategy to anchor to the chromium sites of MIL-101 proline molecules terminated with a pyridine group, which allowed for preparation of a MOF-based organocatalyst.⁹⁵ Long and co-workers have anchored ethylenediamine to the coordinative unsaturations

Scheme 6



of a Cu(II)-containing MOF having a sod-type network.⁹⁶ The authors have observed a higher isosteric heat of CO₂ adsorption for the modified material with respect to the unfunctionalized solid (90 vs 21 kJ/mol, respectively), which resulted in higher uptake of CO₂ and CO₂/N₂ selectivity.

A completely different approach that can also be considered a postsynthesis modification consists of replacing the central metal ions forming the MOF by other suitable elements (isomorphous substitution). This strategy has been reported very recently by Das et al.,⁹⁷ who described a metathesis exchange process leading to the complete and fully reversible substitution of framework Cd²⁺ ions by Pb²⁺ in a MOF single crystal, without altering its crystalline integrity (see Scheme 6). The authors were also able to exchange Cd²⁺ ions by trivalent lanthanide cations Dy³⁺ or Nd³⁺, which resulted in positively charged frameworks. This charge excess was compensated by extraframework NO₃⁻ anions. Although this particular case of metathesis process does not have an immediate application for catalysis, it demonstrates the feasibility of tuning the reactivity of a MOF by postsynthesis selecting the identity and concentration of the metal ions forming the framework.

1.6. Evaluating the Potential of a MOF as Catalyst

It has been commented above that one of the drawbacks for the use of MOFs as catalysts is their relatively limited thermal and chemical stability. The low thermal stability of the crystal structure is certainly a limiting factor for vapor-phase reactions carried out at temperatures above 573 K. Thus, we cannot expect MOFs to play an important role as catalysts for oil-refining or petrochemical processes taking place at temperatures ≥ 573 K. This will be even more so for reactions that are accompanied by formation of coke or heavier residual products that have to be removed by combustion. There is no doubt that, under these circumstances, zeolites will be preferred over MOFs. However, one may think of using MOFs for introducing active sites that allow performing those reactions at lower temperature with a much lower catalyst deactivation. It should also be possible to synthesize MOFs with bifunctional metal/acid sites that, by working in the presence of H₂, can maintain the activity of the catalyst for long time periods. This could be, for example, the isomerization of n-C₅ and n-C₆, and even n-C₇ and n-C₈ alkanes, provided that acid or oxidation sites able to work at low temperatures could be incorporated within the framework.

Besides oil refining and petrochemistry, MOFs can find use as catalysts for reactions requiring lower temperatures, as is the case of organic synthesis and, more specifically, the synthesis of fine chemicals. Then, MOFs can complement

zeolites and structured mesoporous catalysts. For instance, in reactions in where a diffusion control by reactants or products is undesired, MOFs with very large pores could be useful, provided that the adequate active sites could be introduced and the structure remains stable during activation and reaction. If this occurs, then MOFs can be of interest, since they allow high density of catalytic sites, in particular when these active sites are transition metals. In this regard, it is interesting to note the need of theoretical work rationalizing/anticipating the catalytic activity of MOFs and predicting appropriate active sites and crystal structures. Considering the flexibility in the synthesis and design characteristic of MOFs, these theoretical studies will be very welcome since they can lead the research in this field, proposing new structures and assisting in the finding of highly active MOF catalysts.

When evaluating the potential of a given MOF structure as heterogeneous catalyst, the main point is its stability under the reaction conditions and its possibility to reactivate the material when it becomes deactivated. Stability of MOF to certain solvents upon heating for long periods can be limited. In principle, because of their composition, MOFs are more suited for being used in hydrocarbons and apolar solvents, although in some cases water and alcohols can be used. X-ray diffraction (XRD) is a suitable technique to assess the structural stability. In some cases, minor changes in the XRD pattern, particularly in the relative intensity of some peaks, have been attributed to the presence in the interior of the MOF void space of organic species and not to a real destruction of the crystallinity.^{71,98} This can be assessed by determining the microporosity of the used material after the reaction and observing the isothermal gas adsorption data characteristic of MOFs.

Thermogravimetric techniques are frequently used to establish the thermal stability of organic materials. Most MOFs are thermally stable at temperatures higher than 573 K. This temperature is sufficiently high to ensure the applicability of the material in many liquid-phase reactions that are typically performed at temperatures below 473 K. However, it should be commented that data from thermogravimetric analyses have to be used cautiously since structures that are stable over 573 K for the limited time of the thermogravimetric measurement may undergo extensive damage when heated at lower temperature for much longer times.

Leaching of some metal species from the solid to the liquid phase, even in minute amounts, can also be possible, and this possibility has to be addressed by performing chemical analyses of the solution. This leached metal species could be responsible totally or in part for the catalysis. In these cases, the solid could be the precursor of the real catalytic species and will act by dispensing a certain amount of metal into the solution. In principle, leaching is an undesirable process in heterogeneous catalysis because it produces at long term the decay of the catalytic activity of the material and manifests the instability of the solid catalyst.

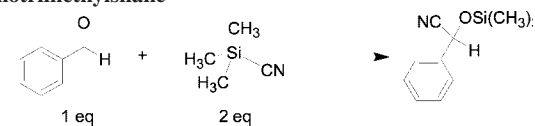
From the above comments, it can be concluded that any MOF tested in catalysis has to be carefully surveyed for stability and that MOF stability also has to be considered suspicious. Even the presence of moisture can affect the structural stability of MOFs upon long-term storage, as in the case of MOF-5.^{99–101}

1.6.1. Determining the Maximum Productivity of a MOF

An ideal heterogeneous catalyst should exhibit high activity and selectivity and should not deactivate over the course of the reaction. Obviously, there are no perfect heterogeneous catalysts and all solid catalysts, including MOFs, will deactivate after sufficiently long operation time. In this regard, several reports have performed reusability tests to prove that MOF does not deactivate upon reuse. The problem is that data confirming the reuse for a given number of runs under certain conditions do not ensure or anticipate the same or similar activity in the next subsequent run. In this regard, one should consider the maximum catalyst productivity (turnover number, TON) rather than the number of reuses under certain conditions. To determine this maximum productivity, a single experiment can be performed in which a large excess of substrate is used and the process is allowed to occur for sufficiently long time up to the point in which the catalyst becomes deactivated. If at this point the TON is still too low, catalyst regeneration becomes mandatory when considering a potential industrial use. In that case, it is of much interest to determine which are the causes of catalyst deactivation and if the catalyst can be regenerated. Among the possible causes for catalyst deactivation, one may highlight (a) strong adsorption of products or side products (that perhaps can be reversed by liquid extraction, since catalyst regeneration by burning out the adsorbed products can drive into catalyst destruction) and (b) the irreversible collapse of the structure due to the migration of the framework metal ions.

It is clear that, to find the causes of catalyst deactivation, the reacted MOF should be collected and analyzed by textural, microscopy, and spectroscopic techniques. Isothermal gas adsorption would inform on the plugging of the micropore system, while powder XRD of the deactivated catalyst could serve to determine the integrity of the crystal structure. Fourier transform infrared (FTIR) spectroscopy can be used to determine the presence of adsorbed organic poisons and the formation of new functional groups in the linker. One approach that has been used in the case of zeolites to determine the nature of the poisons is dissolving the solid and proceeding to extraction and analysis of the occluded organic matter. This methodology could be easily applied to the case of MOFs, since most of them can be readily dissolved in mild acids. Electron microscopy can also be applied to establish whether or not the morphology of the MOF particles has changed during reaction together with the eventual formation of metal micro/nanoparticles on the solid. When MOF is used as support of metal nanoparticles (see section 2.4.1), electron microscopy and chemical analysis can be used to assess variations on particle size and the occurrence of aggregation or metal leaching, with the concomitant loss of catalytic activity. It is remarkable that, in most cases, these types of deactivation studies have not been pursued for MOFs as catalysts. This is probably due to the fact that the use of MOFs as catalysts is a recent area of research that is currently more focused on proving the concept that MOFs can be solid catalysts in organic reactions and determining the scope than in developing real, industrial applications of MOFs as catalysts for a certain process. This stage surely will come later.

Table 1. Summary of Different Experimental Conditions Used for the Cyanosilylation of Benzaldehyde with 2 Equiv of Cyanotrimethylsilane




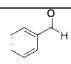
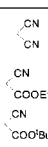
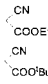
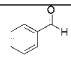
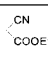
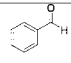
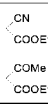
mol % catalyst	solvent	temp, K	time, h	yield, %	ref
20	CH ₂ Cl ₂	313	24	77	115
11.2	CH ₂ Cl ₂	r.t.	16	69	118
15.75	CH ₂ Cl ₂	313	48	50	71
	pentane	313	48	40	
			72	57	
	THF	313	48	2	
	heptane	333	48	55	
	toluene	353	24	20	
11	CH ₂ Cl ₂	r.t.	9	98	166
1.5	heptane	313	3	98.5	127

1.6.2. Selecting a Suitable Reaction Test and the Right Substrates

There exist several MOFs for which a potential catalytic activity can be envisaged from a direct inspection of their structure, like those containing, e.g., redox active centers in a given coordination environment, organic groups with basic properties (such as amides or amines), or metal sites with potential coordinative unsaturations, which could behave as active centers for certain Lewis catalyzed processes. In such cases, a catalytic reaction experiment can be performed to demonstrate that the material presents the required active sites for the reaction. However, as we will see in this section, the selection of the catalytic reaction, the experimental conditions, and the substrates chosen have to be done properly in order to obtain a fair appraisal of the true potential of the material as catalyst. This is particularly relevant when shape- or size-selective properties of the solid catalyst are being evaluated (an obviously targeted characteristic when dealing with porous crystalline solids such as MOFs). In these cases, one can select for a given reaction a set of substrates with different dimensions relative to the pore system of the MOF, and the possible occurrence of shape- or size-selectivity is evaluated from the different reaction rates measured for each substrate. However, we have to be completely sure that the observed differences in reactivity are only due to the different dimensions of the substrates, and that other possible factors, such as activating or deactivating electronic effects due to the substituents introduced, are not determinant.

Common choices of catalytic “test” reactions to demonstrate Lewis acid and Lewis basic properties of a MOF have been cyanosilylation of aldehydes and Knoevenagel condensation, respectively. However, a general, standardized experimental procedure has not been adopted to perform these test reactions, so that it is very difficult to establish fair comparisons between the different MOFs. This can be clearly appreciated in Tables 1 and 2, in which different conditions reported for cyanosilylation of benzaldehyde with Me₃SiCN and Knoevenagel condensation of various aldehydes are summarized. In these two particular reactions, the selection of the substrates, solvent, and reaction temperature can have a critical effect on the observed catalytic activity. If the aim of the catalytic study is only to demonstrate that the material contains the necessary active centers for these reactions (i.e., Lewis acid or basic sites), a simple experiment with a readily convertible substrate might be satisfactory.

Table 2. Summary of Different Experimental Conditions Used for the Knoevenagel Condensation Reaction of Different Aldehydes


React 1	React 2	Solvent	Temp, K	%mol cat.	time	Yield %	Ref.
		Benzene	r.t.	4	12 hr	98	177
						7	
		Cyclohexane	353	2.08 ^(a)	19 hr	97.7	94
					7 hr	97.7	
					19 hr	97.7	
					19 hr	96.3	
		DMSO	313	2.86	2 hr	99	179
						58	

^a Catalyst used (mol %) calculated for ED-MIL-101. ^b Catalyst used (mol %) calculated for ED-MIL-101(D). ^c Catalyst used (mol %) calculated for DETA-MIL-101. ^d Catalyst used (mol %) calculated for APS-MIL-101.

However, it would be of more use to provide a fair evaluation of the potential of the MOF as a heterogeneous Lewis acid or basic catalyst by screening a range of different substrates. A good way of assessing the activity of the MOF is to perform the reaction with substrates of increasing difficulty. For instance, the more demanding ketones can be used instead of the aldehydes in both Knoevenagel and cyanosilylation reactions, or a series of different activated methylene compounds can be used for the Knoevenagel condensation of different pK values and thus of decreasing reactivity: malononitrile > ethyl cyanoacetate > ethyl acetoacetate > diethylmalonate.^{102,103} In these tests, the initial reaction rate, corresponding to the intrinsic catalytic activity of the fresh catalyst, the maximum productivity, and studies on the stability of the MOF catalyst should be provided in addition to the conversion at a given reaction time. Proceeding in this way, it is possible to find the limits (and, thus, the true potential) of the catalyst.

Finally, it will always be of interest to compare the catalytic behavior of MOFs with other state-of-the-art homogeneous and heterogeneous catalysts for the particular reaction studied. Particularly interesting is to compare the catalytic activity of MOFs with that of metal carboxylates in solution. These types of comparative studies can be used to determine the nature of the active sites and to establish what is the influence of the spatial structuring of the sites in a fixed environment.

2. Catalysis by MOFs

2.1. Types of MOFs Used in Catalysis

In all MOF compounds, three different parts can be clearly differentiated: (i) the metallic component, (ii) the organic ligand, and (iii) the pore system. It is, therefore, possible to think of three different types of catalysts based on MOFs, and in practice, all of them have been described.

2.1.1. MOFs with Metal Active Sites

The catalytic activity observed for these materials is directly related to their metallic components, either as isolated metal centers or as clusters¹⁰⁴ (dimers,³⁶ trimers,¹⁰⁵ tetramers,¹² etc.), chains,¹⁰⁶ or sheets,^{107,108} connected through the organic linkers. This group of MOFs includes materials with only one type of metal center (M), which simultaneously acts as a structural building component and a catalytic active site. Other MOFs contain two different types of metals: one of them (M₁) is responsible for the catalytic activity, while the second metal (M₂) has only a structural role and is not directly involved in catalysis. Whereas M₁ is commonly a single metal site, M₂ can be either a single metal ion or a cluster. A representation of the general structure of these materials is shown in Scheme 7.

2.1.2. MOFs with Reactive Functional Groups

These are materials in which the catalytic activity is associated with the functional groups of the organic component. These MOFs have functional groups in the organic ligands that are able to catalyze a given reaction, i.e., the active sites are located at the organic molecule and not at the metal ion. The organic ligands used for constructing this class of MOFs must present two different types of functional groups: coordinative groups, L₁, which are required for constructing the MOF structure through coordination to the metals, and reactive groups, L₂, which will be responsible for the catalytic properties of the material, as shown in Scheme 8. The number of MOFs belonging to this category with demonstrated catalytic activity is very limited. This is because the reactive groups L₂ need to be free and accessible to interact with the catalytic substrates and not be coordinated to the metal ions of the MOF. Therefore, the difficulty in preparing MOFs containing organic reactive groups lies in the natural tendency of metals to interact with all the available functional groups of the ligand.

2.1.3. MOFs as Host Matrices or Nanometric Reaction Cavities

None of the components of the MOF is directly involved in catalysis. The porous system of the material provides the physical space where the catalysis occurs (nanometric reaction cavity) or serves as a cage where the catalytic centers are encapsulated (host matrices).

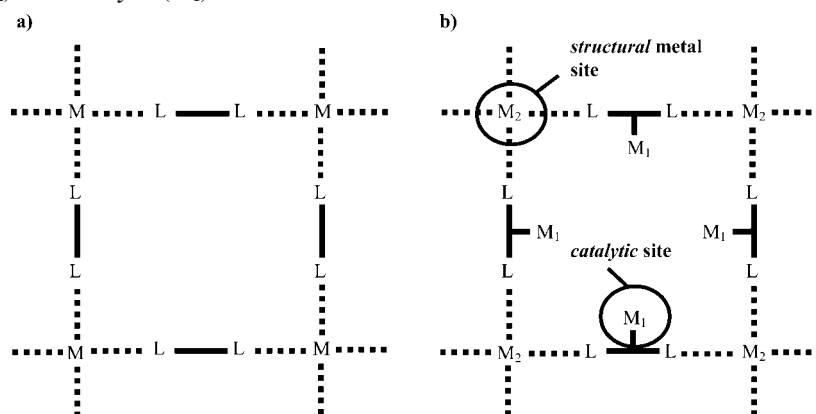
A list of the MOFs with proven catalytic activity that will be discussed in this review is given in Table 3.

2.2. MOFs with Metal Active Sites

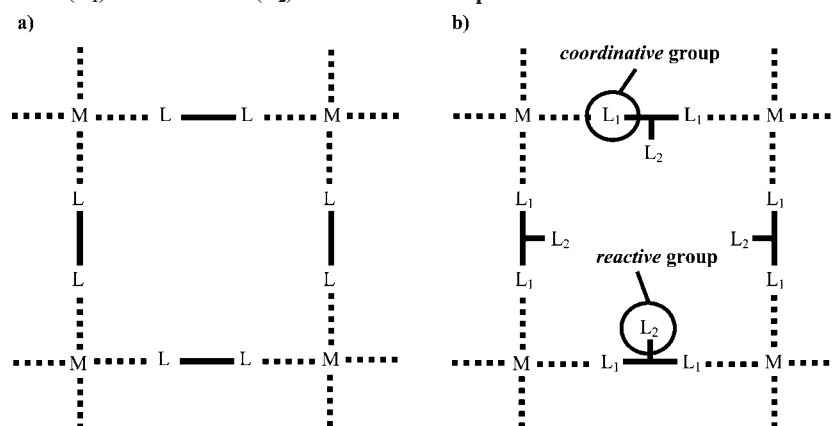
2.2.1. Early Studies

The catalytic activity of CPs has been known for a couple of decades. In 1982, Efraty and Feinstein¹⁰⁹ reported on the preparation of a CP containing Rh(I) and 1,4-diisocyanobenzene (1,4-dicb) by reacting [Rh(CO)₂Cl]₂ with an equimolar amount of 1,4-dicb. Although the structure of this material was not fully known, the authors deduced from IR and diffuse reflectance UV-vis (DRUV-vis) spectroscopies that the ligand 1,4-dicb produced a shift of half of the carbonyl groups initially present in the Rh complex, and weak intrachain Rh-Rh interactions take place in the material. Interestingly, this material was found to be active for the catalytic hydrogenation and isomerization of 1-hexene at

Scheme 7. Representation of (a) a Monometallic MOF with Only One Type of Metal Center (M) and (b) a Bimetallic MOF with Both Structural (M_2) and Catalytic (M_1) Sites



Scheme 8. Representation of (a) a “Classic” MOF with an Organic Spacer Having Only Coordinative Groups (L) and (b) a MOF with Both Coordinative (L_1) and Reactive (L_2) Functional Groups



room temperature at 0.5 bar H_2 pressure. The hydrogenation reaction was proposed to proceed through substitution of the carbonyl ligand by 1-hexene, followed by oxidative addition of H_2 with breaking of the intrachain Rh–Rh interactions, hydrogen transfer to the double bond, and reductive elimination of *n*-hexane. After this first cycle (implying the irreversible displacement of the remaining carbonyl ligand and breaking of the intrachain Rh–Rh interactions), further catalytic cycles proceed via oxidative addition of H_2 and coordination of 1-hexene to Rh(I). The proposed mechanism is shown in Scheme 9. Thus, the material [RhCl(CO)(1,4-dicb)] can be considered as a precatalyst, which evolves to the true catalyst after CO elimination. In agreement with the proposed mechanism and as anticipated by the authors, irradiation of the catalyst at 350 nm accelerates the initial reaction rate, favoring the photolytic rupture of the metal–carbonyl bond.

In successive years, the same group has reported on the preparation and catalytic activity of hybrid materials related with the above Rh-containing CP. In particular, they described the preparation of CPs containing 4,4′-diisocyanobiphenyl (4,4′-dicbp) as the organic ligand and Pd, Pt (both metals in 0 or II oxidation state),^{110,111} and Rh(I)¹¹² as the metallic components. These materials were also found to be active for the heterogeneous hydrogenation of alkenes and alkynes.

Related with the above materials, Tannenbaum reported on the synthesis of Ru(II)-containing CPs using 1,4-dicb as the organic spacer.^{113,114} Depending on the ruthenium precursor used in the synthesis, either cubic or tetragonal 3D

materials could be prepared. While the tetragonal material presented Ru–Ru stacking interactions in the *z* direction, in the cubic form all the Ru(II) ions were separated by 1,4-dicb ligands. The presence of Ru–Ru interactions confers catalytic potential to the tetragonal solid, because breaking these weak intermetallic interactions leads to coordinative unsaturation of the Ru(II) ions. The metal sites thus become prone to perform the oxidative addition of the substrates. On the contrary, this is not possible for the cubic form, in which all Ru(II) ions are coordinated to six ligand molecules. Tannenbaum demonstrated the catalytic potential of the tetragonal solid by studying the hydrogenation of 1-hexene. This reaction proceeded smoothly over the tetragonal form of the Ru(II)–1,4-dicb solid, while no conversion was observed when the cubic form was used. However, hydrogenation of 1-hexene to hexane was not selective, since isomerization products (mainly *trans*-2-hexene) were also obtained. An induction period was observed, which indicates that cleavage of the Ru–Ru interactions was necessary before the hydrogenation reaction can start. Irradiation at 350 nm was found to suppress the observed induction period, since this energy was enough to break the Ru–Ru intermetallic bonds.

In 1994, Fujita et al. prepared a network material containing Cd^{2+} and 4,4′-bipyridine, [Cd(4,4′-bpy)₂](NO₃)₂ (4,4′-bpy = 4,4′-bipyridine).¹¹⁵ This material consists of stacked two-dimensional square networks of Cd^{2+} ions at the corners and 4,4′-bpy at the sides of the square. Stacking of layers defines square cavities, which were found to show shape-specific clathration toward some aromatic compounds. Thus,

Table 3. MOF Compounds with Reported Catalytic Properties^a

MOFs with metal active sites			
MOF	active metal	catalyzed reaction(s)	ref
[RhCl(CO)(1,4-dicb)]	Rh ⁺	1-hexene hydrogenation/isomerization	109
[M(4,4'-dicbp) _x]	M = Pd ⁰ ($x = 1.82 \pm 0.12$) M = Pt ⁰ ($x = 1.25 \pm 0.2$)	1-hexene hydrogenation/isomerization	110, 111
[MC1 ₂ (4,4'-dicbp)]	M = Pd ²⁺ , Pt ²⁺	alkene and alkyne hydrogenation/isomerization	110, 111
[RhCl(4,4'-dicbp) ₂]	Rh ⁺	1-hexene hydrogenation/isomerization	112
[RuCl ₂ (1,4-dicb) ₂][RuCl ₂ (1,4-dicb) ₃]	Ru ²⁺	1-hexene hydrogenation/isomerization	113, 114
[Cd(4,4'-bpy) ₂](NO ₃) ₂	Cd ²⁺	(shape-selective) cyanosilylation of aldehydes/imines	115, 116
[<i>cis/trans</i> -(OArO) _x Ti(py) _y] (OArO = aryldioxide)	Ti ⁴⁺	ethylene and propylene polymerization	117
[Ln(7-H ₂)(7-H ₃)(H ₂ O) ₄]	Ln = La, Ce, Pr, Nd, Sm, Gd, Tb	cyanosilylation of aldehydes ring opening of <i>meso</i> -anhydrides	118
[In ₂ (OH) ₃ (bdc) _{1.5}]	In ³⁺	hydrogenation of nitroaromatics oxidation of sulfides	107
[Pd(2-pymo) ₂]	Pd ²⁺	(shape-selective) hydrogenation of olefins oxidation of alcohols Suzuki C–C coupling	61
IRMOF-3-SI-Au (SI-salicylideneimine)	Au ³⁺	3-component coupling and cyclization hydrogenation of 1,3-butadiene	93
IRMOF-3-SI-VO(acac) (SI-salicylideneimine)	V(O)acac ₂ (acac = acetylacetonate)	oxidation of cyclohexene	92
PIZA-3	Mn ³⁺	hydroxylation of linear and cyclic alkanes	129
[Cu(2-pymo) ₂]	Cu ²⁺	oxidation of tetralin (with air)	79
[Co(bzim) ₂] (ZIF-9)	Co ²⁺		
MIL-101(Cr)	Cr ³⁺	oxidation of tetralin (with ^t BuOOH)	130
[Zn ₂ (bpc) ₂ (salenMnCl)]	Mn ³⁺	enantioselective olefin epoxidation	132
[Co(bpb)] (MFU-3)	Co ²⁺	cyclohexene oxidation	135
[Cu ₂ (1,4-chdc) ₂]	Cu ²⁺	oxidation of alcohols	137
V ₆ O ₁₃ -Co-MOF	V ₆ O ₁₃	oxidation of thiols	141
V ₆ O ₁₃ -Tb-MOF	V ₆ O ₁₃	oxidation of thiols	142
RPF-4	Ln = La, Ce, Pr, Nd, Sm, Eu, Gd, Tb, Dy, Er, Yb	oxidation of sulfides	143
[Yb(C ₄ H ₄ O ₄) _{1.5}]	Yb ³⁺	acetalization of aldehydes oxidation of sulfides hydrodesulfurization	144
[Zn ₂ (bdc)(L-lact)(dmf)]	Zn ²⁺	oxidation of sulfides	106, 145
MIL-101(Cr)	Cr ³⁺	oxidation of sulfides	131
[Na ₂₀ (Ni ₈ (4,5-IDC) ₁₂)]	Ni ²⁺	CO oxidation to CO ₂	147
[Cu(5-mipt)]	Cu ²⁺	CO oxidation to CO ₂	148
[Ni ₂ (H ₂ O) ₂ (2,3-pydc) ₂ (4,4'-bpy) ₂ - U ₅ O ₁₄ (H ₂ O) ₂ (OAc) ₂ ·2H ₂ O	U ₅ O ₁₄	photocatalysis	149
[Co ₂ (4,4'-bpy)(oba) ₂][Ni ₂ (4,4'-bpy) ₂ (oba) ₂]- [Zn ₂ (4,4'-bpy)(oba) ₂]	Co ²⁺ /Ni ²⁺ /Zn ²⁺	photocatalysis	152
[Zn ₄ (O)(bdc) ₃] (MOF-5)	Zn ₄ O ₁₃	photocatalysis	62, 153
IRMOF's	Zn ₄ O ₁₃	photocatalysis	162
[Cu ₃ (btc) ₂] (HKUST-1)	Cu ²⁺	aldehyde cyanosilylation	71
Mn ₃ [(Mn ₄ Cl) ₃ (btt) ₈ (CH ₃ OH) ₁₀] ₂	Mn ²⁺	cyanosilylation of carbonyls Mukaiyama-aldol condensation	166
MIL-101(Cr)	Cr ³⁺	aldehyde cyanosilylation	127
Yb-RPF-5	Yb ³⁺	hydrodesulfurization	167
Ti-MOF homochiral	Ti ⁴⁺	ZnEt ₂ addition to aldehydes	76, 169
[Cu ₃ (btc) ₂] (HKUST-1)	Cu ²⁺	various acid-catalyzed reactions	63
MIL-100(Fe)	Fe ³⁺	Friedel–Crafts benzylation	170
IRMOF's	Zn ²⁺ -OH	alkylation of aromatics	173
MOFs with reactive functional groups			
MOF	active ligand	catalyzed reaction(s)	ref
POST-1	pyridyl group	(size-/enantioselective) transesterification	105
[Cu ₂ (pzdc) ₂ (4,4'-bpy)]	carboxylate oxygen	polymerization of acidic acetylenes	176
[Cd(4-btapa) ₂](NO ₃) ₂	amide	Knoevenagel condensation	177
[Zn ₄ (O)(ata) ₃](IRMOF-3) MIL-53(NH ₂)	amino	Knoevenagel condensation	179
MIL-101(Cr)-ED	amino	Knoevenagel condensation	94
MIL-101(Cr)-proline	proline	asymmetric aldol reaction	95

^a See section 4 for a list of the abbreviations used for the ligand molecules. The materials are grouped according to the three main types described in section 2.1 and sorted by order of appearance in the text.

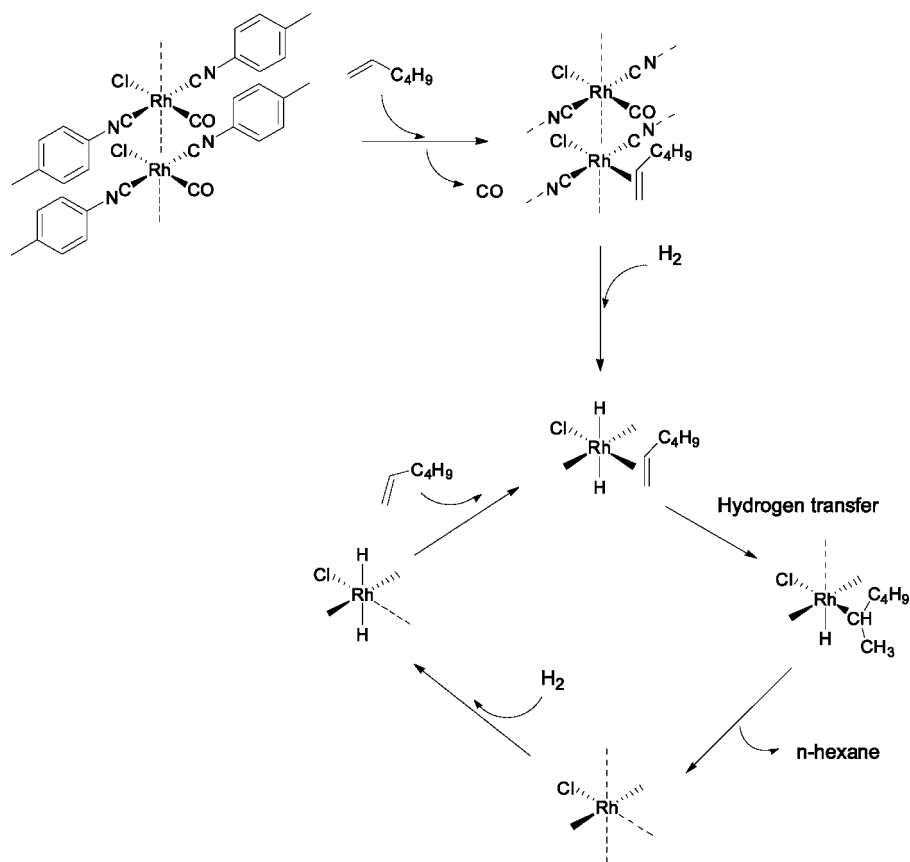
o-dihalobenzenes were selectively clathrated from mixtures containing *ortho*-, *meta*-, and *para*-isomers. Interestingly, the material showed catalytic activity and shape selectivity during cyanosilylation of aldehydes¹¹⁵ and imines.¹¹⁶

Tanski and Wolczanski¹¹⁷ have studied the potential of a series of 1D, 2D, and 3D CPs containing titanium and aryldioxides, for the polymerization of ethylene and propylene using methylaluminumoxane (MAO) as cocatalyst. How-

ever, the authors concluded that all the materials studied gave poor catalytic performance (i.e., low activity and high polydispersity).

Evans et al.¹¹⁸ have prepared a series of isomorphous homochiral porous lamellar lanthanide bisphosphonates of general formula [Ln(7-H₂)(7-H₃)(H₂O)₄]_x·xH₂O, with Ln = La, Ce, Pr, Nd, Sm, Gd, Tb, $x = 9-14$, and (7-H₄) = 2,2'-diethoxy-1,1'-binaphthalene-6,6'-bisphosphonic acid. The

Scheme 9



material containing Gd and the enantiomer *R*-7 crystallized in the chiral $P2_12_12_1$ space group and consisted of a lamellar structure with 8-coordinated Gd centers and bridging binaphthylbiphosphonate ligands (see Figure 2). Each Gd was linked to four phosphonate oxygen atoms from four different ligands and four water molecules. The linkage of these structural units leads to the formation of elongated 2D rhombohedral grids on the *ac* plane, which stacks along the *b* axis via interdigitation of the binaphthyl rings. Three of the four crystallographically independent phosphonate groups are monodeprotonated, while the fourth phosphonate group remains protonated. The material was found to be stable to dehydration. Although desolvation was accompanied by severe changes and peak broadening in the XRD patterns, the original structure was recovered after reexposure to water. The changes were attributed to distortion of the long-range

order of the material while maintaining the local coordination environment. Given the presence of both Lewis and Brønsted acidity, the authors tested the catalytic activity of the materials for cyanosilylation of aldehydes. Reaction of cyanotrimethylsilane and different aldehydes over one of the lamellar compounds afforded isolated yields ranging from 55 to 69% of the pure nitriles after 16 h and acidic workup. The obtained products were essentially racemic (*ee* < 5%). The authors claimed that the indiscriminate catalytic efficiency observed with aldehydes of different size was due to swelling of the lamellar catalyst to facilitate substrate transport under reaction conditions. However, the lack of kinetic data precludes the evaluation of the catalytic activity with the different substrates in terms of turnover frequency (TOF), so that any consideration about the influence of the substrate size is meaningless. Finally, the authors also

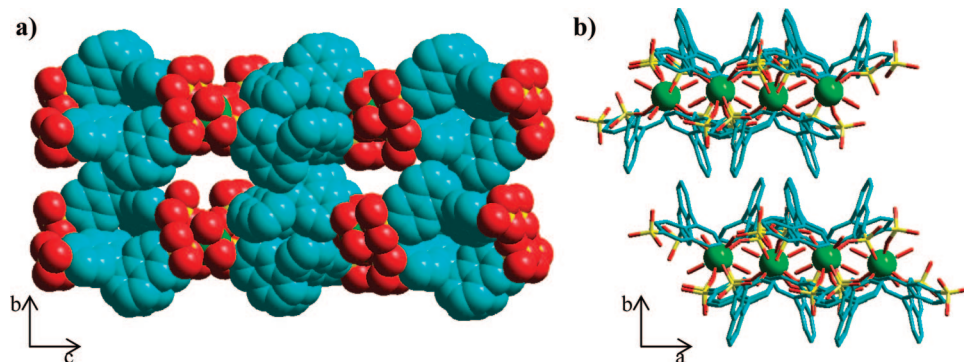
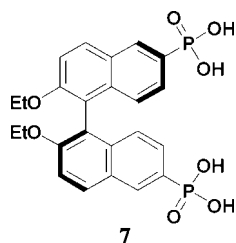


Figure 2. (a) Projection on the *bc* plane of the lamellar structure of the compound $[\text{Gd}(\text{R-7-H}_2)(\text{R-7-H}_3)(\text{H}_2\text{O})_4] \cdot 12 \text{H}_2\text{O}$, in which the presence of asymmetric channels can be seen; (b) structure seen along the *c* axis, showing interdigitation of the binaphthyl rings of two consecutive layers. Ethoxy chains and hydrogen atoms have been omitted for clarity. La, Green; C, Light blue; O, Red; P, Yellow. Figure adapted from ref 118.

demonstrated the catalytic activity of the materials for the acid-promoted ring opening of *meso*-anhydrides. Treatment of *meso*-2,3-dimethylsuccinic anhydride with methanol in the presence of one of the biphosphonate compounds produced the corresponding hemiester in 81% yield, although the obtained product was racemic (*ee* < 5%).



According to the definition given in section 1.2, some of the compounds described so far cannot strictly be considered as MOFs, since they do not fulfill all the requirements of crystallinity, porosity, and a 3D network supported by strong metal/ligand interactions over the three dimensions. In some compounds, the lack of experimental characterization data does not allow one to conclude if the material would fit the definition of MOF or not. Nevertheless, we have considered it interesting to include a discussion on these compounds because they represent the first attempts to use structured coordination polymers as catalysts. These studies have thus paved the way for the development of MOF catalysts in present days.

2.2.2. Hydrogenation Reactions

The work of Efraty and Feinstein^{109–112} and Tannenbaum,^{113,114} discussed in section 2.2.1, constituted the first examples of coordination polymers as hydrogenation catalysts. In all the above cases, the chosen target for hydrogenation was the unsaturated C–C bond of an alkene or an alkyne. Since these pioneering papers appeared, other reports have been published describing new materials with a demonstrated hydrogenation activity.

Gómez-Lor et al.¹⁰⁷ have prepared and characterized a 3D indium terephthalate MOF, $[\text{In}_2(\text{OH})_3(\text{bdc})_{1.5}]$. In this material, indium atoms were coordinated to three μ^2 -OH groups

and three oxygen atoms from three different bdc ligands. The structure can be described as infinite hexagonal sheets formed by $[\text{In}_2(\text{OH})_3]^{3+}$ repetitive units, in which the resulting sheets are linked by bdc molecules. There, each bdc ligand is coordinated to four In atoms, two from each sheet, thus acting as pillars. The bdc pillars are built parallel to the *ac* plane, 2/3 of them oriented in the $[101]$ direction and 1/3 of them oriented in the $[1\bar{0}1]$ direction (see Figure 3). This orientation, probably caused by π – π repulsion of the aromatic rings, precludes the occurrence of open channels in the *b* direction. According to the XRD, the structure of this MOF was found to remain unchanged after heating at 673 K. Given this high thermal stability, the authors tested the catalytic activity of the MOF for hydrogenation of nitroaromatic compounds and for the oxidation of sulfides (see section 2.2.3.5). The small size of the pore in the material avoided accessibility of the substrates to the metal centers, and consequently, the reaction should occur at the external surface of the catalyst.

Reduction of nitrobenzene and 2-methyl-1-nitronaphthalene over the In–MOF occurred without induction period, with a high yield and with TOFs of 489 and 385 min^{-1} , respectively. Even bulky molecules, such as 2-methyl-1-nitronaphthalene, were converted with a 100% yield within 6 h under mild conditions (batch reactor, 313 K, $p(\text{H}_2) = 4$ bar, with metal/substrate molar ratio of 1/1000). The catalyst was reused without any deactivation at least four times, while no changes were observed in the X-ray diffractograms of the recovered materials. The liquid filtrates after each reaction were tested in the same reaction conditions and were found to be inactive, and no indium or bdc traces were detected in solution. Owing to the fact that the hydrogenation reaction only occurs at the external surface, it is clear that the real TOF must be much larger than the one calculated on the basis of the total number of metal atoms. Furthermore, the activity of this catalyst should be a function of the size of the crystal.

Navarro et al.⁸⁰ described the preparation of a Pd-containing MOF using 2-hydroxypyrimidine as organic ligand, $[\text{Pd}(2\text{-pymo})_2] \cdot 3\text{H}_2\text{O}$. This material is structurally related to 3D sodalite-type frameworks, with two different hexagonal windows with free openings of 4.8 and 8.8 Å and

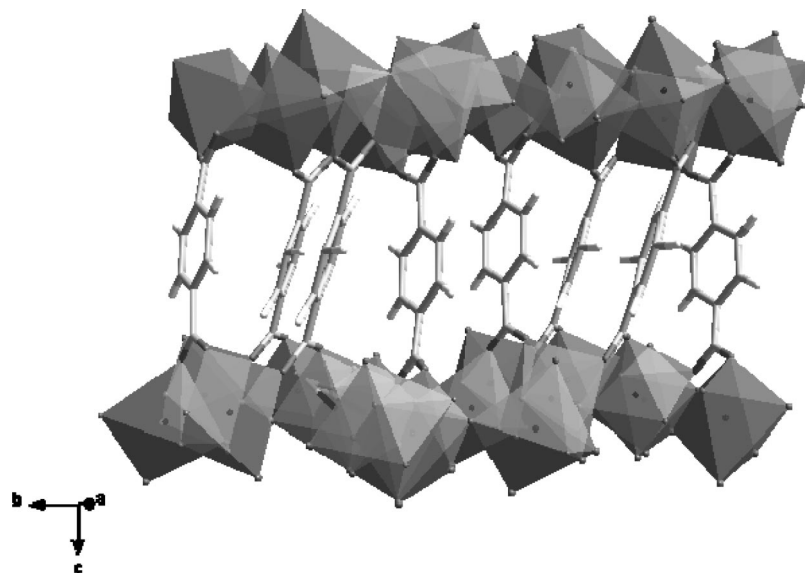


Figure 3. Projection on the *bc* plane of the 3D structure of the $[\text{In}_2(\text{OH})_3(\text{bdc})_{1.5}]$ material, in which the alternate disposition of the interlayer bdc ligands can be appreciated. Figure adapted from ref 107.

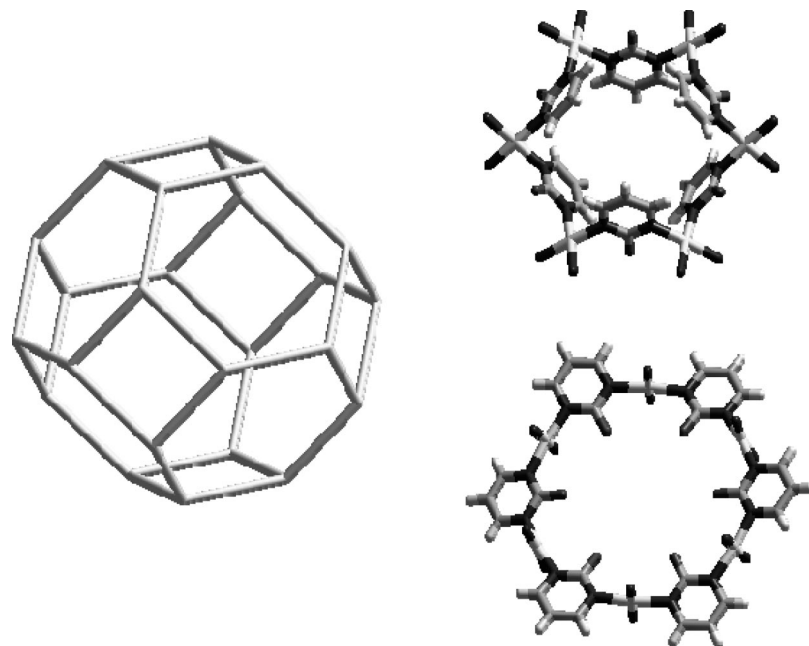


Figure 4. 3D structure of the material [Pd(2-pymo)₂] showing (left) the sodalite cages (only Pd ions are shown) and (right) the two types of hexagonal windows. Figure adapted from ref 80.

with a fraction of 42% of the crystal volume available to reacting molecules (see Figure 4). We have recently demonstrated the utility of this material for Pd-catalyzed reactions, such as alcohol oxidation, Suzuki C–C coupling, and olefin hydrogenation.⁶¹ We will describe here the results obtained with olefin hydrogenation, while the other two reactions will be presented in forthcoming sections (see sections 2.2.3.3 and 2.2.8).

When 1-octene was contacted with the Pd–MOF under mild conditions (2 bar H₂ and 308 K), a complete conversion of the substrate was observed after ca. 40 min. Analysis of the products showed a 59% yield (at 40 min reaction time) of octane, with the rest of the products being 2-octene. When the reaction time was prolonged, the 2-octene formed was ultimately hydrogenated to octane, with the selectivity to octane being 100% after 2 h reaction time. Furthermore, the Pd–MOF behaves as a heterogeneous catalyst and can be reused without structure degradation or leaching of Pd. The presence of a regular pore system in the Pd–MOF can introduce shape-selectivity effects for hydrogenations, as only smaller olefins that can diffuse through the pores will be hydrogenated, while bulkier molecules will not. To explore the potential shape selectivity of the Pd–MOF, and following the method proposed by Chang et al.,¹¹⁹ the hydrogenation rates of 1-octene and cyclododecene were compared over the Pd–MOF. Total conversion of 1-octene was obtained after 40 min, while no reaction was observed with cyclododecene even after 5 h reaction time, with this being a clear consequence of shape-selectivity effects imposed by Pd–MOF.

Very recently, we have reported on the catalytic properties of a gold(III)-containing MOF prepared via a covalent postsynthesis modification.⁹³ The material was prepared through the two-step process depicted in Scheme 5. This catalyst was prepared from the zinc aminoterephthalate IRMOF-3 (isoreticular to MOF-5), by reacting the available –NH₂ groups with an aldehyde to form the corresponding imine, followed by complexation of a metal precursor (NaAuCl₄) to form the corresponding Au(III) Schiff base complex. In a related precedent to our work, Ingleson et al.⁹²

described the preparation of a MOF containing a vanadyl Schiff base complex following a similar postsynthesis modification of IRMOF-3 with salicylaldehyde, but incorporating V=O instead of Au(III). These authors also performed a preliminary catalytic investigation using the (V=O)–MOF for the oxidation of cyclohexene with ^tBuOOH (*tert*-butylhydroperoxide) as the oxidant, but they recognized that the obtained TOF was very low and that the material loosed its framework integrity.

Concerning our gold-containing MOF, the preparation procedure used leads to accessible isolated Au(III) ions lining the pore walls of the material, while the crystalline structure was preserved.⁹³ The +3 oxidation state was confirmed by the amount of H₂ consumed during a temperature-programmed reduction measurement (TPR), which corresponded to 1.5 the total molar amount of gold of the material. Furthermore, the TPR experiment also demonstrated that Au(III) was highly stabilized by the Schiff base complex, as deduced from the H₂ consumption peak appearing at a sensibly higher temperature (512 K) than that found for gold(III) supported on nanocrystalline CeO₂ or on ZrO₂, which are known to stabilize surface cationic gold species.^{120–122} But at difference with gold deposited on these metal oxide supports, in which the fraction of Au(III) with respect to total gold is only 0.2–0.3,^{122b} the Au–MOF contains exclusively cationic gold(III). Therefore, we anticipated the catalytic activity of this material in reactions in which cationic gold is claimed as the active species, such as the selective hydrogenation of 1,3-butadiene^{122a} and the three-component coupling of aldehydes, amines, and alkynes/N-protected ethynylaniline to yield propargylamines and indoles (see section 2.2.8).^{122b}

Hydrogenation of 1,3-butadiene was performed using the Au(III)–MOF as catalyst (fixed-bed reactor, atmospheric pressure, and 403 K). For comparison, samples of Au/TiO₂ (1.5 wt % gold) provided by the World Gold Council, pretreated either in Ar at 403 K or in H₂ at 523 K, were also measured under the same conditions. The activities and selectivities obtained for the hydrogenation over the different catalysts are shown in Figure 5. When

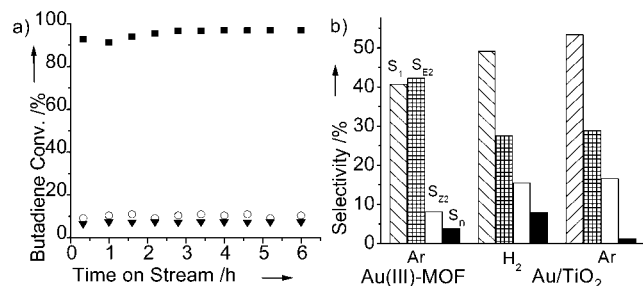


Figure 5. (a) 1,3-Butadiene conversion versus time on stream and (b) product selectivity over the Au(III)-MOF (■), and Au/TiO₂ pretreated in flowing H₂ at 523 K (○) or in Ar at 403 K (▼). S₁, S_{E2}, S_{Z2}, and S_n represent the selectivity to 1-butene, *E*-2-butene, *Z*-2-butene, and *n*-butane, respectively. Reproduced with permission from ref 93. Copyright 2009 Elsevier.

the Au(III)-MOF was used as catalyst, almost total conversion of 1,3-butadiene was obtained, while much lower conversions (ca. 9%) were achieved with both Au/TiO₂ catalysts. The TOF calculated for Au(III)-MOF on the basis of total gold weight (540 h⁻¹) was 1 order of magnitude higher than the values calculated for Au/TiO₂ (50.4 h⁻¹). Analysis of the reaction with Au(III)-MOF at a lower level of conversion and shorter time on stream¹²³ showed no evidence of any induction period. Considering that both Au/TiO₂ catalysts contain exclusively metallic gold, as well as the lack of any induction period for the reaction catalyzed by Au(III)-MOF, the results demonstrated that the oxidation state of gold is of paramount importance for the hydrogenation of 1,3-butadiene. Interestingly, the Au(III)-MOF showed a very high selectivity (up to 97%) for butenes (mainly 1-butene and *E*-2-butene), while production of butane was kept at a low value (3%) even at total conversion of 1,3-butadiene. The Au(III)-MOF catalyst also showed a high stability with time on stream (for at least 17 h under continuous operation).¹²³ This is one of the few examples existing in the literature in which a MOF catalyst has demonstrated better catalytic performances, stability, and reusability than any of the alternative state-of-the-art catalysts.

A totally different approach to the development of hydrogenation catalysts based on MOFs is the preparation of metal nanoparticles incorporated inside their structural pore system.^{124–127} In this context, hydrogenation catalysts consisting of Pd nanoparticles encapsulated inside MOF-5 and MIL-101 MOFs have been prepared by following different preparation procedures, including chemical vapor deposition, incipient impregnation, and coprecipitation. In these composite materials, the MOF acts as a host matrix in where the metal nanoparticles, which are the true catalysts for hydrogenation, are encapsulated. We will deal with these Metal@MOF composite materials in section 2.4.1.

Hydrazine can be used to effect C–C multiple bonds hydrogenation using MOFs as heterogeneous catalyst.¹²⁸ The main advantage is the experimental simplicity that avoids the use of flammable and explosive gas, being replaced by aqueous solutions of hydrazine that can be manipulated more easily.

2.2.3. Oxidation of Organic Substrates

There are some reported examples on the use of MOFs as catalysts for the oxidation of organic substrates, using either O₂ (or air) or hydroperoxides as oxidants. To demonstrate the performance of the material in these types of reactions, different substrates have been chosen. In this section, we

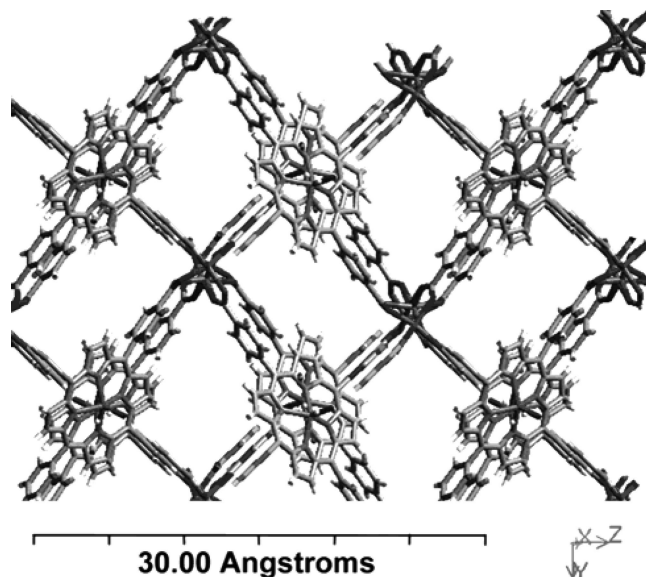


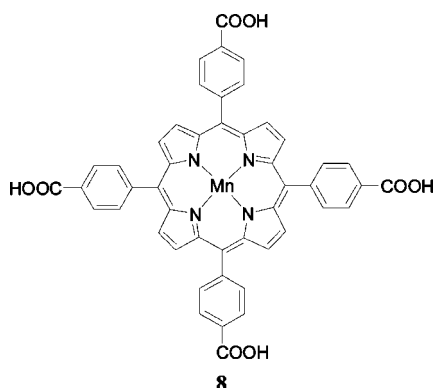
Figure 6. Crystalline structure of the compound [Mn(TpCPP)-Mn_{1.5}] (PIZA-3) viewed along the crystallographic *a* axis. Reproduced with permission from ref 129. Copyright 2005 American Chemical Society.

present the results obtained using MOFs as catalysts for oxidations of alcohols to aldehydes, paraffins or naphthenes to alcohols or carbonyl compounds, olefins to epoxides, sulfides to sulfoxides, and thiols to disulfides.

2.2.3.1. Alkanes to Alcohols and Carbonyl Compounds.

Suslick and co-workers prepared a series of robust microporous metal organic framework compounds termed PIZA-*n* (Porphyrinic Illinois Zeolite Analogue), containing metalloporphyrin complexes acting as ligands and metallic clusters at the nodes.¹²⁹ One of them, PIZA-3, contained Mn(III) tetra(*p*-carboxyphenyl)porphyrins (tpcpp, **8**) coordinated to bent trinuclear Mn(II) clusters. The 3D structure of this material contained alternating 5 × 9 Å and 7 × 8 Å pores down the *a* crystallographic axis and 3 × 5 Å pores down the *c* axis, creating an open framework with 56% void volume (see Figure 6). This material was tested as an oxidation catalyst for the hydroxylation of linear and cyclic alkanes, using either iodosylbenzene or peracetic acid as oxidants. All the reactions were carried out in acetonitrile at room temperature and with a catalyst/substrate ratio of 1:1000. According to the authors, the catalytic results obtained with PIZA-3 were comparable with those using other manganese porphyrins in homogeneous systems or immobilized inside inorganic supports as heterogeneous catalysts. After 2 h of reaction time, the oxidation of cycloalkanes (cyclohexane and cycloheptane) yielded the corresponding cycloalcohol as the main product, in ca. 45% yield and alcohol-to-ketone ratios of 8.0–8.9. However, the yields were referred to the oxidant iodosylbenzene (which was in a 1:100 ratio with respect to the substrate), meaning that the real alkane conversions were 100-fold lower. For linear alkanes (hexane and heptane), a mixture of alcohols was obtained with the hydroxyl group on different secondary carbons, with total yields of products of 17–22%. Finally, a branched alkane (3-methylbutane) produced the corresponding tertiary alcohol in 27% yield as the sole product. PIZA-3 was also found to be active for the oxidation of 1-hexanol to hexanal with 17% yield. The authors did not observe traces of metalloporphyrin or degradation products in the supernatant liquid after the catalytic reaction. When

peracetic acid was used as the oxidant, the solid MOF recovered after filtration was reused without loss of activity.



We have recently reported on the catalytic activity of two metal organic frameworks in the liquid-phase oxidation of alkanes using air as the oxidant.⁷⁹ The materials studied were [Cu(2-pymo)₂]⁸¹ and [Co(bzim)₂].³⁴ Both materials crystallized in the sod network, like the [Pd(2-pymo)₂] shown in Figure 4, in which isolated metal ions (Cu²⁺ or Co²⁺) occupy the nodes and are linked through N-atoms of diazaheterocyclic ligands (pyrimidinolate or imidazololate). As a substrate for the oxidation reaction, we chose tetralin (T-H), because of the industrial interest of the α -tetralone product (T=O), as an oxygenated diesel additive and a precursor in drug synthesis. The oxidation reaction was carried out in a batch reactor with bubbled air at ambient pressure and 363 K, and with a T-H-to-metal molar ratio of 2000. In these conditions, [Cu(2-pymo)₂] was found to be active and readily reusable, attaining a maximum T-H conversion of about 50% after 48 h. The time evolution of products of T-H oxidation over this Cu-MOF revealed an initial stage in which the only product formed was tetralinhydroperoxide, T-OOH, reaching a maximum yield of about 20–25 mol % after 15 h of reaction. At this point, the concentration of T-OOH started to decrease at the expense of T=O and α -tetralol (T-OH). After ca. 30 h, and coinciding with the disappearance of T-OOH, conversion of T-H reached a plateau. The obtained tetralone-to tetralol ratio, T=O/T-OH, was 2.7 after the first run, and this value slightly increases up to 3.4 for the two successive catalytic cycles. The T=O/T-OH ratio is a relevant indicator of the catalyst performance as it measures the selectivity of T-H oxidation to T=O. A thorough characterization of the catalytic reaction, including hot filtration test, analysis of copper in the catalyst and in the filtrate before and after reaction, and comparison with homogeneous catalysts, allowed us to conclude that leaching of Cu²⁺ from the Cu-MOF was not occurring, and that the catalytic process was heterogeneous.⁷⁹

T-H oxidation using the Co²⁺ containing MOF as catalyst revealed a totally different behavior. A maximum T-H conversion of ca. 23 mol % was reached, with a T=O/T-OH ratio of 6.8 for the first cycle, which increased up to 11.3 after three runs, i.e., the total conversion was significantly lower but the selectivity to T=O sharply increased as compared to that obtained with Cu-MOF. The kinetic evolution of products was also different for the two solids. In the case of Co-MOF, a clear induction period was observed in which no T-H was converted. After that, T-H was converted to T=O and T-OH, while the level of T-OOH accumulated throughout the whole reaction was very low. In other words, Co-MOF is very inefficient in

generating T-OOH (the primary product of the reaction), but once formed it can convert it very efficiently to T=O. On the contrary, Cu-MOF is very active in producing T-OOH and less selective to T=O.

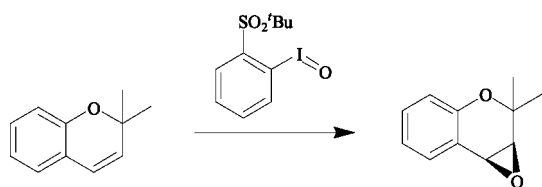
In light of the results obtained with Cu-MOF and Co-MOF for tetralin oxidation, and the observed differences between the two materials, we designed a strategy to improve the performance of the catalytic system by preparing mixtures of the two solids. This mixture could combine the advantages of both materials while overcoming the limitations of the two separate solids.⁷⁹ Indeed, an optimum composition was found at Co-MOF/Cu-MOF 90/10 wt %, which was the best compromise between activity, selectivity to T=O, low T-OOH accumulation, and no induction period.

Very recently, Kim et al. have reported on the catalytic activity of the chromium terephthalate MIL-101 for the liquid-phase oxidation of T-H, using as oxidant either ¹BuOOH or acylperoxy radicals generated in situ by reaction between trimethylacetaldehyde and O₂.¹³⁰ The authors have presented a thorough catalytic study in which the effect of temperature, amount of catalyst, and nature of the solvent and oxidant are contemplated. When ¹BuOOH was used as the oxidant, T-H conversions between 60 and 68% were obtained, with selectivities to T=O of ca. 85%. The amount of MIL-101(Cr) catalyst used was varied between 10 and 50 mg, which roughly corresponds to a T-H-to-active chromium site molar ratio of ca. 800 and 160, respectively (assuming that the concentration of coordinatively unsaturated Cr³⁺ sites in the fully dehydrated MOF is 1.0 mmol g⁻¹, as determined in ref 131). The authors found a dependence of the solvent on both T-H conversion and selectivity to T=O: the catalyst performed better in noncoordinating solvents (such as chlorobenzene or benzene) than in solvents with coordinating heteroatoms (such as CH₃CN or tetrahydrofuran, thf). This was explained by a strong coordination of the solvent molecules to the Cr(III) vacancies, which cannot be completely displaced by ¹BuOO[•] or the acylperoxy radicals.¹³⁰ The catalytic reaction over MIL-101 was found to be heterogeneous, as indicated by the hot filtration experiments and by the maintenance of the catalytic activity and selectivity for at least 5 runs. Also the crystallinity of the catalyst recovered after 5 uses was virtually identical to that of the fresh sample. Oxidation of benzylic positions of aromatic hydrocarbons using hydrogen peroxide as oxidizing reagent and Fe(BTC) MOF as catalyst has also been reported.⁹⁸

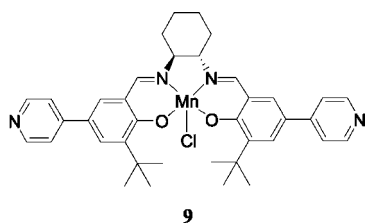
2.2.3.2. Oxidation of Olefins. As already mentioned in the previous section, the material referred to as PIZA-3¹²⁹ containing Mn-porphyrin units coordinated to trinuclear Mn clusters showed interesting oxidation capabilities, and it was found also to be active for the epoxidation of cycloalkenes using iodosylbenzene or peracetic acid as the oxidant. The substrates used for this reaction were cyclooctene, cyclohexene, cyclopentene, and limonene. In all the cases, the corresponding epoxide was formed as the main product, with yield to products of 74% for cyclooctene and ca. 20% for all the other olefins. In the case of limonene, the oxidation occurred at the ring position 1,2, producing a mixture of *cis*- and *trans*-limonene epoxide.

Probably the most promising results reported up to now concerning the use of a MOF catalyst for olefin oxidations were obtained by the group of Hupp.¹³² The compound used consisted of a bimetallic mixed ligand MOF. The structure of this compound can be described by the linkage of paddle-

Scheme 10



wheel carboxylate Zn_2 dimers and 4,4'-biphenyldicarboxylate ligands (bphdc) forming square planar layers, stacked by a bipyridine-like ligand containing a chiral Schiff base Mn(III) complex, **9** (salenMn). The formula of the material was $[Zn_2(bphdc)_2(salenMnCl)] \cdot 10 \text{ dmf} \cdot 8H_2O$. The MOF crystallized in the triclinic *P1* space group, and it was doubly interpenetrated, featuring distorted-rectangular and rhombic channels along the *c* and *a* directions of $6.2 \times 15.7 \text{ \AA}$ and $6.2 \times 6.2 \text{ \AA}$, respectively. The particular structure of the Schiff base ligand provided a chiral environment to the Mn(III) ions, similar to that found in other previously described Mn–salen heterogeneous systems.^{133,134} This material represents a clear example of the type of MOFs depicted in Scheme 7b, containing two types of metal ions with separate catalytic (M_1) and structural (M_2) roles. At the same time, this material exemplifies the second strategy described in section 1.5.2, Synthesis of MOFs with metal complexes as building blocks.



The authors compared the catalytic activity of the MOF with that of the free (salenMn) complex for the asymmetric epoxidation of 2,2-dimethyl-2H-chromene using 2-(*tert*-butylsulfonyl)iodosylbenzene as the oxidant (Scheme 10). The homogeneous free (salenMn) complex initially showed a high activity, but it started to be deactivated after a few minutes of reaction time, losing almost all its activity after a few hours. On the contrary, the MOF showed a steady catalytic activity with no signs of deactivation during the first 3.4 h of reaction time, achieving a total conversion nearly four times that of the homogeneous complex. Deactivation of the homogeneous (salenMn) complex was attributed to the oxidation of the salen ligands mediated by reactive encounters with other catalyst molecules. Immobilization of the salen complex in the MOF structure prevents these reactive encounters and thus deactivation, resulting in an increase of the catalyst lifetime. The enantioselectivity of the reaction was essentially the same for the two catalysts: 88% and 82% enantiomeric excess (ee) for the homogeneous (salenMn) and the MOF, respectively. The slightly lower enantioselectivity observed for the MOF was proposed to arise from the electronic effect of binding the pyridyl groups to zinc cations, owing to the known negative influence of electron-withdrawing substituents on enantioselectivity of salen complexes.

According to the thermogravimetric analysis of the MOF after being used in catalysis and reimmersed in dmf, the authors concluded that the solid remained porous, although no gas adsorption isotherms were presented to corroborate this assumption and to evaluate the changes in porosity with respect to the pristine sample. The XRD of the MOF after

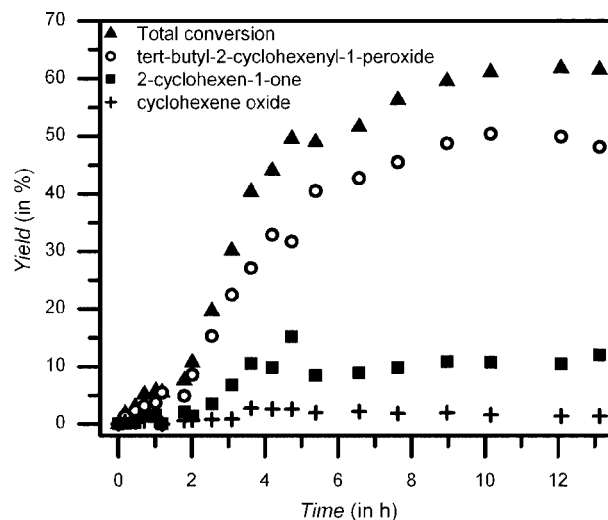
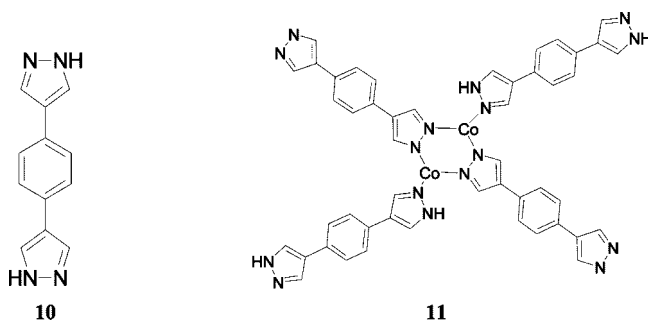


Figure 7. Time–conversion plots of cyclohexene oxidation with $t\text{-BuOOH}$ using $[Co^{II}(\text{BPB})]$ as catalyst. Reproduced with permission from reference 135. Copyright 2008 Wiley-VCH Verlag GmbH & Co. KGaA.

catalysis was not shown either, so no information was given on the structural integrity of the MOF under reaction conditions. Nevertheless, the material was reused three times without loss of enantioselectivity and only a small loss of activity. According to elemental analysis, a loss of about 4–7% of Mn occurred after each catalytic cycle.¹³²

Volkmer and co-workers have prepared a MOF containing Co^{2+} redox active centers and 1,4-bis(4'-pyrazolyl) benzene ligands (bpb) (**10**).¹³⁵ The structure of this MOF consisted of infinite chains of tetrahedral Co^{2+} ions running along the *b* direction and connected through bpb ligands pointing toward the other two directions of the crystal. Two Co^{2+} ions are bridged by two adjacent bpb ligands through the N atoms of the pyrazole ring forming Co_2N_4 rings (**11**). The authors studied the oxidation of cyclohexene as a test reaction using $t\text{-BuOOH}$ as oxidant to demonstrate the catalytic activity of the $[Co^{II}(\text{bpb})]$ compound (reaction in CH_2Cl_2 , 353 K, with $t\text{-BuOOH}/\text{cyclohexene}/Co$ molar ratio of 214:71:1). The results obtained (Figure 7) demonstrated that this Co–MOF was active. A maximum cyclohexene conversion of 62% was achieved after 12 h, yielding *tert*-butyl-2-cyclohexenyl-1-peroxide as the main product (ca. 50% yield) and 2-cyclohexen-1-one (ca. 10% yield) and cyclohexene oxide (<5% yield) as minor products. However, the crystalline structure and porosity of the material suffered important changes after the catalytic reaction, reflecting the instability of the material under the reaction conditions. Additionally, a clear induction period was present in the time–conversion plot, indicating the existence of an activation step before cyclohexene conversion started.



Balkus Jr. and co-workers have used 3-dimensional $[\text{Cu}(\text{OOC}-\text{C}_6\text{H}_4-\text{C}_6\text{H}_4-\text{COO})_{0.5}\text{C}_6\text{H}_{12}\text{N}_2]_n$ MOF to immobilize a microperoxidase that is able to act as a heterogeneous biocatalyst and effect the oxidation of *a*-methylstyrene as well as methylene blue.¹³⁶

2.2.3.3. Alcohols to Aldehydes and Ketones. Selective oxidations of alcohols to the corresponding aldehydes or ketones using MOFs as heterogeneous catalysts have been performed with either air⁶¹ or hydrogen peroxide¹³⁷ as the oxidant. Kato et al.¹³⁷ described the preparation of a MOF containing paddlewheel carboxylate Cu_2 dimers bridged by *trans*-1,4-cyclohexanedicarboxylate linkers, $[\text{Cu}_2(1,4\text{-chdc})_2]$. The structure consisted of stacked 2D layers, in which a carboxylate oxygen atom belonging to one layer was coordinate to the vacant site of a copper of an adjacent layer, thus forming a 3D structure (see Figure 8). The authors used this material as a heterogeneous catalyst for the oxidation of various alcohols (2-propanol, cyclohexanol, benzylalcohol, 1-octanol, and 2-octanol) with H_2O_2 as the oxidant. They found moderate activities at 293 K (TOFs between 1.1×10^{-4} and $5.8 \times 10^{-3} \text{ s}^{-1}$) and good selectivities (>99%) to the corresponding aldehyde or ketone. According to FTIR, UV-vis, XRD, and BET measurements of the recovered solid catalyst, the structure of the MOF was maintained during the catalytic reaction. This is in contrast with other copper carboxylate MOFs (i.e., copper terephthalate and copper fumarate),¹³⁸ which decompose in the presence of H_2O_2 . The occurrence of leaching of copper species into solution was ruled out, thus indicating that the solid behaves as a heterogeneous catalyst. Interestingly, the authors were able to isolate and characterize a green-colored solid intermediate, which was identified as the corresponding copper peroxo material $\text{H}_2[\text{Cu}_2(1,4\text{-chdc})_2(\text{O}_2)]$. In this material, peroxide O_2^{2-} anions intercalate between two copper ions from two adjacent layers, thus forming μ -1,2-*trans*-Cu-O-O-Cu moieties. This results in a negatively

charged framework, with the two H^+ coming from H_2O_2 acting as charge-balancing cations. This copper peroxide intermediate was found to be catalytically active, since the authors demonstrate that addition of the solid to 2-propanol in the absence of H_2O_2 resulted in the formation of acetone.¹³⁷

As we have already mentioned in section 2.2.2, the $[\text{Pd}(2\text{-pymo})_2]$ compound was found to be an active heterogeneous catalyst for a number of palladium catalyzed reactions and, among them, for partial oxidation of alcohols to the corresponding carbonyl compound.⁶¹ We demonstrated this activity of the Pd-MOF for the case of 3-phenyl-2-propen-1-ol (cinnamyl alcohol). Cinnamyl alcohol is a suitable substrate to probe the activity and chemoselectivity of a catalyst for the aerobic alcohol oxidation,^{139,140} since allylic alcohols can also yield side products of polymerization and C=C bond isomerization, which decrease the overall selectivity to the carbonyl compound. When the Pd-MOF was used as catalyst (1.75 mol % Pd, $T = 363 \text{ K}$, atmospheric air as the oxidant), total conversion of cinnamyl alcohol was obtained after 20 h, with a selectivity of 74% to cinnamylaldehyde, while the crystalline structure of the MOF remained intact under the reaction conditions. The obtained selectivity to the aldehyde is similar to that found for palladium-catalyzed oxidations of allylic alcohols.¹³⁹

2.2.3.4. Thiols to Disulfides. Hill et al. reported the synthesis of a MOF compound with catalytic activity for the air-based oxidation of thiol, *n*-PrSH, to the corresponding disulfide, Pr-S-S-Pr.¹⁴¹ The material contained hexavanadate units terminated in two benzoic functions, which reacted with 4,4'-bpy and $\text{Co}(\text{NO}_3)_2 \cdot 6\text{H}_2\text{O}$ to form a ladder-type structure. The material was found to be slightly active for the oxidation of thiols, affording an 8% conversion of *n*-PrSH to PrSSPr at 318 K after 7 days of reaction time (TON = 3), while no reaction was observed in the absence of the solid compound.

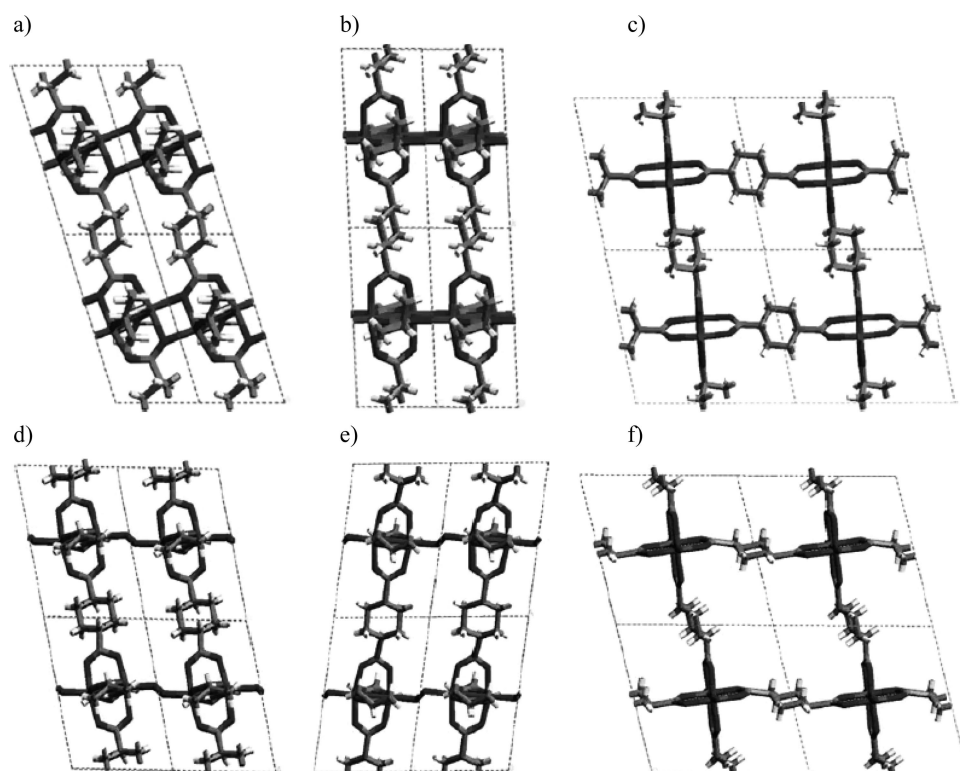


Figure 8. (Top) Structure of $[\text{Cu}_2(1,4\text{-chdc})_2]$ viewed along the (a) *a*, (b) *b*, and (c) *c* axes; (Bottom) structure of $\text{H}_2[\text{Cu}_2(1,4\text{-chdc})_2(\text{O}_2)]$ viewed along the (d) *a*, (e) *b*, and (f) *c* axes. Reproduced with permission from ref 137. Copyright 2005 Elsevier.

Following a similar approach, the same group reported one year later on a MOF compound containing the same hexavanadate units, linked by dodecahedrally Tb(III) ions and 4,4'-bis(pyridine-*N*-oxide) pillars.¹⁴² In this case, the authors observed *n*-Pr-SH oxidation to PrSSPr using the MOF as catalyst and air as the oxidant: a 41% yield of the disulfide was obtained after 30 days at 318 K in chlorobenzene, corresponding to a TON of 18.5. Control reactions with no catalyst, TbCl₃, or a strong acid (*p*-TsOH) gave no thiol conversion under the same conditions, while an equivalent molar quantity of the soluble hexavanadate ligand afforded only one-half of the conversion observed for the solid MOF. The solid could be reused after the catalytic reaction without loss of activity, while the supernatant showed no catalytic activity. When the reaction was conducted in N₂ instead of air, reduction of the hexavanadate units was observed (as deduced from a color change from orange to green), accompanied by the loss of the catalytic activity. Reexposure to oxygen reoxidized the V₆ units.

2.2.3.5. Sulfides to Sulfoxides. Gomez-Lor et al. have described the preparation of the [In₂(OH)₃(bdc)_{1.5}] material shown in Figure 3.¹⁰⁷ As we have already described in section 2.2.2, this material was found to be active for hydrogenation of nitroaromatic compounds. We will now comment on the results obtained using this In-containing MOF for the oxidation of sulfides using H₂O₂ as the oxidant. The authors studied the oxidation of two different substrates for this reaction: methylphenylsulfide and (2-ethylbutyl)phenylsulfide. When the reaction was performed at room temperature in the presence of 5% catalyst, total conversion was observed after 3 and 6 h reaction time, for the two substrates, respectively. In both cases, a high selectivity was observed to the corresponding sulfoxide (73 and 95%) with similar values of TOF (273 and 253 min⁻¹, respectively). When the oxidation reaction was performed at higher temperature, the selectivity to the sulfoxides decreased drastically. The results indicated that sulfoxide was the primary unstable product, while the corresponding sulfone was the stable product. The catalyst can be recovered after the catalytic cycle by filtration and reused without appreciable loss of activity or selectivity. No traces of In were detected in the supernatant. When longer reaction times or a large excess of the oxidant was used, the corresponding sulfone was obtained instead of the sulfoxide. The authors proposed a mechanism of reaction involving In species with coordinative unsaturation, formed by either ligand dissociation or an increase of the coordination number of indium, as being responsible for the observed catalytic reaction.¹⁰⁷

The same research group reported years later the synthesis of a family of rare-earth polymeric framework compounds RPF-4, formed by 9-coordinated Ln(III) ions (Ln = Y, La, Ce, Pr, Nd, Sm, Eu, Gd, Tb, Dy, Ho, Er, Yb) linked by 4,4'-(hexafluoroisopropylidene)bis(benzoic acid) (H₂hfipbb, **12**).¹⁴³ Ln(III) ions formed chains along the *a* axis, which were linked in the other two directions by the ligands defining two square-shaped (A and B) channel families and one hexagonal (C) channel family parallel to the *a* axis (see Figure 9). The capability of the lanthanide RPF-4 materials as redox catalysts was demonstrated by the oxidation of PhSMe using H₂O₂ as oxidant. The results obtained (Table 4) revealed a dependence of both activity and selectivity on the metal ion incorporated, which in general followed opposite trends: upon increasing the atom number (from La to Yb), conversion and TOF increased while selectivity to

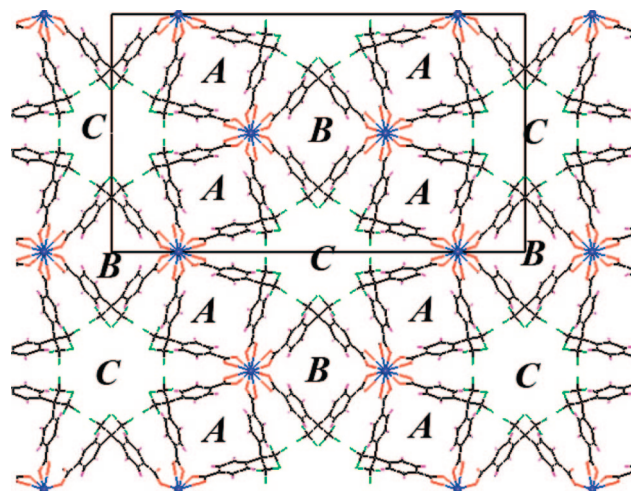
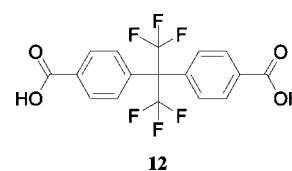


Figure 9. RPF-4 framework viewed along the (100) direction, showing three different types of straight channels, A, B, and C. Reproduced with permission from ref 143. Copyright 2008 American Chemical Society.

Table 4. Oxidation of PhSMe over RPF-4 Materials; Data Taken from Ref 143

rare earth	time (min)	conv. (%)	sel. sulfoxide (%)	TOF (h ⁻¹)
Yb	180	92	30	60
Er	300	85	52	32
Gd	300	82	60	48
Sm	300	78	72	22
Nd	300	80	70	20
La	300	80	75	18

the sulfoxide decreased. Thus, a maximum conversion of PhSMe of 92% was obtained after 3 h (TOF = 60 h⁻¹) for the RPF-4(Yb) compound, yielding the corresponding sulfoxide in 30% selectivity, while the maximum conversion obtained for RPF-4(La) was 80% after 5 h (TOF = 18 h⁻¹) with a 75% selectivity to the sulfoxide.¹⁴³ In all the cases, an induction period was observed, which was attributed to the time needed for the formation of the hydroperoxo Ln-OOH reactive intermediate, as suggested by the appearance of new absorption bands in the IR spectrum of the used materials at 1090 and 1448 cm⁻¹ (not present in the fresh solids).¹⁴³



Reaction of ytterbium nitrate with succinic acid yielded a crystalline MOF with formula [Yb(C₄H₄O₄)_{1.5}] that can exist in two different polymorphic phases, which can be reversibly transformed one into the other by temperature changes.¹⁴⁴ In the room-temperature phase, α , each Yb(III) ion is surrounded by 8 carboxylate oxygen atoms, and these YbO₈ are linked by sharing edges to form zigzag chains along the *a* axis. The chains are linked in the *b* and *c* directions through succinate anions to give a 3D structure. Upon increasing the temperature above 403 K, a reversible single crystal-to-single crystal phase transformation to the polymorph β occurs. In polymorph β , each Yb(III) is surrounded by 7 oxygen atoms forming edge-sharing dimers linked in the three directions by succinate anions.¹⁴⁴ Both polymorphs α and β have been

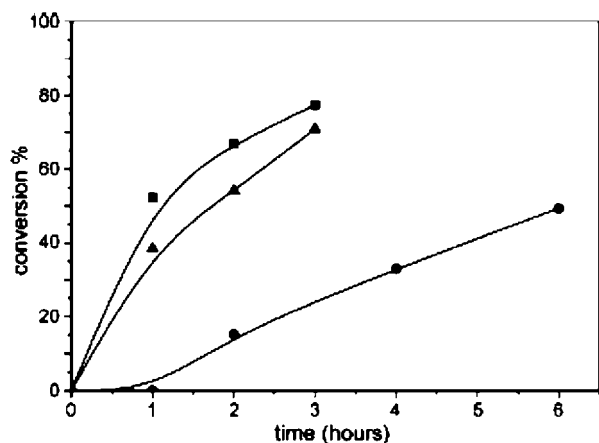
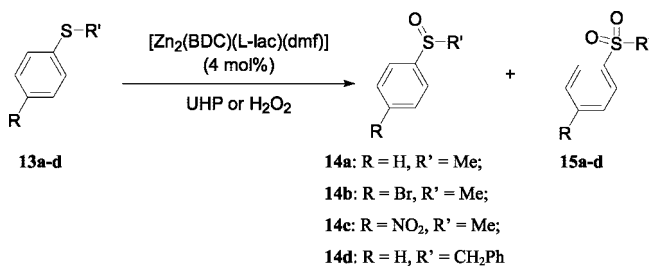


Figure 10. Time–conversion plots of PhSMe oxidation over polymorph α corresponding to first (●), second (▲), and third (■) consecutive catalytic runs. Reproduced with permission from ref 144. Copyright 2009 Wiley-VCH Verlag GmbH & Co. KGaA.

tested as heterogeneous catalysts for a number of different reactions. Reactions that need a low temperature (i.e., below the phase-transition temperature) were only performed with polymorph α . Thus, polymorph α has been employed as Lewis acid catalyst for acetalization of aldehydes (see section 2.2.8) and as redox catalyst for the oxidation of sulfides. Additionally, the authors used a further reaction, i.e., thiophene hydrodesulfurization (HDS), to compare the catalytic activity of the two polymorphs, since this reaction can be performed at temperatures at which both polymorphs can exist (see Section 2.2.7). PhSMe oxidation over the α polymorph using 1.5 equiv of H_2O_2 as the oxidant was performed at 333 K. Under these conditions, a maximum PhSMe conversion of 50% was achieved after 6 h (TOF = 457 min^{-1}), with the sulfoxide being the only product detected (92% selectivity).¹⁴⁴ However, an induction period of about 1 h was observed (see Figure 10), which was absent in successive catalytic runs. Moreover, the activity of the catalyst was found to increase sharply from the first to the second run, and again increased in the third run. X-ray analysis of the samples before and after the catalytic reaction showed that the catalyst structure resisted, although inspection of the IR spectra revealed the appearance of several new absorption bands. These bands were attributed to the formation of Yb–OOH species, which were formed during the reaction upon contacting the MOF with H_2O_2 . According to the authors, these hydroperoxo species would be the actual active intermediates for the catalytic reaction, and this would explain the disappearance of the induction period after the first catalytic run and also the increased activity of the MOF after consecutive cycles.

Dybtsev et al. have studied the catalytic activity of a zinc-containing homochiral metal organic framework for the oxidation of sulfides, using either H_2O_2 or urea hydroperoxide (UHP) as the oxidant.¹⁰⁶ The MOF compound featured 1D chiral chains along the a axis, formed by Zn^{2+} ions and lactate ligands, which were further linked by bdc ligands in the other two dimensions. The 3D framework structure presented pores of about 5 Å in diameter interconnected in three dimensions, with a homochiral environment provided by the chiral lactate ligands.¹⁰⁶ The framework presented two crystallographic independent Zn^{2+} sites, one of them coordinated to a dmf molecule. Coordinated dmf molecules and guest dmf molecules present in the pores can be partially removed (263 K under a vacuum for 3 h) without loss of

Scheme 11



crystallinity. However, complete evacuation cannot be achieved, since treatment under vacuum for longer periods caused a loss of the crystallinity. The partially evacuated material showed a specific surface area (Langmuir) of $190 \text{ m}^2 \text{ g}^{-1}$, which is rather low compared to the typical values encountered for a MOF. Nevertheless, the material showed enantioselective adsorption properties of substituted thioether oxides. When a racemic mixture of sulfoxides with small substituents, such as H/Me (**14a**) and Me/Br (**14b**), was contacted with the homochiral MOF, the adsorbed product showed enantiomeric excess of 20 and 27%, respectively, with the *S*-enantiomer being in excess in both cases (for the MOF containing *L*-lactate ligands). However, sulfoxides with larger substituents (**14c** and **14d**) were not adsorbed in the pores. This MOF was further studied as catalyst for the catalytic oxidation of thioethers (**13**) to the corresponding sulfoxides (**14**) using urea hydroperoxide (UHP) or H_2O_2 as the oxidant (see Scheme 11). In agreement with the adsorption behavior discussed above, sulfides containing small substituents were converted with reasonable conversions (64 and 58% for **14a** and **14b**) and high selectivity (92% and 83%, respectively) to the sulfoxide. On the contrary, thioethers with larger substituents (**14c** and **14d**) were hardly converted. When H_2O_2 was used instead of UHP and after adjusting solvent composition, both conversion and selectivity for the smaller substrates were quantitative. The size selectivity of this MOF indicated that the reaction occurred inside the pores.¹⁰⁶ Filtration tests were also performed to demonstrate the heterogeneous nature of the catalytic process. The authors did not observe loss of activity after 30 catalytic cycles. However, in spite of the good conversions and selectivities achieved with this catalyst, no enantioselectivity was observed, and the reasons for this remained unexplained.

One year later, the same group used the homochiral $[\text{Zn}_2(\text{bdc})(\text{L-lact})(\text{dmf})]$ solid (*L*-Lact = *L*-lactic acid) as stationary phase to prepare a chiral chromatographic column for the separation of racemic mixtures of chiral alkyl aryl sulfoxides.¹⁴⁵ In this study, the authors combined the known catalytic activity of this MOF for the selective oxidation of sulfides to sulfoxides, with its enantioselective adsorption properties of sulfoxides, to develop a one-pot process for the synthesis of enantiomerically enriched sulfoxides starting from the corresponding sulfides. Thus, a mixture containing PhSMe and H_2O_2 was fed to a chromatographic column containing the Zn–MOF, and the products were eluted with a $\text{CH}_2\text{Cl}_2/\text{CH}_3\text{CN}$ mixture. The chromatograms obtained are shown in Figure 11. The results obtained depended on the $\text{H}_2\text{O}_2/\text{PhSMe}$ ratio used. When a 5-fold oxidant excess was used, overoxidation took place (ca. 5% sulfone was detected, chromatogram a). If the amount of H_2O_2 was decreased to a 1.5-fold excess, a fraction of unreacted PhSMe remained (total conversion 91%). Nevertheless, and despite some peak overlap, the method was appropriate to obtain both (*R*-) and (*S*-) sulfoxide enantiomers separately, with a net isolated yield

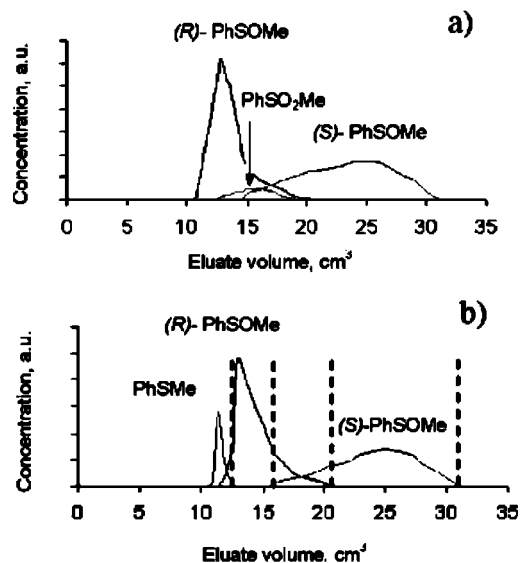


Figure 11. Chromatograms obtained for the combined catalytic oxidation of PhSMe and racemic resolution of the products over the homochiral $[\text{Zn}_2(\text{bdc})(\text{L-lact})(\text{dmf})]$ MOF. The $\text{H}_2\text{O}_2/\text{PhSMe}$ ratio used was 5:1 (a) or 1.5:1 (b). The column consisted of a glass tube (8 mm i.d.) charged with 14 g of the MOF to obtain a 33 cm high column. Elution rate was $2 \text{ cm}^3 \text{ h}^{-1}$. Reproduced with permission from ref 145. Copyright 2007 American Chemical Society.

of the optically pure enantiomers of about 70% (35% each enantiomer).¹⁴⁵

Very recently, Hwang et al. demonstrated that the coordinative unsaturated Cr(III) sites of MIL-101 can catalyze the selective oxidation of aryl sulfides to aryl sulfoxides using H_2O_2 as the oxidant.¹³¹ The activity of the catalyst depended upon the concentration of coordinative unsaturated Cr(III) sites (as determined from FTIR spectroscopy of adsorbed CO) in MIL-101 samples prepared with different activation procedures. As substrates for the oxidation reaction, phenylmethylsulfide and other compounds having different ring substituents in *para*-position were chosen (CH_3 , Cl, CN, NO_2). A direct correlation was found between the measured activity and the nature of the group in *para*-position, in the sense that electron-donating groups enhanced the oxidation reactivity (the determined Hammett parameter was $\rho = -1.8$). The authors did not find appreciable deactivation of the catalyst after five catalytic runs.

2.2.4. CO Oxidation to CO_2

Selective catalytic oxidation of CO to CO_2 is a very interesting reaction for its implications in the production of clean hydrogen for the chemical industry from hydrocarbon feeds.¹⁴⁶ At the industrial scale, production of H_2 occurs in three steps: (i) steam reforming: $\text{fuel} + \text{H}_2\text{O} \rightarrow \text{H}_2 + \text{CO}$; (ii) water-gas shift reaction to eliminate CO and produce more hydrogen: $\text{CO} + \text{H}_2\text{O} \rightarrow \text{CO}_2 + \text{H}_2$; and (iii) any remaining CO is reduced to ppm levels by selective catalytic oxidation. A particularly interesting field of application of the CO oxidation reaction is in the production of H_2 (essentially free of CO) for fuel cells. Proton exchange membrane (PEM) fuel cells need to operate with clean H_2 to avoid deactivation of the Pt anode electrode by traces of CO that could be present in the feed. Ideally, the catalyst has to be capable of selectively converting CO into CO_2 in the presence of a large excess of H_2 , CO_2 , and H_2O . After the water-gas shift reaction, the CO content in the steam is

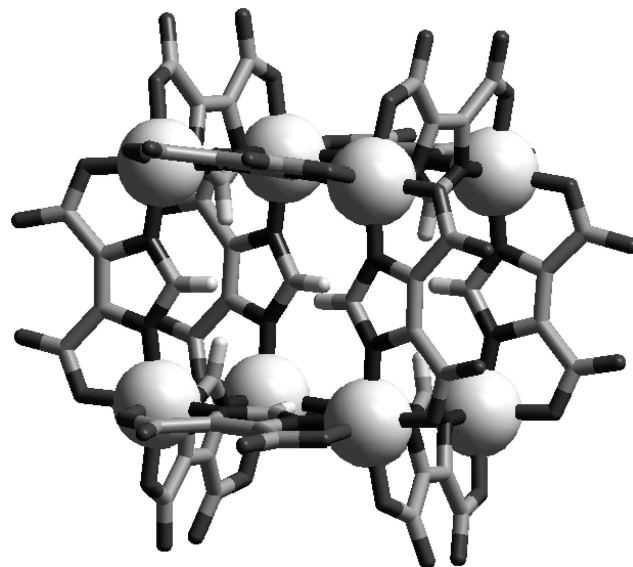


Figure 12. $[\text{Ni}_8(4,5\text{-icd})_{12}]$ cubic structural units present in both Li^+ - and Na^+ -containing MOFs described in ref 147.

typically of about 1%, and it needs to be reduced to less than 5 ppm without oxidizing any of the 30–70% H_2 present. Selective catalytic oxidation of CO for fuel cells is performed at 70–80 °C under ambient pressure. The crystalline structure of a MOF could reasonably withstand these relatively mild operation conditions, so that development of selective CO oxidation catalysts for fuel cells could be a possible future application of MOFs.

Zou et al. have reported on the preparation of two different MOFs built up by nickel and 4,5-imidazoledicarboxylate (4,5-icd) and an additional alkali metal cation consisting of either Na^+ , $[\text{Na}_{20}(\text{Ni}_8(4,5\text{-icd})_{12})(\text{H}_2\text{O})_{28})(\text{H}_2\text{O})_{13}(\text{CH}_3\text{OH})_2$, or Li^+ , $[\text{Li}_{11}(\text{Ni}_8(4,5\text{-icd})_{12})(\text{H}_2\text{O})_{12}]\text{Li}_9(\text{H}_2\text{O})_{20}$.¹⁴⁷ Both MOFs featured discrete $[\text{Ni}_8(4,5\text{-icd})_{12}]^{20-}$ cubic building blocks, with nickel at the vertices and the ligand molecules at the edges (see Figure 12). In these cubic building blocks, nickel atoms are coordinated to three N and three O atoms, NiN_3O_3 , from three different imidazolate ligands, in a slightly distorted octahedral coordination geometry. The oxygen atoms of the ligand not coordinated to nickel are linked to alkali metal cations, in a different manner for Li^+ and Na^+ cations. With both cations, the arrangement of the cubic units leads to a 3D network defining open channels, with BET surface areas of 145 and $186 \text{ m}^2 \text{ g}^{-1}$ and pore volumes of 0.28 and $0.33 \text{ cm}^3 \text{ g}^{-1}$ for the Li^+ - and Na^+ -containing MOFs, respectively. When Na^+ was used, the resulting material was found to be thermally stable up to 653 K, while the material containing Li^+ was less stable, owing to the weaker coordinative interactions of $\text{Li}-\text{O}$ bonds compared to $\text{Na}-\text{O}$ bonds. The sodium containing material was found to be catalytically active for oxidation of CO to CO_2 , at temperatures between 475 and 578 K. This catalytic activity was ascribed to the nickel clusters present in the structure. The observed reaction rate at 473 K for the Na^+ -MOF was between that of a Ni-exchanged Y zeolite and NiO, and the activation energy for the MOF (64.9 kJ mol^{-1}) was also between that of Ni–Y ($108.8 \text{ kJ mol}^{-1}$) and NiO (39.8 kJ mol^{-1}). Interestingly, the stability of the MOF with time on stream was considerably higher than that of Ni–Y and NiO. The MOF showed stable activity for the initial 20 min of reaction time at a $T \geq 475 \text{ K}$. XRD indicated that the framework of the MOF remained intact after the catalytic reaction and that no crystalline NiO was present. On the contrary, the authors did not observe

catalytic activity for the MOF containing Li^+ cations, and they attributed the lack of activity to the lower thermal stability of the material.

One year later, the same authors described the preparation of a new copper MOF using 5-methylisophthalate ligands, $[\text{Cu}(5\text{-mip})_2(\text{H}_2\text{O})_2](\text{H}_2\text{O})_2$.¹⁴⁸ The material features the well-known paddlewheel carboxylate bridged Cu_2 dimers, with each copper ion being coordinated to an apical water molecule. The structure defines two types of square 2D grids: type I grids exhibit open windows of $8.33 \times 8.33 \text{ \AA}^2$ (all four isophthalic rings in *cis* mode) and type II grids (alternate *cis-trans* mode of the aromatic rings), which are self-closed to form cavities with a diameter of 9.4 \AA . Two adjacent 2D grids are eclipsed to form a microporous material with two types of open channels. Both uncoordinated and coordinated water molecules can be thermally eliminated to obtain the corresponding dehydrated material, while the original framework remains intact as determined by XRD. Dehydration is accompanied by a color change, from blue to black-violet. Dehydration of the MOF is reversible, and the dehydrated material recovers its original blue color after exposure to moisture. Once the coordinated water molecules are eliminated, copper sites located at the channel walls become potential Lewis acids sites for adsorption and catalysis. The calculated free crystalline volume amounted to ca. 29%. The accessibility of the copper sites after water elimination was demonstrated by FTIR spectroscopy using CO as a probe molecule at room temperature. A $\nu(\text{C}-\text{O})$ stretching band was observed at 2113 cm^{-1} after ^{12}C adsorption, which was assigned to CO adsorbed onto Cu Lewis acid sites. This band shifted to 2064 cm^{-1} when ^{13}C was used.

The authors demonstrated that the copper MOF was active for air oxidation of CO to CO_2 . The catalytic activity was considerably higher than for the previously reported nickel-containing MOF discussed above. Indeed, 100% conversion of CO was reached over the Cu-MOF at 473 K, while a conversion of only 3% was obtained over Ni-MOF at the same temperature (fixed-bed reaction conditions: flowing CO (1%) + O_2 (20%) + He (balance) gas mixture, $\text{SV} = 20\,000 \text{ mL h}^{-1} \text{ g}(\text{cat})^{-1}$). The activity of the Cu-MOF was found to be similar or higher than that reported for CuO and CuO/ Al_2O_3 , with an activation energy (70.1 kJ mol^{-1}) close to that of CuO (69.9 kJ mol^{-1}). Furthermore, the activity of the copper MOF was stable with time at temperatures of 378 K or higher, and the material retained the framework integrity after the catalytic use, as determined by XRD.

2.2.5. Photocatalysis by MOFs

Yu et al.¹⁴⁹ reported on the synthesis, structure, and photocatalytic properties of a 3D bimetallic coordination polymer containing uranium and nickel, with the formula $[\text{Ni}_2(\text{H}_2\text{O})_2(2,3\text{-pydca})_2(4,4'\text{-bpy})_2\text{U}_5\text{O}_{14}(\text{H}_2\text{O})_2(\text{OAc})_2] \cdot 2\text{H}_2\text{O}$ (2,3-pydca = pyridine-2,3-dicarboxylate, quinolinic acid). The material contains polyoxouranium ribbons connected with Ni-containing layers through 2,3-pydca ligands. The polyoxouranium ribbons are composed of UO_8 hexagonal bipyramid and two different UO_7 pentagonal bipyramid linked by $\mu^3\text{-O}$ bridges forming a trinuclear uranium core. Two of these U trimers are linked by $\mu^3\text{-O}$ atoms to form a pentanuclear U_5O core, which is repeated along the *b* axis. Given the reported photocatalytic activity of uranyl (UO_2^{2+}) units for the oxidative degradation of organic substrates,¹⁵⁰ the authors anticipated that the presence of the polyoxouranium ribbons could provide photocatalytic activity to their material. To demonstrate this,

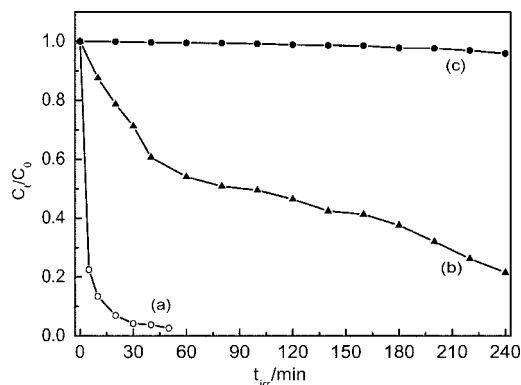


Figure 13. Plots of concentration versus irradiation time for (a) MB irradiated with UV light in the presence of $[\text{Ni}_2(\text{H}_2\text{O})_2(2,3\text{-pydca})_2(4,4'\text{-bpy})_2\text{U}_5\text{O}_{14}(\text{H}_2\text{O})_2(\text{OAc})_2] \cdot 2\text{H}_2\text{O}$, (b) MB under xenon-lamp irradiation in the presence of the same photocatalyst, and (c) MB under xenon-lamp irradiation without photocatalyst. C_t and C_0 stand for the dye concentrations after and before irradiation, and t_{irr} stands for the irradiation time. Reproduced with permission from ref 149. Copyright 2004 Royal Society of Chemistry.

the photodecomposition of methyl blue (MB) was studied under UV light irradiation and in the presence of the nickel-uranium bimetallic compound. The progress of the reaction (see Figure 13) was estimated by monitoring the absorbance characteristic of MB at $\lambda = 600 \text{ nm}$. After complete decolorization of the MB solution, the authors determined that about 45% mineralization was achieved, according to the total organic carbon analysis. The authors also reported a photocatalytic activity of the material irradiating with a xenon lamp (with the wavelength of the main output being longer than 400 nm).

Following this research line, the same group described one year later the preparation of two novel bimetallic 2D silver-uranium coordination polymers, $[\text{Ag}(2,2'\text{-bpy})(\text{UO}_2)_2(\text{bdc})_{1.5}]$ and $[\text{Ag}_2(\text{phen})_2\text{UO}_2(\text{btec})]$ (phen = 1,10-phenanthroline, btec = 1,2,4,5-benzenetetracarboxylate).¹⁵¹ Note that, according to the definition given in the Introduction section for MOFs, these two materials are not to be considered MOFs. Indeed, both solids feature laminar structures held together by weak $\pi-\pi$ interactions between the aromatic ligands: edge-to-face $\pi-\pi$ interactions between 2,2'-bpy and bdc in the former solid and face-to-face $\pi-\pi$ interactions between phen and btec in the latter. However, we still mention this work here for its implications in the understanding of the photoactivity of uranyl UO_2^{2+} species commented above. The two silver-uranyl laminar materials were found to be active photocatalysts for the degradation of rhodamine B (RhB), with higher efficiencies than that obtained with TiO_2 P-25 under the same experimental conditions (see Figure 14). The authors demonstrated that the materials retained their crystalline structures after the photocatalytic reaction, and the observed activities were not due to soluble species leached from the original solids. The material containing 2,2'-bpy ligands was also active photocatalytically under visible light irradiation with a xenon lamp. The authors proposed the following mechanism to explain the observed photoactivity of the uranium containing materials: upon light excitation, a ligand-to-metal charge transfer (LMCT) occurs in UO_2^{2+} species between the 2p bonding orbitals of oxygen (HOMO) and the empty orbitals of uranium (LUMO) to produce an excited state, $^*\text{UO}_2^{2+}$, with uranium in the +5 and oxygen in the -1 oxidation states. In the presence of RhB, $^*\text{UO}_2^{2+}$ can abstract one α -hydrogen

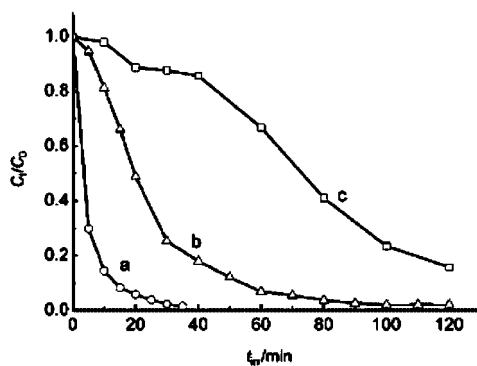
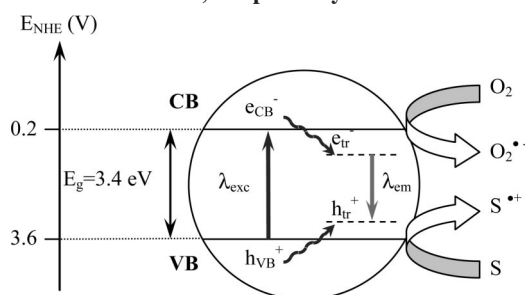


Figure 14. Concentration changes of RhB irradiated with UV light as a function of irradiation time, t_{irr} , in the presence of (a) $[\text{Ag}(2,2'\text{-bpy})(\text{UO}_2)_2(\text{bdc})_{1.5}]$, (b) $[\text{Ag}_2(\text{phen})_2\text{UO}_2(\text{BTEC})]$, and (c) Degussa P-25. C_t and C_0 stand for the RhB concentrations after and before irradiation. Reproduced with permission from 151. Copyright 2005 Wiley-VCH Verlag GmbH & Co. KGaA.

atom of the methylene group bonded to the nitrogen atom of RhB. This results in the cleavage of the C–N bond of RhB, producing the stepwise *N*-deethylation of RhB. The excited electron is captured by O_2 in solution, thus generating highly active oxygenated species that can further oxidize and produce total degradation of RhB. The mechanism was supported by the detection of intermediate species generated during the degradation of RhB from positive-ion ($\text{M} + \text{H}$) spectra. The dye was found to be degraded from m/z 443.2 (RhB) to m/z 415.2 (*N,N',N'*-triethylrhodamine), 387.1 (*N,N'*-diethylrhodamine), 359.0 (*N*-ethylrhodamine), corresponding to the stepwise loss of C_2H_5 units. Also, the presence of O_2 during the photocatalytic reaction was found to be essential to reoxidize the formed uranium(V) species back to uranium(VI) to close the cycle. When argon was bubbled through the system for 30 min before and during irradiation, the photocatalytic reaction rate decreased for the material with 2,2'-bpy ligand and dropped to zero for the material containing phenanthroline ligands. The former material was so active that trace amounts of O_2 in the reaction medium are enough to produce the efficient degradation of RhB.

Mahata et al.¹⁵² described the preparation of three novel photocatalysts for the decomposition of organic dyes based on metal organic framework compounds. The materials were obtained with 4,4'-oxybis(benzoate) (oba) and 4,4'-bpy as the organic linkers and contained either Co, Ni, or Zn as the metal components: $[\text{Co}_2(4,4'\text{-bpy})(\text{oba})_2]$, $[\text{Ni}_2(4,4'\text{-bpy})_2(\text{oba})_2] \cdot \text{H}_2\text{O}$, and $[\text{Zn}_2(4,4'\text{-bpy})(\text{oba})_2]$, respectively. DRUV–vis spectra of the three compounds showed absorption bands assigned to the corresponding LMCT bands from the oba ligand to the central metal ion. Additionally, the MOFs containing Co^{2+} (d^7) and Ni^{2+} (d^8) also showed the $d-d$ transition, as expected for the geometry of the metal sites, which were absent in the spectrum of the MOF containing Zn^{2+} (d^{10}). From the absorption edge of the corresponding LMCT bands (311, 294, and 290 nm), values for the band gap of the three materials were determined to be 3.11, 3.89, and 4.02 eV, for the Co-, Ni-, and Zn-containing MOFs, respectively.¹⁵² In order to demonstrate the photocatalytic activity of the three compounds, the authors studied the photodegradation of four dyes in water: Orange G (OG), RhB, remazol brilliant blue R (RBBR), and MB. The course of the degradation was followed by monitoring the characteristic absorbances of the dyes (at $\lambda = 482, 554, 590,$ and 661 nm for OG, RhB, RBBR, and MB, respectively). All three materials were found to be active

Scheme 12. Energetic Diagram of MOF-5 and Processes Occurring upon Band Gap Irradiation: CB, Conduction Band; VB, Valence Band; Subindex tr Indicates Electrons or Holes Trapped in Defect States; λ_{exc} and λ_{em} Refer to Excitation and Emission, Respectively



in the photodegradation of all the tested dyes. For all the dyes, the efficiency of degradation followed the order $\text{Co} > \text{Ni} > \text{Zn}$, which is, as expected, the reverse order observed for the corresponding band gaps. The authors assumed that the photodegradation of the dyes occurred through a mechanism analogous to that suggested by Yu et al. for materials containing UO_2^{2+} species that we have commented on previously.¹⁵¹ In the present case, the active centers would be the central M^{2+} ions, which would be excited upon irradiation at the LMCT band.

We have recently shown^{101,153} that the $[\text{Zn}_4\text{O}_{13}]$ units found in MOF-5¹² behave as a wide band gap semiconductor, as deduced from fluorescence and laser flash photolysis studies and by comparison with the photochemistry of aqueous zinc terephthalate solutions. This study has been lately confirmed and completed by Tachikawa et al.¹⁰⁰ According to these studies, band gap irradiation ($E_g = 3.4$ eV, $\lambda_{\text{exc}} = 350$ nm) produces a charge separation state, with electrons and holes in the conduction and valence bands (e_{CB}^- and h_{VB}^+). The charge separation state was proposed^{153,154} to occur via electron injection from the organic linker (terephthalate anions) to the $[\text{Zn}_4\text{O}_{13}]$ clusters of MOF-5, i.e., a so-called ligand-to-cluster charge transfer (LCCT). Once formed, the photogenerated charge carriers can be trapped into singlet defect states (e_{tr}^- and h_{tr}^+) that, upon recombination, give rise to a fluorescence emission ($\lambda_{\text{em}} = 540$ nm, $\tau_0 \approx 600$ ns).¹⁵³ The whole process is shown in Scheme 12. The photogenerated charge carriers are accessible to interact with appropriate substrates, as we have previously demonstrated: electron acceptors (such as methyl viologen dichloride) can interact with the photogenerated electrons, and electron donors (such as *N,N,N',N'*-tetramethyl-*p*-phenylenediamine) can trap the photogenerated holes. Thus, MOF-5 revealed a semiconductor behavior that opened the possibility of using the material as a photocatalyst. To explore this possibility, the photodegradation of phenol in aqueous solution was studied using hydrated MOF-5 as photocatalyst.^{62,153} The photocatalytic activity of hydrated MOF-5 was compared with that of ZnO and TiO_2 P-25 under the same reaction conditions. According to the photodegradation curves of phenol shown in Figure 15, hydrated MOF-5 showed a remarkable photocatalytic activity, which is comparable to that measured for ZnO and TiO_2 . This comparison can be made either per mass unit (plot a) or per metal of active atom (plot b). Moreover, the presence of a regular pore system in hydrated MOF-5, with an internal surface area determined by cavities with well-defined dimensions, opens up the possibility of performing shape-selective photocatalysis. This was demonstrated by studying the competitive

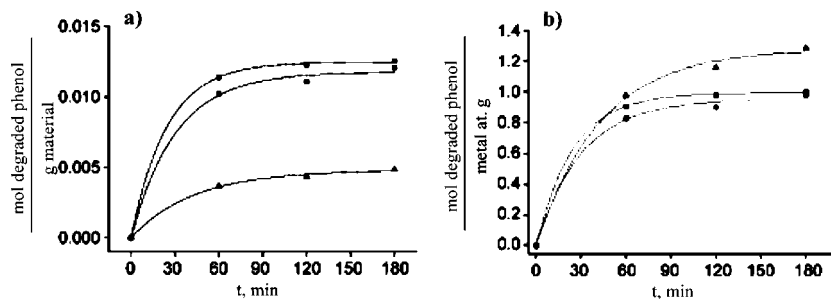


Figure 15. Time–conversion plots of phenol disappearance (a) per mass unit and (b) per metal atom in the presence of MOF-5 (▲), TiO₂ (■), and ZnO (●). Reproduced with permission from ref 153. Copyright 2007 Wiley-VCH Verlag GmbH & Co. KGaA.

Table 5. Photodegradation Rates (k , ppm·min⁻¹) for Phenol (P) and 2,6-Di-*tert*-butylphenol (DTBP), Irradiated Separately or in a Mixture And Using MOF-5 as a Photocatalyst; Data Taken from Ref 62

	separate irradiation		mixture
$k(\text{P})_{\text{pure}}$	0.352	$k(\text{P})_{\text{mix}}$	0.067
$k(\text{DTBP})_{\text{pure}}$	0.387	$k(\text{DTBP})_{\text{mix}}$	0.296
$k(\text{DTBP})_{\text{pure}}/k(\text{P})_{\text{pure}}$	1.10	$k(\text{DTBP})_{\text{mix}}/k(\text{P})_{\text{mix}}$	4.42

photodegradation of phenol (P) and 2,6-di-*tert*-butyl phenol (DTBP), a considerably bulkier molecule. The results obtained are reported in Table 5. When aqueous solutions containing either P or DTBP were separately irradiated in the presence of MOF-5 derived photocatalyst, very similar initial rates (as determined from the slope of the time–conversion plots at short irradiation time) were obtained in both cases, thus giving a rate constant ratio close to one: $k(\text{DTBP})_{\text{pure}}/k(\text{P})_{\text{pure}} = 1.10$. This indicates that the intrinsic degradability of both molecules on hydrated MOF-5 is very similar. However, when a solution containing equimolar concentrations of the two molecules was contacted with MOF-5 derived photocatalyst (i.e., competitive photodegradation), the initial degradation rates were remarkably different: 0.067 and 0.296 ppm·min⁻¹ for P and DTBP, giving a rate constant ratio of $k(\text{DTBP})_{\text{mix}}/k(\text{P})_{\text{mix}} = 4.42$. This value represents a selectivity toward DTBP degradation of 82%, that cannot be accounted for by a different intrinsic reactivity. We attributed the observed differences between the two molecules to a reverse shape-selectivity effect, in line with previous studies made on the titanosilicate ETS-10.^{155,156} The explanation to this reverse shape selectivity would be that small molecules can freely diffuse to the internal space of the material, where they are less prone to undergo photodegradation. In contrast, bulky molecules remain at the external surface of the photocatalyst, where they are rapidly degraded. In other words, degradation of the organic molecules takes place at a different rate in the internal and on the external surface of the photocatalyst (being significantly lower at the internal surface).

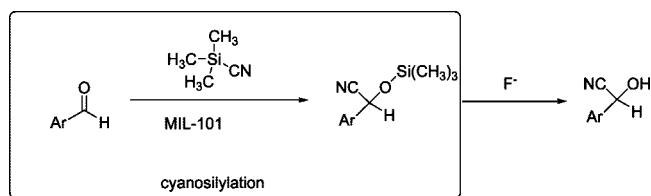
The [Zn₄O₁₃] cluster found in MOF-5 is a structural model that can be taken as a starting point to design other materials with semiconductor properties, which could have potential use in optoelectronics, photocatalysis, and in other related applications.⁶² In principle, it would be possible to control these semiconducting properties by tuning the band gap of the material by either modifying the inorganic [Zn₄O₁₃] cluster or the organic components. Fuentes-Cabrera et al.¹⁵⁷ concluded by first-principles calculations (LDA method) that a hypothetical series of IRMOFs, generated by replacing the Zn²⁺ ions by other elements in MOF-5 (i.e., Be, Mg, Ca, and Cd), would all show very similar band gaps (ca. 3.5 eV). Accordingly, modification of the band gap through

substitution of the inorganic clusters could be ruled out as a means for altering the properties of a semiconductor MOF. Conversely, Choi et al. performed density functional theory (DFT) calculation at B3-LYP level of the electronic properties of a series of materials isoreticular to MOF-5 in which some or all of the Zn²⁺ ions in the [Zn₄O₁₃] clusters were replaced by Co²⁺, yielding bimetallic clusters of composition [Zn_{4-n}Co_nO₁₃] ($n = 0, 0.25, 0.5, 1, 2, \text{ and } 4$).¹⁵⁸ The conclusions of this study were that the electronic structure of the bimetallic material could be tuned to achieve band gaps ranging from semiconductor to metallic states by only changing the concentration of the Co²⁺ ions in the [Zn_{4-n}Co_nO₁₃] clusters while keeping the same organic ligand.

The other alternative to modify the band gap energy is the substitution of the organic ligands by other lineal dicarboxylate molecules. This possibility was explored by Civalleri et al.¹⁵⁹ by ab initio periodic calculations at B3-LYP level using the CRYSTAL code. The calculated band gap for MOF-5 was 5.0 eV, which was rather high compared to the values of 3.5 and 3.53 eV found, respectively, by Fuentes-Cabrera¹⁵⁷ and by Choi.¹⁵⁸ These discrepancies were accounted for by the different calculation methods used in both works. Nevertheless, what is more interesting for the present discussion is that Civalleri et al. found out that valence bands in MOF-5 are dominated by the contribution of the p atomic orbitals of carbon atoms of the aromatic rings. Accordingly, they proposed to modulate the band gap by substituting the linker. Indeed, their preliminary calculations, replacing the terephthalate ligands in MOF-5 (IRMOF-1) by 2,6-naphthalenedicarboxylate (IRMOF-8) or by biphenyldicarboxylate (IRMOF-10) resulted in a decrease of the band gap from 5.0 to 4.0 eV. The substitution would cause a change in the LMCT transition responsible for the semiconductor behavior of the material, and this in turn would indicate that replacement of the organic linker in the isoreticular series of MOFs is an effective method for tuning the band gap of the resulting semiconductor material. As anticipated by Civalleri,¹⁶⁰ increasing the aromaticity of the organic linker could be a useful means to design a specific ligand acting as a light-harvesting antenna that would sensitize the inorganic component.

The above conclusions by Fuentes-Cabrera¹⁵⁷ and Choi¹⁵⁸ on the influence of the metal, and by Civalleri¹⁵⁹ on the influence of the organic ligand, were all extracted from ab initio theoretical calculations. Up to now, there is no experimental evidence to refute or to confirm the calculations made by Fuentes-Cabrera and by Choi, since the calculated isoreticular series of materials [M₄O(bdc)₃] (M = Zn, Be, Mg, Ca, Cd) and [Zn_{4-n}Co_nO₁₃] have not yet been synthesized. In a related precedent, Volkmer and co-workers have

Scheme 13



recently described the preparation of isoreticular MOFs containing pentanuclear $[MZn_4]$ clusters ($M = Co^{2+}$ or Zn^{2+}) and 1,2,3-benzotriazolone ligands.¹⁶¹ However, the composition and structure of the bimetallic clusters of these materials and those studied by Choi are too different to allow comparing the dependence of band gap on composition among the two isoreticular series. On the contrary, it has been possible to prepare the isoreticular series of MOFs containing $[Zn_4O_{13}]$ clusters and different linear dicarboxylates calculated by Civalleri, i.e., the well-known IRMOF-n series reported by Eddaoudi et al.⁸⁸ Therefore, in this case, it is possible to compare the predictions on band gap energies with experimental data. This has been recently done by Gascon et al.,¹⁶² who found a direct correlation between the band gap of the materials and the resonance effects of the organic linkers due to the different substituents. They reported (optical) band gaps of 4.0, 3.8, and 3.3 eV for MOF-5, IRMOF-10, and IRMOF-8, respectively, thus following the trend anticipated by Civalleri. The authors have also prepared IRMOF-7, a material containing 1,4-naphthalenedicarboxylate as organic linker that was not calculated by Civalleri et al., and found the same band gap (3.3 eV) for IRMOF-7 and for IRMOF-8, thus suggesting that the band gap depends on the substituent (naphthalene ring in both materials) rather than on the substitution pattern or on the distances between $[Zn_4O_{13}]$ clusters.¹⁶² Gascon et al. have also studied the gas-phase photooxidation of propylene over different IRMOFs,¹⁶² following the reaction by operando diffuse reflectance IR spectroscopy (DRIFTS). MOF-5 was found to be inactive under the selected conditions, while the other IRMOF-n materials tested, with smaller band gaps, proved to be active photocatalysts. On the basis of the intensity of the IR absorption bands of the products, IRMOF-8 (i.e., with 2,6-naphthalenedicarboxylate) was found to be the most active material, more active than IRMOF-7 (i.e., with 1,4-naphthalenedicarboxylate) because of its more open pore structure.

2.2.6. Carbonyl Cyanosilylation

The Lewis acid-catalyzed cyanosilylation reaction of carbonyl compounds with trimethylsilyl cyanide yields the corresponding cyanohydrin trimethylsilyl ethers, which can be further hydrolyzed to the cyanohydrin. Cyanohydrins are versatile intermediates that can be readily converted into more interesting compounds, such as α -hydroxy acids, α -hydroxy aldehydes and ketones, β -hydroxyamines, and α -amino acid derivatives. Cyanosilylation of aldehydes (Scheme 13) is a reaction that does not require strong Lewis acid sites, and it is typically carried out under very mild conditions (see section 1.6). For this reason, this reaction has been frequently chosen as a test to demonstrate the presence of Lewis acid centers in MOFs. The examples discussed in this section rely on the presence of coordinatively unsaturated metal sites in the MOF framework to carry out the cyanosilylation. Nevertheless, a point that has never

been addressed up to now is the application of MOFs for the synthesis of asymmetric cyanohydrins.¹⁶³ This would require the presence of chiral Lewis acid sites in the MOF structure, so that MOFs containing coordinatively unsaturated metal sites produced by solvent evacuation cannot be used (since they are not chiral). On the contrary, chiral Lewis acid sites could readily be introduced in the MOF by either using the second or the third design strategies already discussed in section 1.5. Alternatively, homochiral MOFs could also be applied to the synthesis of asymmetric cyanohydrins. Homochiral MOFs can in principle be produced either from achiral building units or by using chiral ligands.¹⁶⁴

The first example of a MOF with catalytic activity for cyanosilylation of carbonyl compounds was reported by Fujita et al.,¹¹⁵ and these results have already been discussed in section 2.2.1. Table 1 shows a comparison of the different MOF catalysts used for cyanosilylation of benzaldehyde.

Kaskel and co-workers⁷¹ have reported on the catalytic activity for cyanosilylation of aldehydes of the well-known copper trimesate H-KUST-1 (or $Cu_3(btc)_2$). This material contains copper carboxylate paddlewheel dimers, $[Cu_2(COO)_4(H_2O)_2]$, with one apical water ligand on each copper that exposes a coordinative unsaturation on the metal ion when removed (see Scheme 2). The authors observed that the dehydrated material was able to chemisorb different ligands with electron-donor groups, such as carbonyl compounds or amines. Among them, adsorption of benzaldehyde was studied by IR spectroscopy, which revealed the formation of an absorption band at 1687 cm^{-1} , corresponding to the adsorbed molecule (pure benzaldehyde shows an IR band at 1702 cm^{-1}). The adsorption of benzaldehyde on the copper sites was found to be irreversible, since it is not possible to remove the adsorbed molecules without decomposition of the framework.⁷¹ HKUST-1 was used for the liquid-phase cyanosilylation of benzaldehyde. First, the material was outgassed under a vacuum at 373 K to remove adsorbed water molecules and create vacancies on the copper ions. When the reaction was carried out at 293 K, the observed conversion was very low (below 5% after 24 h). Benzaldehyde conversion increased upon increasing the temperature up to 313 K (ca. 60% conversion after 70 h). The nature of the solvent of the reaction was found to be very important: solvents with a low polarity were preferred to minimize dissolution of the catalyst. Additionally, donor type solvents, such as tetrahydrofuran and other ethers, compete against the reaction substrates for the copper Lewis acid, so they can block the catalytic active sites, resulting in a diminution of the reactivity. Solvents such as pentane, heptane, toluene, and CH_2Cl_2 can be used, but the temperature needs to be kept below 313 K to avoid catalyst decomposition (reduction).

Long and co-workers have described the preparation of a MOF with sodalite-type framework containing Mn and the ligand 1,3,5-benzenetris(4-yl) (btt).⁶⁵ This material consisted of Mn_4Cl square planar clusters surrounded by eight btt ligands to form sodalite-type cages. The as-synthesized material contained one $[Mn(dmf)_6]^{2+}$ complex clathrated inside each sodalite cage to preserve the electric neutrality of the framework. Upon exchanging the dmf molecules by methanol and evacuating at 423 K, the resulting material shows two types of exposed Mn sites: five-coordinated sites I originated from framework Mn^{2+} ions of the Mn_4Cl clusters and two-coordinated sites II, which correspond to Mn^{2+} ions formerly in the extraframework $[Mn(dmf)_6]$ complexes and which remain coordinated to two N atoms of adjacent

tetrazole rings after removal of the dmf molecules (see Scheme 3). Owing to the presence of exposed Mn^{2+} metal sites, this MOF was found to adsorb up to 2.2 wt % H_2 at $-200\text{ }^\circ\text{C}$ and 1.2 bar, reaching an excess H_2 adsorption of 5.1 wt % at saturation. The isosteric heat of H_2 adsorption (up to 10.1 kJ mol^{-1} at zero coverage) was at that moment the highest ever reported for a MOF,⁶⁵ although later this value was overcome up to $12.29 \pm 0.53\text{ kJ mol}^{-1}$ at zero coverage.¹⁶⁵ The high accessibility of the Mn^{2+} sites prompted the study of the catalytic properties of this material as a Lewis acid catalyst. The authors thus chose two reactions that required Lewis acid sites of increasing strength: carbonyl cyanosilylation and the Mukaiyama–aldol reaction between an aldehyde and a silyl enolate, a reaction that is only catalyzed by very active Lewis acid catalysts.¹⁶⁶ The material was found to be an active heterogeneous catalyst for the cyanosilylation of carbonyl compounds, both aldehydes and ketones. A filtration test was performed to demonstrate that the catalyst was heterogeneous. The authors also studied the size-selective properties of the MOF by changing the size of the aldehyde: while benzaldehyde and 1-naphthaldehyde readily reacted with Me_3SiCN (98 and 90% conversion after 9 h), 4-phenoxybenzaldehyde and 4-phenylbenzaldehyde gave lower conversions (19 and 18% conversion after 9 h). These different reaction rates of the substrates were interpreted as being due to the difficulty to accommodate the transition state of the large substrates inside the 10 \AA pores.¹⁶⁶ Under similar reaction conditions, ketones gave lower conversions than the aldehydes, as expected due to their reduced reactivity. Nevertheless, also in the case of ketones, the authors observed a size selectivity of the MOF: 28% conversion of acetophenone was achieved after 24 h of reaction, while 4-acetylbiphenyl ketone gave only 1% conversion after the same reaction time.¹⁶⁶

In chromium terephthalate MIL-101, two of the three chromium ions of the μ_3 -oxo bridged trimeric building block contain one water molecule that can be replaced in the catalytic cycle by the substrate, reagent, or intermediate.¹⁶ As commented before, the lack of these exchangeable positions around the coordination sphere of the metallic ions or clusters has been considered as one of the main limitations for the use of MOFs in catalysis. Since MIL-101 has in its structure this exchangeable ligand, it should be especially interesting for testing catalytic properties. It has to be noted that MIL-101 having water as one of the pseudo-octahedral ligands of chromium can be outgassed to remove this ligand under moderate temperature without causing the collapse of the crystal structure, as already described for $\text{Cu}_3(\text{btc})_2$.⁷¹ Other interesting properties of MIL-101 for its potential use in catalysis are its thermal stability and its durability upon storage and ambient moisture exposure for extended time periods.¹⁶ On the other hand, MIL-101 has very large pores, which is advantageous for catalysis with fine chemicals that are typically large molecules and can have several functionalities. Compared to $\text{Cu}_3(\text{btc})_2$,⁷¹ MIL-101 is more active for carbonyl cyanosilylation using a catalyst/substrate ratio as low as 0.5%. Chromium(III) has the advantage that it cannot be reduced by the aldehyde. In contrast, in $\text{Cu}_3(\text{btc})_2$, it has been proposed that one of the origins of deactivation is the damaging of the crystal structure as a consequence of the change in the coordination of Cu when it is reduced from Cu(II) to Cu(I) by the aldehyde. The catalytic process has been shown to be heterogeneous, and no changes in the peak position of the MIL-101 XRD after being used were

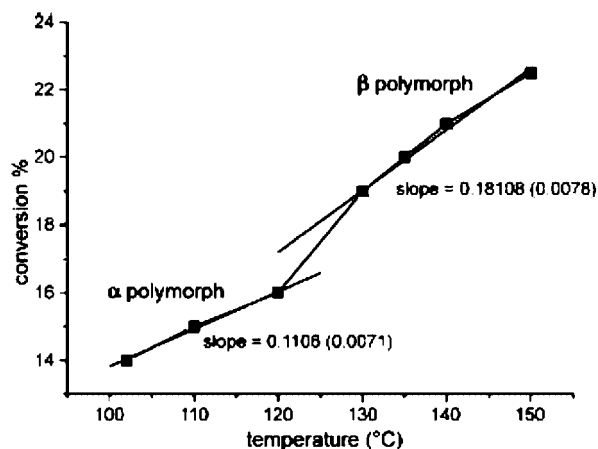


Figure 16. Thiophene conversion obtained after 4 h over the ytterbium succinate $[\text{Yb}(\text{C}_4\text{H}_4\text{O}_4)_{1.5}]$ as a function of temperature, showing a different dependence for the two polymorphs α and β . Reproduced with permission from ref 144. Copyright 2009 Wiley-VCH Verlag GmbH & Co. KGaA.

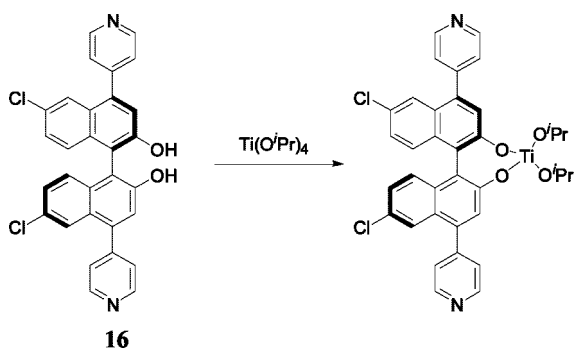
observed.¹²⁷ The redistribution in the intensity of the XRD peaks was interpreted as indicating that some heavy organic material is trapped inside the solid. This organic material blocking the pores and not the structure collapse is proposed to be the main cause of the long-term deactivation of MIL-101 as catalyst for aldehyde cyanosilylation.

2.2.7. Hydrodesulfurization

Hydrodesulfurization (HDS) is a catalytic process widely employed for removing sulfur compounds from natural gas and fossil fuels, with the aim of reducing SO_x emissions. Another important reason for removing sulfur compounds from the feedstocks is that they can poison the noble metal catalysts used for the ensuing catalytic reforming of the fuel. The HDS process consists of converting sulfur compounds into H_2S , which is then captured and transformed into elemental sulfur or sulfuric acid. The catalytic process occurs through the coordination of the sulfur atom to a coordinative unsaturation of the active metal site (usually molybdenum), which is followed by rupture of the C–S bond and eventually hydrogenation of the C=C bonds.

Monge and co-workers have recently applied different ytterbium containing materials for the HDS reaction of thiophene, chosen as a model compound for sulfur containing molecules in fuels. Both polymorphs α and β of the ytterbium succinate $[\text{Yb}(\text{C}_4\text{H}_4\text{O}_4)_{1.5}]$ were found to be active catalysts for HDS.¹⁴⁴ The reaction was carried out in a batch reactor at $p(\text{H}_2) = 6$ bar and with a thiophene/catalyst molar ratio of 1000. The authors performed the reaction at different temperatures below and above the phase-transition temperature, in order to evaluate the influence of the structure and the coordination around the Yb sites. The values obtained for the thiophene conversions after 4 h of reaction as a function of the temperature followed a straight line for temperatures below 393 K (see Figure 16). Above this temperature, in which the phase transition occurs, this increasing linear trend was also obeyed, but with a higher slope, which indicated a higher activity of the polymorph β with respect to α . This was explained in terms of the lower coordination around Yb in polymorph β (coordination number (c.n.) = 7) than in polymorph α (c.n. = 8). Additionally, the breaking of one Yb–O bond per Yb center occurring when the phase transition takes place produced a

Scheme 14



more open structure that facilitated diffusion of the substrates to the active sites.¹⁴⁴ Finally, a maximum thiophene conversion of 68% was obtained at 423 K after 18 h of reaction.

The same group have reported the preparation of the material named Yb-RPF-5 (rare-earth polymeric framework-5), containing anthraquinone-2,6-disulfonate (AQDS²⁻) as the organic ligand.¹⁶⁷ In this 3D MOF, Yb ions are hepta-coordinated to two μ_2 -(OH) groups, one water molecule, and four oxygen atoms from four different sulfonate groups. Two Yb are linked sharing an edge of OH groups, thus forming Yb₂O₁₂ dimers. This material was used for the HDS reaction of thiophene, yielding total conversion after 24 h at 443 K (substrate/catalyst molar ratio = 1:1000 and $p(\text{H}_2) = 7$ bar). As expected, the activity increased with the temperature (total conversion after 16 h at 373 K and 90% conversion after 4.3 h at 393 K).

2.2.8. Other Reactions

Besides the reactions mentioned above, MOFs have also been applied successfully as heterogeneous catalysts in a number of other reactions. In general, the articles that we will describe in the following section represent the only existing reports on the use of MOFs as catalysts for that particular reaction. Therefore, we have grouped all these papers under the common heading "Other Reactions".

Wu et al. have reported the synthesis of enantiopure chiral MOFs by slow diffusion of diethylether into a MeOH/dmf solution containing the ligand (*R*)-6,6'-dichloro-2,2'-dihydroxy-1,1'-binaphthyl-4,4'-bipyridine (**16**) and Cd²⁺ (in the form of CdCl₂).⁷⁶ This ligand molecule contains the two pyridine units to connect with the structural metal ions, while the accessible chiral 2,2'-dihydroxy-1,1'-binaphthyl groups can react with Ti(O^{*i*}Pr)₄ to produce asymmetric catalytic sites analogous to (BINOLate)Ti(O^{*i*}Pr)₂ (see Scheme 14). A model of the very large chiral channels ($\sim 1.6 \times 1.8$ nm²) of the binaphthyl MOF containing the Ti(O^{*i*}Pr)₂ active sites is shown in Figure 17. Owing to the known catalytic activity of (BINOLate)Ti(O^{*i*}Pr)₂ as a chiral homogeneous catalyst for the addition of Zn(CH₂CH₃)₂ to aromatic aldehydes to afford chiral secondary alcohols, the authors studied the catalytic properties of the homochiral porous MOF for the same reaction. Some of the results obtained are reported in Table 6.⁷⁶ This chiral MOF turned out to be an excellent heterogeneous catalyst for the asymmetric addition of ZnEt₂ to a wide range of aromatic aldehydes with ee values at high conversion very high and similar to those obtained with analogous soluble catalysts. The asymmetric induction of binaphthyl MOF was over 20% higher than that reported for analogous zirconium phosphonates.¹⁶⁸ No leaching was observed by establishing that the reaction stops when the

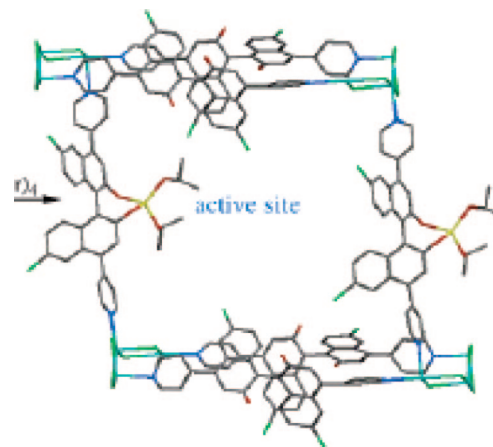


Figure 17. Model of the channel containing Ti(O^{*i*}Pr)₂ active sites of the binaphthyl containing MOF. Reproduced with permission from ref 76. Copyright 2005 American Chemical Society.

Table 6. Results of the ZnEt₂ Addition to Aromatic Aldehydes at Room Temperature Catalyzed by an Enantiopure Binaphthyl MOF Containing Ti(O^{*i*}Pr)₂ (Substrate-to-Ti Ratio 13 mol %); Data Taken from Ref 76

Ar	conversion (%)	enantiomeric excess (%)
1-naphthyl	>99	93
Ph	>99	83
4-ClPh	>99	80
3-BrPh	>99	80

solid chiral MOF is filtered. In addition, in contrast to the homogeneous counterpart, the chiral binaphthyl MOF catalyst exhibits shape selectivity, with the activity decreasing as the size of the aldehyde increases. The absence of leaching and the occurrence of shape selectivity clearly established the heterogeneous nature of the chiral binaphthyl MOF catalyst.

Some years later, the same authors reported that, when two other Cd²⁺ salts were used in the preparation of the MOF (namely, Cd(NO₃)₂·4H₂O or Cd(ClO₄)₂·6H₂O), two different MOF structures can be obtained with the same chiral binaphthyl ligand.¹⁶⁹ This diversity in crystal structures seems to arise from the participation of the anion accompanying Cd²⁺ in the structure and distinct abilities of halides and oxy anions in binding Cd²⁺. Thus, different enantiopure chiral MOFs were synthesized when the same experimental procedure based on the room-temperature diffusion of diethyl ether as precipitating agent is used on different Cd²⁺ salts. The two new enantiopure MOFs based on chiral binaphthyl ligands can, in principle, be used as polymeric 3D ligands of titanium Lewis acids, like in the case reported earlier.⁷⁶ The actual catalysts are obtained by treating the solids with an excess of Ti(O^{*i*}Pr)₄ in toluene. It is supposed that Ti(O^{*i*}Pr)₄ binds to the dihydroxy groups present in the 1,1'-binaphthyl units, although the crystal structure and analytical data of the titanium containing MOFs were not studied. Interestingly, because of the different crystal structure, the two MOFs exhibited a contrasting behavior. The chiral MOF prepared from nitrate acts as an efficient heterogeneous catalyst for the room-temperature, asymmetric addition of diethylzinc to a series of aromatic aldehydes, with ee values from 45 to 90% at full substrate conversion. On the other hand, the MOF derived from the perchlorate salt was inactive under the same conditions. The failure of the MOF prepared from the

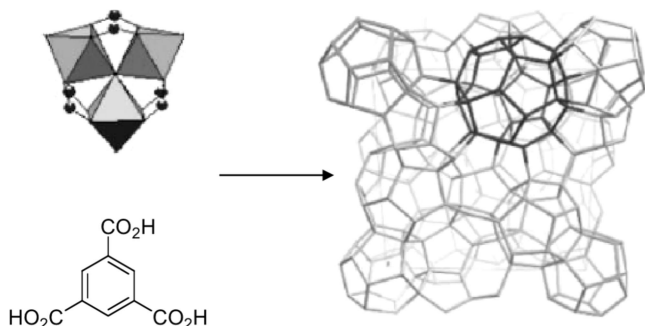


Figure 18. Building blocks and detail of the crystal structure of Fe(III)–MIL100 in which two types of cages of different sizes and accessible through smaller windows can be observed. Reproduced with permission from ref 170. Copyright 2007 Royal Society of Chemistry.

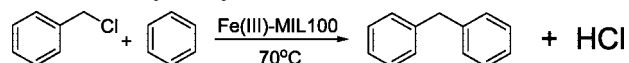
perchlorate salt to act as catalyst was rationalized by considering the strong steric congestion around these chiral dihydroxy groups, which would prevent them to react with $\text{Ti}(\text{O}^i\text{Pr})_4$, effecting the substitution of two isopropoxides.

The occurrence in the dehydrated copper trimesate HKUST-1 of Lewis acid sites has already been demonstrated in previous sections as being due to unsaturated copper sites. However, HKUST-1 also contains carboxylate ligands that could be protonated to some extent, thus contributing to the overall observed acidity. This ambiguity prompted Alaerts et al. to conduct a thorough characterization of the acid properties of the material by selecting suitable test reactions.⁶³ Isomerization of α -pinene oxide to campholenic aldehyde is a Lewis catalyzed reaction. Brønsted acids can also catalyze this conversion, but generally other products are also formed (*trans*-carveol, *p*-cymene, *trans*-sobrerol, and dimerization products), which can lower the selectivity down to 55%, while with Lewis acids selectivities as high as 85% can be attained. When the reaction was performed in the presence of HKUST-1 samples prepared in different ways and using different solvents, the obtained selectivities to campholenic aldehyde were in all cases about 80%, thus reflecting the true Lewis acid nature of the active sites.

Fe(III)–MIL100 is an Fe(III) carboxylate obtained from crystallization of Fe(0), 1,3,5-benzenetricarboxylate, and a mixture of hydrofluoric and nitric acid in water at 423 K for 6 days.¹⁷⁰ XRD shows that Fe(III)–MOF and the previously reported Cr(III)–MIL100 were isostructural.¹⁷¹ The structure formula of Fe(III)–MIL100 was $\text{Fe}_3\text{O}(\text{H}_2\text{O})_2\text{F}(\text{btc})_2 \cdot n\text{H}_2\text{O}$, where the number of water molecules is around 14 and depends on the ambient conditions to which the material is exposed. The crystal structure of Fe(III)–MIL100 is constituted by trimers of iron octahedra sharing a common vertex μ_3 -O. These Fe_3O clusters are then linked through Fe-carboxylates of the benzene-1,3,5-tricarboxylate ligand.¹⁷⁰ This arrangement of trimeric Fe and benzenetricarboxylate delimits two types of mesoporous cages of 2.5 and 2.9 nm dimension that are accessible through windows of ca. 0.55 and 0.86 nm. Figure 18 shows the structure of the resulting Fe(III)–MIL. The resulting specific surface area was 2 800 $\text{m}^2 \text{g}^{-1}$, which is remarkably large, although somewhat smaller than that achieved for Cr(III)–MIL100, which is beyond 3 000 $\text{m}^2 \text{g}^{-1}$.¹⁷¹ The crystal structure of Fe(III)–MIL100 was stable up to 543 K as determined by variable-temperature XRD.

Fe(III)–MIL100 was used as catalyst for the Friedel–Crafts reaction of benzene with benzyl chloride to render diphenylmethane at 343 K (Scheme 15).¹⁷⁰ The catalytic activity

Scheme 15. Friedel–Crafts Alkylation of Benzene by Benzyl Chloride Catalyzed by Fe(III)–MIL100



of Fe(III)–MIL100 was compared with that exhibited by Cr(III)–MIL100 and two acid zeolites, namely, HBEA and HY. It was observed that, while Cr(III)–MIL100 was notably inactive, the activity of Fe(III)–MIL100 surpasses that of the two zeolites under the same conditions. Figure 19 presents the time–conversion plot for benzene benzylation using MOFs or zeolites as catalysts.

With Fe(III)–MIL100, about 100% benzyl chloride conversion affording diphenylmethane with complete selectivity was obtained rapidly after an induction period of 5 min. Catalysis by zeolites occurs also with complete selectivity toward diphenylmethane, but the reaction is considerably slower as compared to Fe(III)–MIL100. It has to be, however, commented that the H-form of the zeolites should contain mainly Brønsted sites and also that catalytic data could have been completed by giving the time–conversion plots for a similar number of sites rather than for the same weight of catalyst.

In this context, it is interesting to comment that the higher activity of Fe(III)–MIL100 in the Friedel–Crafts reaction was attributed to the ability of Fe to swing between +3 and +2 oxidation state. Because Friedel–Crafts are typically catalyzed by acid sites, the authors should have ruled out Lewis acidity as an alternative (or even the main) reaction pathway. Another point of interest that was not addressed for the reaction with benzyl chloride is the stability of the Fe(III)–MIL100 and the possibility of homogeneous rather than heterogeneous catalysis. Considering that hydrochloric acid is the reaction byproduct, stability of MOF to HCl is an issue of considerable importance. Also, leaching of Fe species and occurrence of catalysis in solution are points that deserve much attention, particularly when the medium contains halides ions that can act as Fe ligands and the conditions should be strongly acidic.

The utility of the Pd-containing [Pd(2-pymo)₂] MOF (see Figure 4) as catalyst for olefin hydrogenation and alcohol oxidation has already been described in sections 2.2.2 and 2.2.3.3, respectively.⁶¹ Additionally, we have also demon-

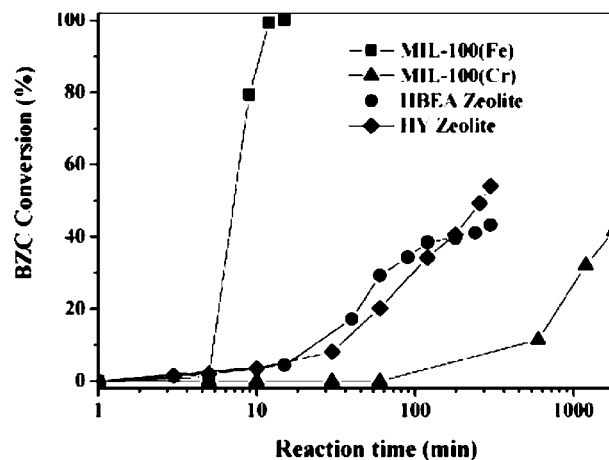


Figure 19. Time–conversion plot for the reaction of benzyl chloride with benzene in the presence of MOFs and zeolites as catalysts. Reaction conditions: 70 °C, 7.8 mL of benzene, benzene/benzyl chloride = 10 (molar ratio), 0.1 g of catalyst. Reproduced with permission from ref 171. Copyright 2004 Wiley-VCH Verlag GmbH & Co. KGaA.

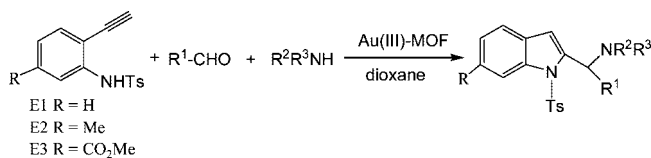
strated that this Pd–MOF can act as a heterogeneous catalyst for the Suzuki C–C coupling. In particular, we chose phenylboronic acid and 4-bromoanisole as the substrates, since this coupling has been proposed as a benchmark reaction to compare highly active palladium catalysts.¹⁷² Using the Pd–MOF as the catalyst (2.5 mol % Pd), we observed 85% conversion of 4-bromoanisole after 5 h (at 423 K in *o*-xylene), with >99% selectivity to the cross-coupling product, 4-methoxybiphenyl. The crystalline structure of the solid was preserved under these experimental conditions, and the solid was reused without a significant loss of activity. According to the inductively coupled plasma (ICP) analysis, no loss of Pd was detected after the reaction. A hot filtration experiment was also performed to exclude the occurrence of metal leaching from the MOF structure. The reaction was also conducted at room temperature, using ethanol as solvent, and total conversion was achieved after 48 h with excellent selectivities. Also in this case, the solid was reused without appreciable loss of activity. The TOF for the Pd–MOF catalyst was calculated for a separate run with a 10-fold lower catalyst concentration (0.25 mol % Pd), and a value of 1230 h⁻¹ was obtained. This represents a reasonably high value of activity for a phosphine-free palladium heterogeneous catalyst.

Ravon et al. have successfully used zinc dicarboxylates IRMOF-1 and IRMOF-8 as heterogeneous catalysts for the alkylation of aromatics.¹⁷³ Alkylation of either toluene or biphenyl with *tert*-butyl chloride was performed at 443 K in the presence of IRMOFs. For both substrates, the reaction was complete after 2 h, thus showing a catalytic activity similar to that of AlCl₃ or an acidic zeolite H-beta. Interestingly, both IRMOFs gave selectivities to the corresponding *para*-substituted product of over 82% in the case of toluene and 95% in the case of biphenyl. In contrast, both AlCl₃ and the acidic zeolite beta gave mixtures of *ortho*- and *para*-substituted molecules and dialkylated products.¹⁷³ The nature of the active centers of IRMOFs was not clear. However, the presence of both Zn–OH and Zn–OH–Zn groups according to IR and NMR spectroscopies suggested the presence in IRMOF-1 of either zinc hydroxide clusters or small crystals of the phase MOF-69C (not detected by XRD), which could be responsible for the observed catalytic activity.¹⁷³

Bernini et al. have reported on the preparation of an ytterbium succinate, [Yb(C₄H₄O₄)_{1.5}], which can exist in two temperature-dependent polymorphic forms: a room-temperature phase, α , and a polymorph β above 403 K.¹⁴⁴ As already mentioned in previous sections, these materials were found to be active catalysts for oxidation of sulfides (section 2.2.3.5) and hydrodesulfurization (section 2.2.7).¹⁴⁴ Additionally, the low-temperature polymorph α was also tested as a Lewis acid catalyst for acetalization of aldehydes. Reaction between benzaldehyde and trimethyl *ortho*-formate in the presence of polymorph α at 333 K was found to produce the corresponding dimethyl acetal with 90% yield after 5 h, thus evidencing the catalytic activity of the MOF.

As we have already mentioned in section 1.5.3, isolated and highly stabilized gold(III) cations were successfully incorporated in a MOF by a postsynthesis modification strategy.⁹³ This strategy (see Scheme 5) consisted of first preparing a Schiff base complex by reaction between the accessible –NH₂ groups of IRMOF-3,⁸⁸ followed by gold(III) complexation. This Au(III)–MOF was applied to the multicomponent domino coupling and cyclization of N-protected

Scheme 16. Reaction Scheme of the Domino Three-Component Coupling and Cyclization Reaction Catalyzed by Au(III)–MOF



ethylaniline, aldehyde, and amine, yielding the corresponding indole (see Scheme 16). The reaction was performed in a batch reactor at 313 K, and the performance of the Au(III)–MOF was compared with other representative examples of soluble gold salt (AuCl₃), soluble gold(III) salen complex,¹⁷⁴ and gold supported on metal oxide capable of stabilizing cationic species (Au/ZrO₂).^{122b} The results obtained (Figure 20) demonstrated the superiority of the Au(III)–MOF over the rest of the catalysts. Soluble gold salts and the gold salen complex were found to suffer from irreversible deactivation, and therefore, the initial reaction rate (TOF) and maximum conversion attained were lower compared to those for the Au(III)–MOF. A lower TOF value was also obtained for Au/ZrO₂ with respect to Au(III)–MOF. This difference was attributed to the fact that Au/ZrO₂ contained only 25% of the total gold in the form of cationic Au(III), while Au(III)–MOF contains exclusively Au(III). When the TOFs for both catalysts were recalculated taking into account the amount of Au(III), the values obtained were much closer: 52 h⁻¹ and 48 h⁻¹ for Au(III)–MOF and Au/ZrO₂, respectively. This finding was taken as evidence that cationic Au(III) species are the true active sites for this reaction,⁹³ thus confirming previous hypotheses.^{122b}

2.3. MOFs with Reactive Functional Groups

Seo et al.¹⁰⁵ reported in 2000 the first example describing the catalytic activity of a MOF containing ligands with reactive groups. This material (referred to as POST-1) was obtained by reaction between Zn²⁺ ions and the chiral molecule **17** (derived from D- or L-tartaric acid) containing a carboxylic acid and a pyridine group. The resulting homochiral MOF contained [Zn₃(μ^3 -O)] units, **18**, in which each Zn²⁺ ion was coordinated to the central μ^3 -oxygen, four oxygen atoms from four carboxylic ligands **17** bridging two Zn²⁺ ions within the same unit, and a pyridine N atom from a neighboring trimer. This structure has 6 pyridyl groups per trimer: three of them are coordinated to three Zn²⁺ ions from three different trimers, but the other three are free and pointing toward the center of the chiral channel. The authors showed that the presence of the uncoordinated pyridyl groups

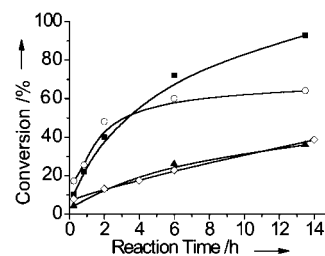
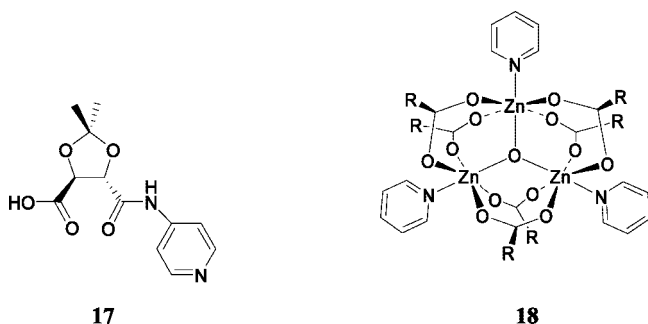


Figure 20. Comparison of the catalytic activity over Au(III)–MOF (■, gold: 0.0008 mmol), Au/ZrO₂ (▲, gold: 0.0014 mmol), homogeneous Au(III) Schiff complex (◇, gold: 0.0008 mmol), and AuCl₃ (○, gold: 0.025 mmol) for domino coupling and cyclization. Reproduced with permission from ref 93. Copyright 2009 Elsevier.

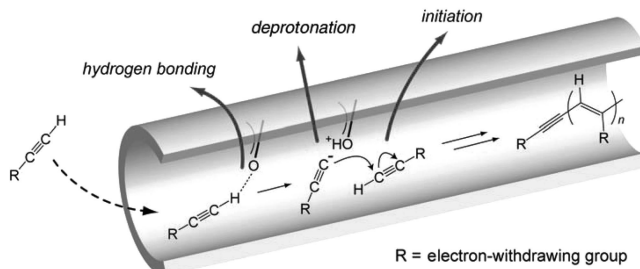
conferred catalytic activity to the material, as they demonstrated for transesterification reactions.¹⁰⁵ Using alcohols of increasing size and steric hindrance also suggested a size-selectivity effect. Moreover, POST-1 also revealed enantioselective catalytic properties for transesterification of 2,4-dinitrophenylacetate with 1-phenyl-2-propanol, although the enantiomeric excess obtained ($\sim 8\%$) using either D- or L-POST-1 was very modest.¹⁰⁵ Although the catalytic results obtained by POST-1 are very poor, the relevance of this paper remains as it is the first report on catalytic activity of a MOF associated to the functional groups of the organic ligands and not to the metal sites.



Kitagawa and co-workers¹⁷⁵ described the preparation of a pillared-layer copper-containing MOF, $[\text{Cu}_2(\text{pzdc})_2(\text{pz})]$ (pzdc = pyrazine-2,3-dicarboxylate, pz = pyrazine), with one-dimensional channels ($4.0 \times 6.0 \text{ \AA}^2$). They found that the carboxylate oxygen atoms of the material have a marked Lewis basic character, since they could act as specific adsorption sites for acetylene, resulting in electron delocalization between the H atoms of acetylene and the carboxylate oxygen atoms of the solid. On the basis of this rationalization and using pillared $[\text{Cu}(\text{pzdc})_2(4,4'\text{-bpy})]$ with channel dimensions of $0.82 \times 0.60 \text{ nm}^2$, it was anticipated that stronger acidic terminal alkynes having electron-withdrawing substituents could form the corresponding acetylide that would undergo anionic polymerization.¹⁷⁶ This is the case of methyl propiolate that undergoes polymerization inside $[\text{Cu}(\text{pzdc})_2(4,4'\text{-bpy})]$ upon standing at room temperature for 12 h. The polymer filled about 40% of the MOF micropore volume as estimated by thermogravimetry. Although there are some variations in the relative peak intensity, preservation of the MOF structure was inferred from the coincidence of the powder XRD pattern before and after methyl propiolate polymerization. The poly(methyl propiolate) can be recovered from the MOF by extracting the solid with dmf at 353 K. Optical and vibrational spectroscopy of the recovered polymer showed that the conjugated polyacetylene formed inside the MOF's micropores has mostly a *trans*-configuration of the C=C double bonds. Interestingly, a control using sodium benzoate as a soluble model for the MOF's basic sites does not lead to the formation of poly(methyl propiolate), supporting the view that spatial confinement inside a reaction cavity provided by MOF with the precise arrangement of basic carboxylate oxygen atoms and appropriate adsorption sites for methyl propiolate is a crucial requirement for the success of the polymerization by enabling a strong interaction between the monomer and the basic carboxylate.¹⁷⁶ This precise arrangement does not occur in solution.

Further support for this rationalization of alkyne polymerization was obtained by performing adsorption of methyl propiolate analogues in different MOFs with various mi-

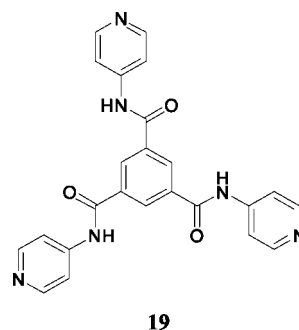
Scheme 17. Proposed Mechanism for the MOF Promoted Anionic Polymerization of Acidic Acetylenes



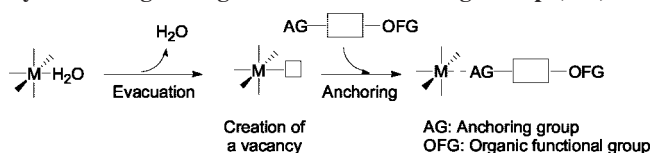
crore sizes and devoid, in one case, of basic carboxylate sites. Thus, formation of poly(methyl propiolate) was only observed when using $[\text{Cu}(\text{pzdc})_2(1,2\text{-di}(4\text{-pyridyl})\text{ethylene})]$ (channel dimensions $1.03 \times 0.60 \text{ nm}^2$).¹⁷⁶ Other acidic terminal alkynes (cyanoacetylene and 2-ethynylpyridine) undergo polymerization like methyl propiolate. In contrast, less acidic terminal alkynes such as phenylacetylene and 1-hexyne or disubstituted acetylenes such as tetrolic acid methyl ester do not polymerize inside $[\text{Cu}(\text{pzdc})_2(4,4'\text{-bpy})]$.¹⁷⁶ On the basis of these results, a mechanistic proposal that has as key steps the formation of acetylide under mild conditions due to spatial confinement and subsequent stereoselective attack to form the *trans*-configured polymer chain is proposed (Scheme 17).

A Knoevenagel condensation reaction is the prototypical example of a reaction catalyzed by MOFs with basic centers, which usually consist of amino or amide groups belonging to the organic ligand.

The first example of a Knoevenagel condensation reaction catalyzed by a MOF was reported by Hasegawa et al.¹⁷⁷ The authors prepared a material with composition $[\text{Cd}(4\text{-btapa})_2(\text{NO}_3)_2] \cdot 6\text{H}_2\text{O} \cdot 2\text{dmf}$ (4-btapa = 1,3,5-benzene tricarboxylic acid tris[*N*-(4-pyridyl)amide], **19**). The ligand used contains three amide groups that are responsible for the catalytic activity (*reactive* groups L_2 in Scheme 8), and three pyridyl groups that coordinate to Cd^{2+} ions (*coordinative* groups L_1 in Scheme 8). The basic catalytic properties of this MOF were demonstrated for the reaction between benzaldehyde and a series of activated methylene compounds: malononitrile, ethyl cyanoacetate, and cyanoacetic acid *tert*-butyl ester; see Table 2. The reaction only proceeded in the case of malononitrile, and this observation was taken as a proof that the reaction occurred inside the pores of the MOF and not on the external surface. However, the authors did not consider that this could also be due to the different intrinsic reactivity of the molecules, since it is well-known that malononitrile is the most reactive among the substrates tested for Knoevenagel condensation.^{102,103} Nevertheless, the authors performed filtration tests, recyclability, and stability measurements of the MOF with positive results.

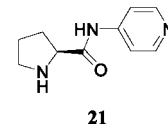
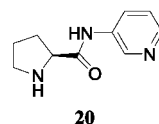


Scheme 18. General Strategy for Introducing an Organic Functional Group (OFG) in a MOF by Postsynthesis Functionalization at a Coordinatively Unsaturated Metal Site by Anchoring through a Suitable Anchoring Group (AG)



Gascon et al. have studied the basic properties of IRMOF-3⁸⁸ and MIL-53(NH₂) (a compound isorecticular to the aluminum terephthalate MIL-53¹⁷⁸ obtained by replacing terephthalate ligands by 2-aminoterephthalate).¹⁷⁹ Both materials contain 2-aminoterephthalate as the organic ligand, which coordinated to the metal ions (Zn²⁺ in IRMOF-3 or Al³⁺ in MIL-53(NH₂)) only through the carboxylic oxygen atoms, thus leaving free the amino group. IRMOF-3 was found to be an active and stable catalyst for the Knoevenagel reaction, comparable with other state-of-the-art solid basic catalysts (see Table 2 for a summary of the best results obtained). MIL-53(NH₂), on the contrary, was found to be much less active, and this was attributed to strong adsorption and diffusion limitations of the products through the 1D channels. However, according to the structure determination of an analogous MIL-53(NH₂) material reported at the same time by Arstad,¹⁸⁰ the amino groups of this material would be oriented parallel to the channel walls and not pointing toward the center of the channels as proposed by Gascon. This orientation of the aminoterephthalate molecule would render the amino groups less accessible to substrates in the case of MIL-53(NH₂) than in the case of IRMOF-3, and this could also explain the sensibly lower catalytic activity.

The next two reports have been included in the category of “MOFs with Reactive Functional Groups”, since in both materials the observed catalytic activity is due to the presence of organic functional groups in the material. However, these organic functional groups responsible for the catalytic reaction were not formerly present in the as-synthesized MOF. They were introduced using a postsynthesis modification consisting of first creating a coordination vacancy on the metal site of the MOF (by removal of a H₂O ligand molecule), followed by coordination of a suitable molecule containing the desired organic functional group (OFG) together with a suitable anchoring group (AG). The process is shown in Scheme 18. Note that this strategy could also be used to introduce an OFG having coordinating properties, which would ultimately allow us to introduce a metal cation coordinated to it. However, as far as we know, this has never been reported so far. Anyway, the strategy was first used by Hwang et al., who used the coordinatively unsaturated Cr³⁺ sites of MIL-101 obtained after evacuation for grafting an amine functional group.⁹⁴ For this purpose, they used ethylenediamine, in such a way that one of the nitrogen atoms coordinated to the Cr³⁺ vacancies, while the other amino group remained free and pointing toward the center of the structural cavities. This material was termed ED-MIL-101. A second example of the use of this strategy was reported recently by Banerjee et al.⁹⁵ Also in this case, the MOF chosen as support was the chromium terephthalate MIL-101, while the anchoring group consisted of a pyridine and the organic functional group was the chiral molecule proline. This was achieved by employing the chiral ligands [(*S*)-*N*-(pyridin-3-yl)-pyrrolidine-2-carboxamide] (**20**) or [(*S*)-*N*-(pyridin-4-yl)-pyrrolidine-2-carboxamide] (**21**).



Concerning ED-MIL-101, this compound was further modified by introducing palladium salt precursors inside the cavities, which, under appropriate conditions, can be reduced to form metallic palladium nanoparticles, as we will describe in more detail in the next section. Interestingly, the pendant amino groups of grafted ethylenediamine before palladium introduction conferred basic properties to the resulting ED-MIL-101. To demonstrate this point, the authors used the ED-MIL-101 material as a catalyst for Knoevenagel condensation of benzaldehyde ethyl cyanoacetate (see Table 2). Reaction between benzaldehyde and ethyl cyanoacetate proceeded smoothly at 353 K, giving quantitative conversion and selectivity to the condensation product after about 7 or 19 h (depending on the amount of grafted ethylenediamine). As expected, when the more demanding ketone 2-hexanone was used as substrate, the reaction was considerably slower, even when ethyl cyanoacetate was replaced by the more activated malononitrile. Conversely, benzophenone was not at all converted. This result was taken as an indication of the shape-selective properties of ED-MIL-101, owing to the large size of the 1,1-dicyano-2,2-diphenylethene product that would be formed in this reaction.⁹⁴ However, this suggestion seems unlikely in light of the large cavities of MIL-101 accessible through windows of ca. 16 Å.

A similar strategy was used by Banerjee et al., who used the Cr³⁺ vacancies of degassed MIL-101 to graft a chiral proline moiety through a pyridine anchoring group.⁹⁵ The resulting materials were used as heterogeneous catalysts for the asymmetric aldol reaction between various aldehydes and ketones. Depending on the particular substrates used, good to excellent conversions (60–90%) were achieved, with ee between 55 and 80%. For comparison, the parent, unmodified MIL-101 gave conversion of only 10% after 5 days, with 0% ee.⁹⁵

2.4. MOFs as Host Matrices or Nanometric Reaction Cavities

2.4.1. MOFs as Host Matrices to Incorporate Metal Nanoparticles

Fischer and co-workers^{124,181,182} have studied the inclusion from the vapor phase of a series of ten organometallic compounds inside MOF-5 and occasionally in IRMOF-8 (0.95 nm pore opening).⁸⁸ Incorporation from solution proved to be much more inefficient.¹²⁴

Table 7 lists the organometallic molecules hosted inside MOF-5 and their corresponding molecular dimensions. Under vacuum and dry argon, it was observed that both the crystal structure of MOF-5 and that of the organometallic compounds remain intact after the inclusion. Moreover, MOF-5 micropores behave like a solid solvent interacting weakly with the organometallic guest as concluded from the lack of remarkable differences in the IR and MAS ¹H NMR spectra of the guest between solution and included inside MOF-5. Also powder XRD shows no variation in the peak positions, and the changes in the relative peak intensity were interpreted as arising from the variations in the X-ray scattering properties from empty voids to micropores filled with organometallic guest. For highly volatile organometallics,

Table 7. Characteristic Molecular Dimensions of the MOCVD Precursors Used to Be Adsorbed by the MOF-5 Matrix; Data Taken from Ref 181

precursor	x	y	z	max.
[Pd(η^3 -C ₃ H ₅)(η^5 -C ₅ H ₅)]	4.5	4.5	4.5	5.5
[Pt(η^5 -C ₅ H ₅)(CH ₃) ₃]	4.3	4.7	4.7	6.5
[Fe(η^5 -C ₅ H ₅) ₂]	3.5	4.5	4.5	5.2
[Cu(η^5 -C ₅ H ₅)(CN ^t Bu)]	4.5	4.5	7.6	8.2 ^a
[Cu(η^5 -C ₅ H ₅)(P(CH ₃) ₃) ₂]	5.0	5.0	6.0	7.5
[Au(CH ₃)(P(CH ₃) ₃) ₂]	4.5	4.5	6.5	7.0
[Sn((C ₄ H ₉) ₂)(OOC ₂ H ₅) ₂]	6.5	7.8	10.0 ^a	10.0 ^a
[Zn(C ₂ H ₅) ₂]	1.8	3.0	8.0 ^a	8.0 ^a
[Fe(CO) ₅]	4.2	4.2	5.1	5.9
[Cu(OCHMeCH ₂ NMe ₂) ₂]	6.5	7.9 ^a	8.3 ^a	8.7 ^a

^a Opening diameter of MOF-5: 7.8 Å.

the inclusion in MOF-5 was fully reversible and the guest could be completely desorbed from MOF-5.

As expected, the maximum amount of incorporated organometallic guest depended on the size of the organometallic compound. Large molecules such as Cu(OCHMeCH₂NMe₂)₂ were size-excluded and could not be incorporated inside MOF-5. An intriguing observation was that the saturation complex loading follows a certain stoichiometry in the sense that the average number of molecules per cavity was an integer number. Sometimes, as in the case of Pd(η^3 -C₃H₅)(η^5 -C₅H₅), the filling by the guest complex accounts for 43% of the initial empty volume.¹²⁴ Although no explanation for this finding was given, the stoichiometric adsorption suggests that all the cavities are equally full with the maximum possible number of accommodated guests. It is also interesting that, when two organometallic compounds are simultaneously coadsorbed, the stoichiometry of the adsorption is lost, suggesting that the mismatch in shape of the two complexes makes impossible a good packing inside the MOF-5 cavities.

Following an analogous chemical vapor deposition procedure, Kim et al.¹⁸³ prepared a ferrocene containing MOF-5, and they were able to perform its structural characterization by single-crystal X-ray diffraction using synchrotron radiation. As already suggested by the stoichiometric adsorption of the organometallic compounds mentioned previously,¹²⁴ single-crystal data revealed an ordered array of ferrocene molecules in the pores of the host MOF that are stabilized by π - π interactions.

What is important for this review is that, once the organometallic complexes have been incorporated and because of their inherent lability, it is possible to generate small metal nanoparticles (~1.4 nm particle size) in a weakly coordinating environment. The nanoparticles can be generated by chemical reduction or photochemical treatment.¹²⁴ For instance, treatment of Pd(η^3 -C₃H₅)(η^5 -C₅H₅) with hydrogen at -35 or 23 °C renders palladium nanoparticles inside MOF-5. These naked palladium nanoparticles are highly reactive and extremely air-sensitive. In spite of the reduction or even disappearance of the characteristic XRD pattern, it is believed that the MOF-5 crystal structure is largely preserved upon formation of Pd nanoparticles based on the high residual BET surface area (1600 m² g⁻¹) and on the lack of terephthalate hydrogenation that was excluded by IR spectroscopy. However, it has to be commented that aromatic ring vibrations of terephthalate linker are almost absent in the IR spectrum of MOF-5, which is dominated by the carboxylate absorption bands at 1572 and 1507 cm⁻¹ (asymmetric stretching) and a peak at 1391 cm⁻¹ (symmetric

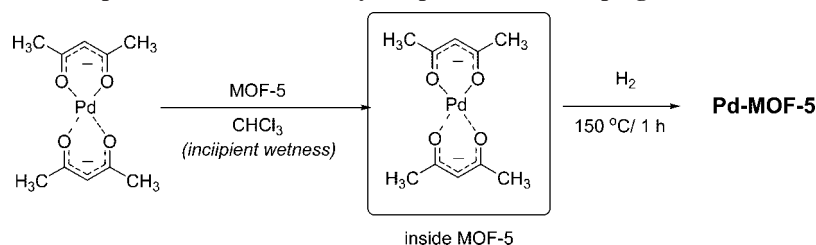
stretching). Thus, it might be difficult to assess the transformation of some terephthalate units just by IR spectroscopy. In addition to hydrogenation and C-C coupling products arising from cyclopentadiene and allyl reaction during the formation of the nanoparticles from Pd(η^3 -C₃H₅)(η^5 -C₅H₅), palladium encapsulated inside MOF was able to effect the hydrogenation of cyclooctene, although the catalytic activity was only moderate (47.34 (μ mol of cyclooctane) g_{cat}⁻¹ h⁻¹).¹²⁴

Copper nanoparticles (3–4 nm) inside intact MOF-5 (XRD pattern and residual surface area 1100 m² g⁻¹) can also be formed through the sequence consisting of adsorption from the gas phase of Cu(PMe₃)(η^5 -C₅H₅) and subsequent reduction with hydrogen at 423 K for 1 h.¹²⁴ The issue of how nanoparticles larger than the diameter of a single cavity are accommodated inside the micropores has not been addressed. In this sense, it is worth noting here that Alledorf et al. have recently reported on the preparation of silver clusters inside MOFs,¹⁸⁴ and they have demonstrated that observations of large metal nanoparticles by TEM are the result of damage to the MOF by the electron beam, so that probably the observation of metal nanoparticles with sizes larger than the MOF pore size could be artifacts of the image technique. Nevertheless, the resulting copper nanoparticles prepared inside MOF-5 were found to be excellent catalysts for the formation of methanol from syn gas (70 (μ mol of cyclooctane) g_{cat}⁻¹ h⁻¹), matching the activity of other supported mesoporous catalysts of the type Cu/ZnO@MCM-41/48.¹²⁴ Apparently the Zn₄O clusters of MOF-5 are able to promote copper, rendering these nanoparticles catalytically active, or the claimed promotion of Cu nanoparticles by ZnO may not be a prerequisite for activity.

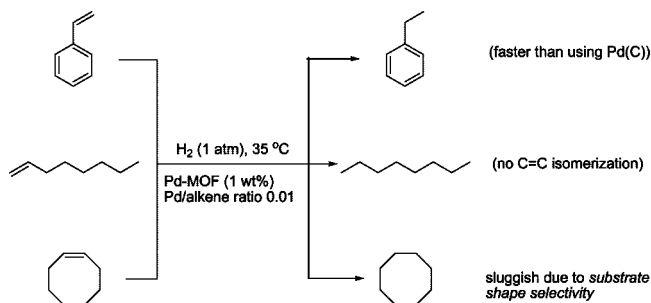
In contrast to palladium and copper, analogous treatment of Au(CH₃)(PMe₃) adsorbed inside MOF leads to nanoparticles with a broad size distribution from 5 to 20 nm outside the structure of MOF-5.¹²⁴ Apparently gold has larger mobility and either the organometallic complex desorbs or the initial gold nuclei migrate outside the crystal. It has to be noted, however, that, in total contrast to palladium, the experimental procedure employed for gold uses a very high reduction temperature (463 K) for a prolonged time (2 h). Not surprisingly in view of the requirements for gold catalysis, this material was unable to catalyze CO oxidation, a reaction that is extremely dependent on the particle size and the nature of the support. It would be interesting to know if milder conditions could avoid migration and agglomeration of gold nanoparticles. Certainly, considering the activity of gold encapsulated in zeolites, it will be of interest to prepare catalytically active gold nanoparticles inside MOFs that could exhibit shape selectivity.

As an alternative to the inclusion from the vapor phase used by Fischer and co-workers, palladium nanoparticles embedded within MOF-5 have also been prepared by Sabo et al. following an incipient wetness procedure using Pd(acac)₂ (acac = acetylacetonate) as precursor and chloroform as solvent.¹²⁵ In the incipient wetness, the pore volume of the material is first determined, and after outgassing and dehydration of the porous solid, a solution of the desired amount of the guest dissolved in the volume corresponding to the pore volume is added dropwise to the solid while mixing mechanically. Typically, a volatile solvent is used to facilitate its removal. In the case considered here, after adsorption of Pd(acac)₂ into MOF-5 in chloroform and

Scheme 19. Procedure for the Preparation of Pd-MOF-5 by Incipient Wetness Impregnation



Scheme 20. Hydrogenation of Three Representative Alkenes with Pd-MOF-5



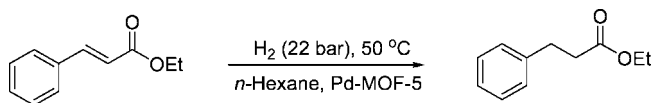
evacuation of the solvent, the precursor was reduced to palladium metal (Scheme 19).

It was found that thermal treatment of Pd(acac)₂-MOF-5 with a hydrogen flow at 423 K renders the most active hydrogenation catalyst. Interestingly, no hydrogenation of the terephthalate ligand was observed by ¹H and ¹³C NMR spectroscopy after destroying Pd-MOF and dissolving the organic component.

A sample containing 1 wt % of palladium embedded with MOF-5 shows a specific surface area of 959 m² g⁻¹ as compared to 2885 m² g⁻¹ of the original MOF-5 sample and exhibits an increase in the reversible hydrogen storage capacity at 1 bar and 77 K from 1.15 to 1.86 wt % under the same conditions for the original MOF-5 precursor.¹²⁵ Pd-MOF-5 prepared by incipient wetness has been used for the hydrogenation of styrene, 1-octene, and cyclooctene under 1 atm H₂ and 308 K and using a catalyst/substrate ratio of 1%. No C=C double-bond isomerization was observed in the hydrogenation of 1-octene, while cyclooctene hydrogenation is comparatively much slower.¹²⁵ The reduced accessibility to the pore system has been proposed as the most likely among the possible reasons for the sluggish cyclooctene hydrogenation. Thus, cyclooctene will only probe the external surface of the MOF-5 crystallite (Scheme 20). No leaching was observed. Provided that the material is not exposed to the air, the crystal structure of the material is preserved upon the catalytic reactions, and the solid was reused three times with some degree of deactivation and reduced performance. However, Pd-MOF-5 was found to be unstable to the air, since the XRD pattern changes significantly when the used catalyst is exposed to the air. Thus, even though under certain conditions (1 atm H₂, 308 K, 8 h) Pd-MOF-5 is more active than commercial Pd on active carbon or Pd prepared on Norit active carbon for the hydrogenation of styrene, it suffers from the serious disadvantage of poor chemical stability and moisture sensitivity.¹²⁵

Although the incipient wetness is a convenient procedure from the experimental point of view, it could be even better if palladium nanoparticles are formed simultaneous with MOF-5. Entrapment of palladium (about 0.5 wt %) simultaneously with MOF-5 formation has been reported by

Scheme 21



adding palladium nitrate together with zinc nitrate and 1,4-benzenedicarboxylic acid to dmf when MOF-5 is being synthesized.¹²⁶ It was found that, although the XRD of the samples obtained by coprecipitation were coincident with those reported for MOF-5, there is a certain range of variation in the textural properties and palladium content of the materials prepared by this method. In any case, the specific surface area and micropore volume of the palladium containing MOF-5 were about 3 times lower than the values reported by Yaghi for this material.¹² Comparison of the catalytic activity of Pd-MOF-5 prepared by coprecipitation with other Pd-MOF-5 prepared by incipient wetness and conventional Pd/C for the hydrogenation of ethyl cinnamate (Scheme 21) showed that the material prepared by coprecipitation was the most active sample, about twice the activity of Pd/C and the sample prepared by incipient wetness. This increased catalytic activity has been explained as derived from a higher metal dispersion on the support when the material is prepared by coprecipitation. However, the fact that the catalytic activity increases significantly in the second run when the material has no pore volume indicates that palladium nanoparticles are located on the external surface of the MOF-5 crystallites and not inside the micropores.¹²⁶

The properties of MIL-101 as a large area catalyst support for Pd has been studied for hydrogenations.¹²⁷ The Pd nanoparticles were obtained by incipient wetness impregnation of Pd(acac)₂ (acac = acetylacetonate) in chloroform followed by palladium(II) reduction with hydrogen at 473 K. The surface area is reduced upon incorporation of palladium from 2046 to 1760 m² g⁻¹, which is still an impressive value and compares very favorably with the residual area when the same process is performed using MOF-5 (67% area reduction). Using hydrogen adsorption and assuming that one palladium atom can form a single palladium-hydride bond, it was estimated that 72% of the palladium atoms embedded in MIL-101 are accessible. This number of external palladium atoms leads to an estimation of average particle size of 1.5 nm that fits well with the dimensions of the internal cavities in MIL-101.

Pd-MIL-101 was air-stable and was considerably more efficient than palladium encapsulated in MOF-5 or supported on active carbon for the hydrogenation of styrene and *cis*-cyclooctene.¹²⁷ The long-term stability of Pd-MIL-101 was assessed for the gas-phase hydrogenation of mixtures of acetylene and ethylene using a continuous fixed-bed reactor operated between 313 and 373 K. Figure 21 shows the observed catalytic performance of Pd-MIL-101. Although the reasons for the selected acetylene/ethylene/hydrogen mixtures and operation conditions were not explained and

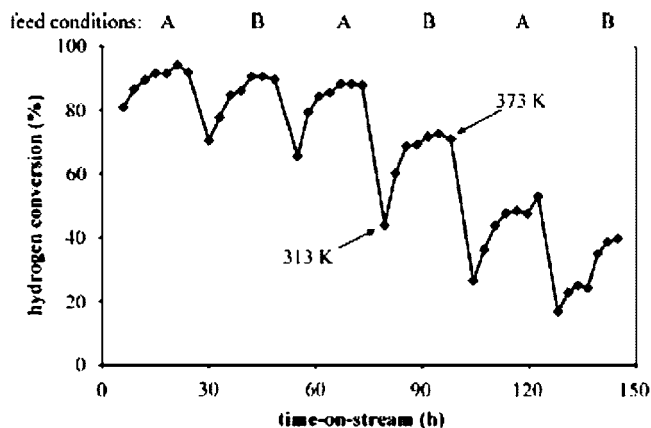


Figure 21. Hydrogen conversion versus time-on-stream in hydrogenation of a mixture of acetylene (1.7%)–ethylene (42.9) using 1 wt % Pd/MIL-101 diluted 1:10 on a SiC matrix in a continuous fixed-bed reactor operated in repeated temperature cycles between 313 and 373 K, feeding a gas mixture with a hydrogen content of 3.4% (condition A) or 2.1% (condition B). Reproduced with permission from ref 127. Copyright 2008 Royal Society of Chemistry.

the applicability of the MIL-101 based palladium catalyst was not discussed, the results show that Pd–MIL-101 exhibits a slow and continuous deactivation attributable to poisoning by heavy oligomers. The catalyst deactivation with time-on-stream renders the use of Pd–MIL-101 still not feasible.

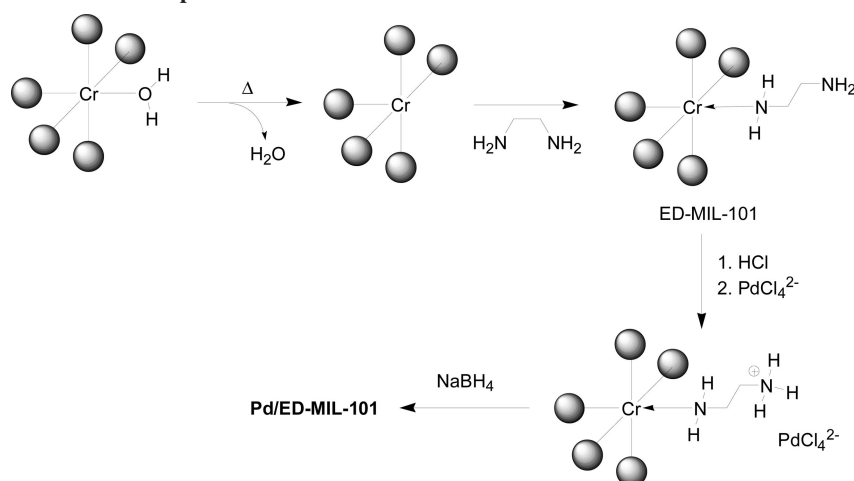
Hwang et al. have prepared Pd nanoparticles (2–4 nm) inside MIL-101 having amine groups anchored to the coordinatively unsaturated chromium sites of the dehydrated material, as already mentioned in section 2.3. Following the procedure depicted in Scheme 22, the authors prepared Pd/ED–MIL-101 and Pd/APS–MIL-101 materials (ED = ethylenediamine, APS = 3-aminopropyl trialkoxysilane). No apparent loss of crystallinity was observed from the corresponding XRD, although incorporation of the metal produced variation in the intensity of the diffraction peaks. TEM images revealed formation of nanoparticles in the range of 2–4 nm. The authors studied the catalytic activity of both Pd/ED–MIL-101 and Pd/APS–MIL-101 samples for the Heck C–C coupling reaction between iodobenzene and acrylic acid at 393 K in dimethylacetamide as solvent (1 mmol of iodobenzene, 1.5 mmol of acrylic acid, 1.5 mmol of triethylamine, and 50 mg of catalyst, which corresponds

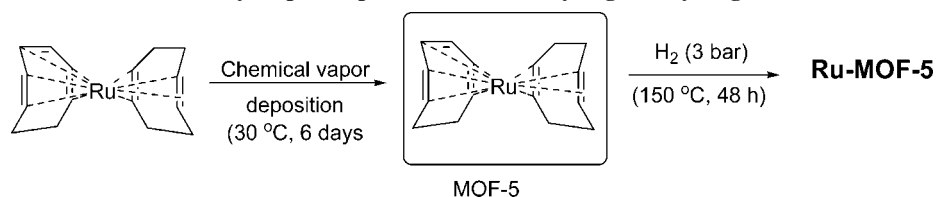
to 0.5 mol % Pd and a Pd/iodobenzene molar ratio of ca. 225). Both Pd/ED–MIL-101 and Pd/APS–MIL-101 showed catalytic activities comparable to that measured in the same conditions for a commercial Pd/C catalyst, achieving total conversion of iodobenzene after about 2 h of reaction time. However, both Pd/ED–MIL-101 and Pd/APS–MIL-101 showed induction periods of about 0.5–1 h, which the authors attributed to slow diffusion of the reactants to reach accessible metal sites in the pores. However, the authors did not perform additional experiments to support this hypothesis, which is a bit surprising on account of the large pores of MIL-101 (cavities accessible through windows of 12 and 16 Å in diameter) and the large area of the support (although the residual area of the material after incorporation of Pd is not reported, the area (S_{BET}) of the starting ED–MIL-101 was 3555 m² g⁻¹). The authors argued that the recyclability of the material proved that the catalytic process was mainly heterogeneous. However, the authors did not indicate the number of runs for which the catalyst was tested, the activity for each run, and the presence or absence of the induction period in all the catalytic runs. Another important piece of information not given concerns the characterization of the solid after the catalytic reaction, i.e., stability of the material under catalytic conditions, comparison of the crystallinity of fresh and used material, Pd content, and size of the nanoparticles after the catalytic reaction. Finally, it should be considered that very small amounts of Pd in solution can be responsible for the observed catalytic activity.

Actually, considering the current interest in the use of small noble metal nanoparticles as catalysts, there is no doubt that much effort should be made in the study of the activity and selectivity of metal nanoparticles inside MOFs. Compared to zeolites, MOFs as hosts of metal nanoparticles can have the advantage of combining the microporous confinement for the nanoparticles and the functionality that can introduce the organic linker. However, also to this respect and before any practical application, the stability of the system upon extensive use should be proved.

Embedding of metal nanoparticles inside MOFs also finds application as heterogeneous oxidation catalysis. Ruthenium nanoparticles embedded within MOF-5 have been prepared by chemical vapor deposition at 303 K under static vacuum of 10⁻⁵ mbar for 6 days of the organometallic Ru(cod)(cot) complex (cod = 1,5-cyclooctadiene; cot = 1,3,5-cyclooctatriene).¹⁸⁵ The process is depicted in Scheme 23. The advantages of vapor deposition are a cleaner nanoparticle

Scheme 22. Procedure Used for the Preparation of Pd/ED–MIL-101

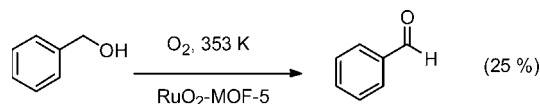
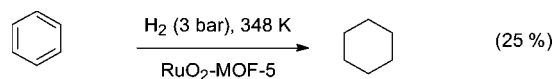


Scheme 23. Preparation of Ru–MOF-5 by Vapor Deposition Followed by Ligand Hydrogenation

deposition without the presence of coadsorbed solvent molecules and a high loading. Up to 30–40% of guest loading can be achieved in a single deposition. Incorporation inside the crystals was supported by performing the procedure using millimetric MOF-5 crystals and observing that it exhibits the characteristic yellow–orange color of the ruthenium complex homogeneously distributed through the cross section.¹⁸⁵ After incorporation, the Ru(cod)(cot) complex (3.5 molecules per unit cell) was expected to be smoothly transformed into embedded Ru metal nanoparticles. Hydrogen converts the C=C double bond of the unsaturated cyclic ligands into cyclooctane, which does not show affinity for ruthenium. Unexpectedly, an intermediate Ru(cod), not observed in solution or in solution containing dimethyl terephthalate, was formed inside MOF-5 as consequence of the hydrogenation under mild conditions. It was assumed that Ru(cod) is stabilized by interaction with the terephthalates of MOF-5. Harsher reduction conditions (3 bar hydrogen, 423 K) and extended treatment times are required to effect the complete transformation of Ru(cod)(cot) into ruthenium metal nanoparticles.¹⁸⁵ One important concept that was introduced by the authors is that the void space of MOFs has many similarities and can be viewed as a rigid solvent cage.¹⁸⁵ Actually, ¹³C NMR of the organometallic Ru(cod)(cot) complex shows the same signals and chemical shifts as in C₆D₆ solution and remarkably different than the spectrum recorded for pure Ru(cod)(cot) in the solid phase, which shows 16 signals corresponding to each individual carbon.¹⁸⁵ This indicates that the Ru(cod)(cot) organometallic complex inside MOF-5 is fluxional and mobile.

The total ruthenium loading was 30 wt % in form of small nanoparticles of 1.5–1.7 nm typical size incorporated uniformly inside the crystal. The surface area of the Ru–MOF-5 was 860 m² g⁻¹, and X-ray absorption spectroscopy reveals a weak interaction of the metal clusters and the arene carbon atoms of MOF-5. These ruthenium metal clusters embedded within MOF-5 can interact reversibly with CO and are able to effect the partial H/D exchange of the 1,4-benzenedicarboxylate linker of MOF-5 upon contacting the solid with D₂. ²D NMR spectroscopy shows a remarkable high mobility of deuterons inside MOF-5 containing ruthenium, even at 40 K, suggesting that the interaction of Ru nanoparticles with the MOF-5 framework should be rather weak and that the system can be viewed as containing naked metal nanoparticles.¹⁸⁵

Ru–MOF-5 can be easily converted into RuO₂–MOF-5 by reaction with diluted O₂ gas. It has been reported that RuO₂ supported on Al₂O₃^{186,187} or zeolites^{188,189} exhibits catalytic activity for the aerobic oxidation of a large variety of alcohols. However, in the presence of RuO₂–MOF-5, benzyl alcohol was only converted in 25% to benzaldehyde and XRD showed the breakdown of the MOF-5 structure (Scheme 24). This unsatisfactory result was attributed to the stoichiometric formation of H₂O during the oxidation and the fact that MOF-5 is highly water-sensitive.¹⁹⁰ Ru–MOF-5 was also tested as solid catalyst for the hydrogenation of

Scheme 24. Use of RuO₂–MOF-5 as Heterogeneous Catalyst for Benzyl Alcohol Oxidation**Scheme 25. Use of RuO₂–MOF-5 as Heterogeneous Catalyst for Benzene Hydrogenation**

benzene at 308 K to cyclohexane, but the conversion was only 25%. (Scheme 25). Altogether, these catalytic results show some promise of ruthenium nanoparticles inside MOFs, provided that the stability of the crystal structure is sufficiently high to withstand the reaction conditions and byproducts.

All information on the internal versus external location of guests on MOFs from electron microscopy must be interpreted cautiously.¹⁹¹ One of the problems is the stability of the sample to the electron beam damage. It has been demonstrated that, at high electron energy or low energy but long exposure times, the beam used to probe the sample by electron microscopy can destroy MOF crystal structure.¹⁹¹ This MOF instability toward electron beam precludes the use of high-resolution TEM imaging, even though the size of MOF micropores is well within the resolution range of this technique. A careful electron microscopy study by three-dimensional tomographic reconstruction of MOF-5 particles loaded with palladium and ruthenium nanoparticles has shown that the procedure to generate these metal nanoparticles after vapor-phase adsorption of the metal precursors [(η^5 -C₅H₅)Pd(η^3 C₃H₅) and Ru(cod)(cot) for Pd and Ru nanoparticles, respectively] by photolysis or hydrogenolysis causes differences in the particle distribution through the MOF matrix.¹⁹¹ It was found that, for palladium nanoparticles obtained by room-temperature photolysis of the monoatomic precursor, a large proportion of the nanoparticles spread within the bulk of MOF-5 framework.¹⁹¹ In contrast, for ruthenium nanoparticles, three-dimensional tomographic images showed a low particle penetration of about 20 nm depth in the MOF-5 crystal.¹⁹¹ Figure 22 shows two representative tomographic images to illustrate the different distribution of the metal nanoparticles through MOF-5 framework.

Formation of the metal nanoparticles from monoatomic precursors requires migration and aggregation of the metallic species through the porous matrix, and the temperature of the process apparently influences this rearrangement. Since no apparent differences on the palladium or ruthenium distribution on MOF-5 are observed in the TEM images, with both TEM images giving the impression that also the distribution of ruthenium nanoparticles within MOF-5 framework is homogeneous and densely packed, it is concluded that projected TEM images have to be interpreted with caution when addressing the internal location of the metal

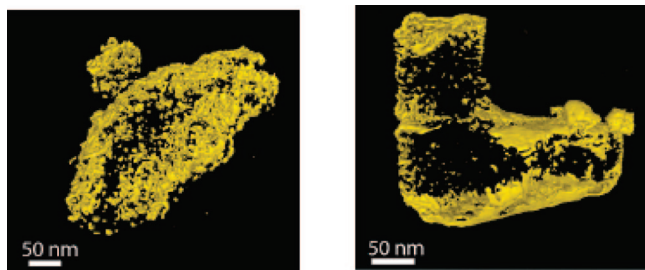
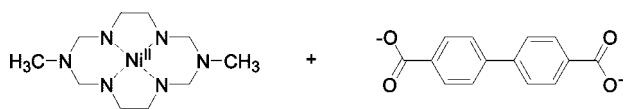


Figure 22. Tomographically reconstructed images of palladium (left) and ruthenium (right) metal nanoparticles inside MOF-5 crystals. Reproduced with permission from ref 191. Copyright 2008 American Chemical Society.

Scheme 26. Building Units of a Nickel-Containing MOF That Has Been Used to Form Silver Nanoparticles of Controlled Size and Shape



nanoparticles.¹⁹¹ Interestingly, this study by electron microscopy firmly reveals the presence of metal nanoparticles as large as 3 nm nestled inside MOF-5 framework (1.5 nm of largest dimension).¹⁹¹ This indicates that some kind of local matrix distortion or the nanoparticles expanding to neighbor micropores occurs to accommodate these metal nanoparticles or that partial framework ruptures occur to allow metal growth. Overall, the intuitive concept that the host framework must limit the size of the included guest does not apply in soft hosts such as MOFs.

In spite of the observation that the metal nanoparticles size can be larger than that expected based on the dimensions of a single cavity, the concept of using the MOF framework to control the metal nanoparticles size has been sometimes used. Monodisperse, regularly shaped silver nanoparticles are more difficult to prepare than gold or platinum nanoparticles.¹⁹² Suh and co-workers have prepared a specially designed MOF [Ni(C₁₀H₂₆N₆)₃(bpdc)₃]·2C₅H₅N·6H₂O (bpdc = 4,4'-biphenyldicarboxylate) to obtain embedded as well as isolated (ca. 3 nm) Ag nanoparticles.¹⁹³ The structure of the required MOF with permanent porosity is constructed by packing of the linear coordination polymer chains formed from the nickel macrocycle complex and bpdc²⁻ ions in a water/pyridine mixture (Scheme 26). As can be seen there, the structure of this Ni-containing MOF is built up by linear polymer chains arising from the coordination of free axial ligand positions of Ni in the aza crown complex and the linear organic dicarboxylic acid. These chains extend in three different directions ([010], [001], and [101]) to construct a double network of 3-fold braids. The resulting structure generates one-directional channels with a honeycomb-like window of 9.7 Å diameter, which are filled with water and pyridine. Similar MOFs based on analogous nickel tetraaza crown complexes coordinated to 2,2'-bipyridyl-5,5'-dicarboxylate cannot be used for the purpose of formation of silver nanoparticles due to the instability of the MOF in an aqueous solution containing Ag⁺.¹⁹⁴

This nickel-containing MOF is insoluble in water, and organic solvents and can be submitted to outgassing at 411 K to evacuate the adsorbed solvent molecules (water and pyridine). This process does not cause the collapse of the

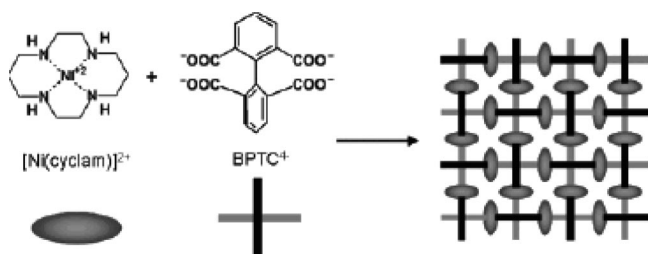
crystal structure if the temperature of the thermal treatment is lower than 523 K. The surface area of the desolvated Ni-MOF was 691 m² g⁻¹.

Addition of desolvated Ni-MOF to a methanolic solution of AgNO₃ (0.08 M) at room temperature leads to the spontaneous formation of silver nanoparticles (3 nm average diameter).¹⁹³ This process cannot be conducted in aqueous medium because the structure of the nickel MOF becomes destroyed in water when AgNO₃ is present. Electron paramagnetic resonance (EPR) shows that the reduction of Ag⁺ to Ag⁰ is accompanied by the oxidation of Ni^{II} to Ni^{III}; this oxidation state is certainly uncommon for nickel ions. A control experiment using the aza crown Ni^{II} complex showed that the complex is unable to effect Ag⁺ reduction, and it is claimed that the MOF structure is necessary to produce the process. It is unclear, however, how the thermodynamics of the process is modified by the incorporation of the redox active complex in a rigid environment.

XRD shows that the structure of nickel MOF is preserved when the desolvated solid is immersed in a methanolic AgNO₃ solution for 10 min. Although under these conditions silver nanoparticles are observed by HR TEM, their presence is not detected by XRD. This failure of XRD to detect Ag nanoparticles has been attributed to their small particle size. Chemical analysis of Ni and Ag indicates that short contact times lead to stoichiometric 1:1 reduction of Ag⁺. The reduction of Ag⁺ represents an example in which a MOF participates in the process as stoichiometric reagent rather than as catalyst. Longer contact times (18 h) of the nickel MOF in the same AgNO₃ solution produce a drastic change of the XRD of the solid, indicating that the crystal structure has been destroyed in the process. Host-guest free silver nanoparticles of 3 nm average diameter can be obtained by treating the solid with boiling dioctyl ether at 563 K in the presence of oleic acid. This fatty acid caps the silver nanoparticles, stabilizing them toward aggregation. If the MOF framework is destroyed with acid or heat treatment in the absence of any capping agent, silver nanoparticles undergo agglomeration in a significant extent. Thus, a procedure in which desolvated Ni-MOF is immersed in methanolic AgNO₃ followed by boiling in dioctyl ether/oleic acid is proposed as a convenient process to obtain monodisperse silver nanoparticles. The obvious drawback of the process is the sacrificial role of MOF that cannot be reformed, making the overall cycle assessment not favorable. Another point that needs clarification is the process of nanoparticles formation and what constraint makes them grow up to 3 nm, which is larger than the pore size (1.5 nm) and eventually leads to framework destruction.

The same authors have studied a similar redox-active bidirectional MOF based on Ni(II)cyclam as a linear bidentate building unit and 1,1'-biphenyl-2,2',6,6'-tetracarboxylic acid as a planar four-connecting organic building block.¹⁹⁵ Self-assembly of Ni(II)-cyclam and biphenyltetracarboxylic acid defines a grid structure in which each biphenyl coordinates to four cyclam complexes and each Ni(II) macrocycle binds axially to two biphenyl units. Scheme 27 illustrates the key structural features of Ni(II)-cyclam/biphenyltetracarboxylic acid. The resulting solid arising from the staking of the bidimensional grids shown in Scheme 27 is soluble in hot water but insoluble in common

Scheme 27. Building Units and Bidirectional Square Grid Based on Ni(II)–Cyclam and 1,1'-Biphenyl-2,2',6,6'-tetracarboxylic Acid; The Resulting Solid Forms Small Ag and Au Nanoparticles upon Contacting It with Ethanolic Solution of These Two Noble Metal Salts



organic solvents such as methanol, acetonitrile, benzene, dimethyl sulfoxide, diethyl formamide, and dimethylformamide.¹⁹⁵

Contacting this bidirectional coordination polymer with ethanolic solutions of $AgNO_3$ (0.13 M) or $NaAuCl_4$ (0.034 M) at room temperature forms Ag (3.7 ± 0.4 nm) or Au (ca. 2 nm) nanoparticles.¹⁹⁵ In both cases, EPR showed the formation of tetragonally distorted Ni(III) complexes, an uncommon oxidation state for Ni that could arise from stabilization by the azamacrocyclic ligand, and quantification determines that the redox process follows a 1:1 (Ni/Ag) or 3:1 (Ni/Au) stoichiometry. This indicates that the bulk solid is participating in the process.¹⁹⁵ However, when the redox reaction with $AgNO_3$ is performed in MeOH, partial dissolution of the $Ni(cyclam)^{2+}$ is observed. Similarly, when other salts of Ni(II)cyclam with 2-naphthalenedicarboxylate were used instead of Ni(II)cyclam/biphenyltetracarboxylic, much larger Ag (7–22 nm) and Au (10–100 nm) nanoparticles are formed, again due to partial dissolution of the solid.¹⁹⁵ This indicates that preservation of the insolubility of the solid is a key issue to obtain small metal nanoparticles.

2.4.2. Incorporation of Metal Oxide Nanoparticles in MOFs

Using tetramethoxysilane as precursor, small silica clusters have been obtained inside a pillared MOF having as molecular formula $[Cu_2(pzdc)_2(L)_n]$, where *pzdc* corresponds to pyrazine-2,3-dicarboxylate (**22**) and the pillar *L* is 1,2-di(4-pyridyl)ethylene (**23**).¹⁹⁶ The dimensions of the channels for this MOF are 1.03×0.60 nm². When an analogous MOF is prepared using pyrazine as the pillar, the resulting smaller channel dimensions (0.40×0.60 nm²) preclude adsorption of tetramethoxysilane, and the loading of silica inside this MOF was negligible.¹⁹⁶



The process followed to obtain the silica clusters consists of immersing the MOF into tetramethoxysilane, followed by removal of the excess of the silane under vacuum and

Scheme 28

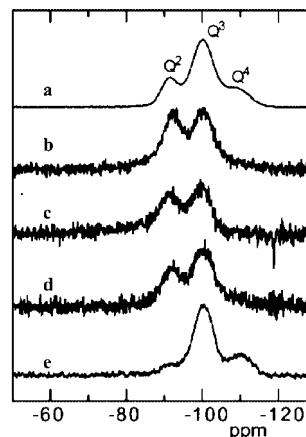
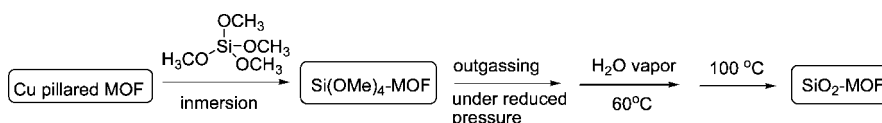


Figure 23. ^{29}Si NMR spectra of silica (a), silica included in MOF (b), silica included in MOF after one year (c), silica included in MOF treated with water (d), and silica recovered from MOF (e). Reproduced with permission from ref 196. Copyright 2008 American Chemical Society.

hydrolysis in a humid atmosphere at 333 K (Scheme 28). Further annealing at 373 K was performed to promote condensation of the silanol groups.

Formation of silica clusters leads to a drastic reduction in the surface area of the composite SiO_2 -MOF; this fact is consistent with the internal location of the silica clusters. In spite of the fact that the loading achieved corresponds approximately to one Si atom per unit cell, the presence of the silica clusters could not be detected by transmission electron microscopy. This was taken as evidence of a uniform distribution of small nanometric silica clusters throughout the MOF particle.¹⁹⁶ ^{29}Si NMR revealed that the incorporated silica clusters are constituted mainly of bipodal $Si(OH)_2O_2$ silicon atoms having two hydroxyl groups in the first coordination sphere of silicon. The chemical shift of these bipodal Si atoms inside MOF appeared as a broad band at about -92 ppm due to the interference of paramagnetic Cu from the MOF.¹⁹⁶ In contrast, a similar condensation procedure of tetramethoxysilane outside the confined environment of MOF leads mainly to tripodal $Si(OH)O_3$ silicon atoms accompanied by tetrapodal SiO_4 and bipodal $Si(OH)_2O_2$ silicon atoms. Figure 23 presents a set of ^{29}Si NMR spectra to show the influence of the confinement on the degree of silanol condensation.

Besides the low degree of silanol condensation, one remarkable consequence of the inclusion of small silica clusters inside a MOF containing copper is the easier transformation of the silica into cristobalite that takes places at 1073 K, whereas this silica crystal phase requires 1743 K to be obtained, with quartz being the prevalent phase below this temperature. The system containing the small silica clusters inside this copper MOF exhibits unique properties since a mechanical mixture of silica and MOF heated at 1073 K forms quartz and CuO oxide.

Titanium dioxide is the most widely used semiconductor.^{197,198} In a semiconductor, absorption of a photon of the same or higher energy than the band gap energy causes

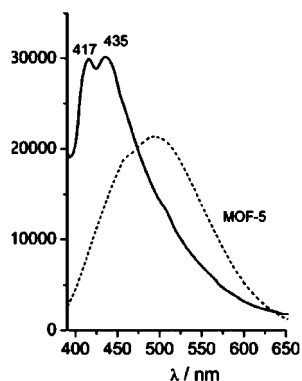
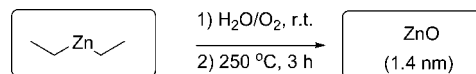


Figure 24. Emission spectra of $\text{TiO}_2@\text{MOF-5}$ (6.3 wt %) and MOF-5 recorded upon excitation at 365 nm. Reproduced with permission from ref 208. Copyright 2009 Royal Society of Chemistry.

charge separation with the formation of a mobile electron on the conduction band and an electron hole in the valence band. When the particle size is in the nanometer range, the photoactivity of titanium dioxide and most of the semiconductors are strongly dependent on the particle size.¹⁹⁹ Considering that electron/hole separation occurring in the bulk of the particle has to migrate to the surface of the particle to result in photoactivity, it is obvious that small particle size is beneficial from this point of view, since the external surface can be easily reached when the diameter of the particle becomes smaller. On the negative side, very small particle size can lead to the operation of quantum size effect, producing an increase in the band gap of the semiconductor. This increased band gap produces the blue shift of the absorption band and, therefore, the onset of the photoactivity in small titania nanoparticles shifts toward shorter wavelengths. It has been reported that, in the case of titanium dioxide, the threshold to observe quantum size effects is in the range of a few nanometers.²⁰⁰

Since encapsulation of small titania clusters inside the micropores of zeolites has been found to increase its photocatalytic activity,^{201–207} it can be anticipated that MOFs could also be appropriate matrices to include titanium dioxide nanoparticles inside the pores. Then, titanium dioxide has been obtained inside MOF-5 by adsorbing from the gas-phase titanium isopropoxide followed by thermal treatment in a dry oxygen stream (4.5 vol % in argon) at 493 K for 8 h and further annealing under Ar (as, for instance, 2 days at 523 K).²⁰⁸ This oxidation procedure effects the transformation of the adsorbed monatomic titanium precursor without damaging the MOF-5 structure. These changes can be monitored by IR spectroscopy. A sample containing ca. 6 wt % of titania, corresponding to a loading of one titanium atom per MOF-5 formula, exhibits a surface area of 2284 $\text{m}^2 \text{g}^{-1}$ as compared to 3400 $\text{m}^2 \text{g}^{-1}$, which is the surface area of the fresh MOF-5.²⁰⁸ TiO_2 clusters at this loading could not be detected by TEM. The small particle size of the MOF-5 encapsulated titania was inferred from the blue-shifted emission onset (350 nm, corresponding to 3.54 eV band gap) and the observation of photoluminescence, a feature that is only observed for small titania clusters.²⁰⁹ This photoluminescence from $\text{TiO}_2@\text{MOF-5}$ upon excitation at 365 nm and peaking at 417 and 435 nm is different from the typical green emission that can be observed for fresh MOF-5.^{153,154} Figure 24 presents a comparison of the photoluminescence from incorporated titanium dioxide clusters

Scheme 29. Transformation of Diethyl Zinc Included Inside MOF-5 into Zinc Oxide Nanoparticles by Exposure to the Ambient Air at Room Temperature and Subsequent Baking



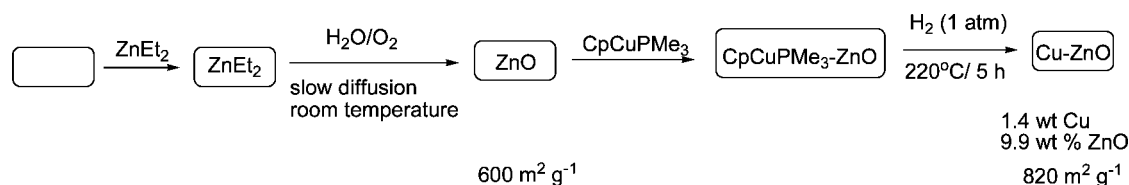
and MOF-5 framework. After having shown the possibility to prepare titania aggregates inside MOF-5, further work could be done to show the photocatalytic activity of the resulting material, particularly compared with the reported properties for analogous materials based on zeolites.¹⁹⁹ Actually it has been claimed that the organic linkers could act as antenna of the semiconductor oxide as it occurs for the photoluminescence of the Zn_4O_{13} clusters of MOF-5.¹⁵⁴

The second most important semiconductor oxide is zinc oxide. Nanoparticles of ZnO have been formed inside MOF-5 by first adsorbing diethyl zinc vapors from the gas phase at 300 K under vacuum and subsequent hydrolysis/oxidation under mild conditions (Scheme 29).¹⁸¹ This organometallic complex is air-sensitive, pyrophoric, and unstable. Upon inclusion of ZnEt_2 into MOF-5 under vacuum, XRD shows that the MOF framework hosting ZnEt_2 remains intact. However, when $\text{ZnEt}_2\text{-MOF-5}$ is exposed to ambient moisture for 28 h and finally heated under vacuum at 523 K for 3 h, the organometallic compound undergoes hydrolysis/oxidation and sintering to render ZnO nanoparticles included inside MOF-5.¹⁸¹

A loading corresponding to a stoichiometry of two ZnO formula units per MOF-5 cavity was obtained. The average particle dimension of ZnO clusters was estimated as 1.4 ± 0.1 nm from the XRD peaks corresponding to this metal oxide.¹⁸¹ This sample of MOF-5 containing ZnO nanoparticles deserves further characterization including TEM and isothermal nitrogen adsorption as well as a detailed study of its photoactivity. Particularly important will be to determine the operation of quantum size and confinement effects and if there is some interaction between the MOF-5 host and the embedded semiconductor particles. In this context, there is an urgent need of theoretical work to rationalize and anticipate some of the results that can be achieved using MOFs as catalysts.

Zinc oxide is the typical promoter of copper to boost its activity in methanol synthesis from CO. Actually, unpromoted copper is almost inactive to catalyze methanol synthesis, and Cu/ZnO is a paradigmatic example of strong metal support interaction in heterogeneous catalysis.^{210,211} Since both copper and zinc oxide have been prepared inside MOF-5,^{124,181} and also considering that the preparation of Cu/ZnO inside mesoporous MCM-41 and MCM-48 boosts the catalytic activity due to the increased interfacial contact, it was of interest to study the catalytic activity for methanol synthesis of a MOF-5 containing simultaneously copper and zinc oxide nanoparticles included inside the micropores.¹⁸²

Co-inclusion of copper and zinc oxide inside MOF-5 was not an obvious task since different strategies lead to destruction of MOF-5. It was found, however, that a process such as the one described in Scheme 30 is successful to prepare Cu/ZnO inside MOF-5. The process requires the initial preparation of ZnO nanoparticles inside MOF-5 by hydrolysis/oxidation of encapsulated ZnEt_2 and the subsequent formation of copper nanoparticles by absorbing cyclopentadienyl trimethylphosphine copper(I) into ZnO-loaded MOF. The main drawback of this procedure is the need of many sequential steps and the low copper content finally

Scheme 30. Procedure to Co-Include Copper and Zinc Oxide Nanoparticles Inside MOF-5; The Box Indicates the Micropore System of MOF-5


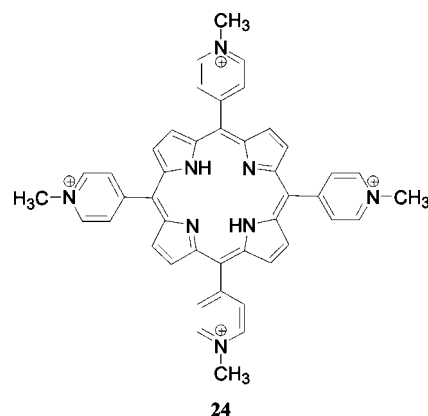
achieved (1.4 wt %) compared to the maximum amount of copper reported in MOF-5 (11 wt %). Other procedures in which the copper loading was higher (up to 7 wt %) showed that the structure of MOF-5 has collapsed.¹⁸² The (Cu–ZnO)–MOF-5 shows some promise as catalyst for methanol synthesis at 493 K, as the initial activity was 212 $\mu\text{mol}_{\text{MeOH}} \text{g}_{\text{cat}}^{-1} \text{h}^{-1}$ during 1 h. The problem is the instability of the material whose activity decays down to 12 $\mu\text{mol}_{\text{MeOH}} \text{g}_{\text{cat}}^{-1} \text{h}^{-1}$, and the deactivated catalyst showed sintering of Cu and ZnO nanoparticles. The deactivated (Cu–ZnO)–MOF-5 catalyst still has a large microporosity with 805 m² g⁻¹ surface area. Overall, although the catalytic results of MOF-5 containing simultaneously copper and zinc oxide nanoparticles was not satisfactory, its preparation constitutes a pioneering example of the opportunities that MOFs offer to obtain multicomponent systems in which each item can have a specific function to achieve the target activity.

2.4.3. MOFs as Host Matrices to Incorporate Catalytically Active Guests

The micropore system of MOFs holds a considerable promise to host guests that can exhibit some catalytic activity. This strategy to transform a homogeneous catalyst into a heterogeneous system has been widely explored in the case of zeolites.²¹² Particularly, large-pore zeolites (those having 12 oxygen member rings with pore size about 0.7 nm), with a tridirectional pore system or presenting large cavities, can have available free space to accommodate some large guests inside their pores. However, the dimensions of the windows might not allow the guests to pass across them and reach the large cavities in where the guests are immobilized. In the case of MOFs, Eddaoudi and co-workers were able to incorporate a porphyrin inside *rho*-ZMOF.²¹³ Metalloporphyrins exhibit catalytic activity for the oxidation of alkanes, epoxidation and cyclopropanation of alkenes, among other reactions, but suffer from a poor stability, with a tendency to form μ -oxo dimers and to self-degrade.^{214–216} These drawbacks were expected to be mitigated by incorporation inside a rigid matrix that isolates individual metalloporphyrin molecules and protects against degradation,²¹⁵ while the substrates and reagents could still diffuse and interact with the metalloporphyrin located into the cavities.

Then, 5,10,15,20-tetrakis(1-methyl-4-pyridinio)porphyrin, [H₂tmpyp]⁴⁺ (**24**), was incorporated directly during the synthesis of the *rho*-ZMOF (Figure 25).²¹³ It was found that the positive charges of this porphyrin are a prerequisite for the successful encapsulation when *rho*-ZMOF is formed from In(NO₃)₃ and 4,5-imidazoledicarboxylic acid in dmf. Since the presence of porphyrin inside *rho*-ZMOF could not be established by single-crystal XRD, the internal location of porphyrin was supported by indirect evidence based on the failure to release the porphyrin by ion exchange with Na⁺ and the absence of leaching. The catalytically active metalloporphyrin was obtained by incubating the *rho*-ZMOF

containing porphyrin free base with 0.1 methanolic solutions of the transition metal nitrates at room temperature for 24 h.



The corresponding manganese complex of the tetrapyrroline porphyrin encapsulated inside *rho*-ZMOF was tested for the solventless cyclohexane oxidation by *tert*-butylhydroperoxide at 338 K (Scheme 31).²¹³ Cyclohexanol/cyclohexanone were selectively formed with an estimated yield of 91.5% based on the ^tBuOOH consumption, assuming that the formation of cyclohexanone consumes 2 equiv. The catalyst was recycled 11 times, maintaining the crystallinity and exhibiting invariable catalytic behavior. The total TON was 258. Blank controls show that this catalytic activity is attributable to the immobilized manganese porphyrin. After this work, it can be easily anticipated that other reactions typically catalyzed by metalloporphyrins can be similarly advantageously promoted by this heterogeneous system.

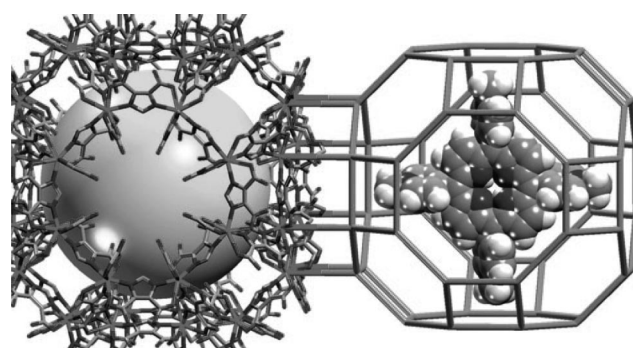
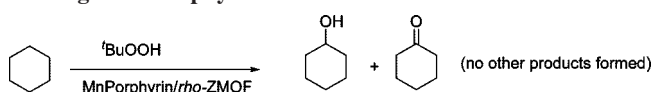


Figure 25. Crystal structure of *rho*-ZMOF (left) and schematic presentation of [H₂TMPyP]⁴⁺ enclosed in *rho*-ZMOF R-cage (right, drawn to scale). Reproduced with permission from ref 213. Copyright 2008 American Chemical Society.

Scheme 31. Cyclohexane Oxidation by *tert*-Butylhydroperoxide Catalyzed by *rho*-MOF Containing a Manganese Porphyrin


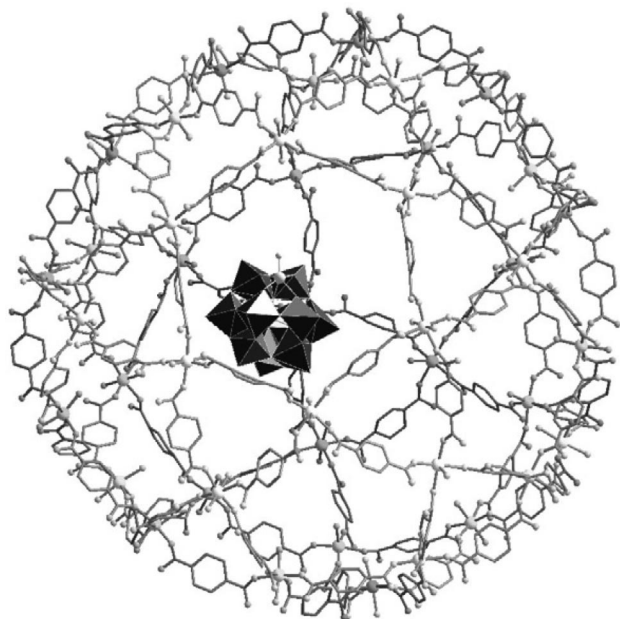


Figure 26. Schematic representation of a polyoxometalate (POM) incorporated inside the cavities of MIL-101. Reproduced with permission from ref 227. Copyright 2008 Elsevier.

Particularly interesting would be their application to the oxidation of alkanes with oxygen.

Polyoxometalates can exhibit strong Brønsted acidity and can be used as catalysts for many acid-catalyzed organic reactions such as alkene hydration, esterification, and alkylation. In addition to acid catalysts, polyoxometalates, particularly those containing transition metals, can also be used as oxidation catalysts.^{217–220} The main limitations of polyoxometalates as acid or redox catalysts are the small surface area of these solids ($<10 \text{ m}^2 \text{ g}^{-1}$) and their agglomeration. Having as a starting point the reported incorporation of polyoxometalates in MOFs,^{221–226} Kholdeeva and co-workers²²⁷ have adsorbed Keggin heteropolyoxoanions containing a single titanium $[(\text{PW}_{11}\text{TiO}_{40})^{5-}]$ or cobalt $[(\text{PW}_{11}\text{CoO}_{39})^{5-}]$ atom inside MIL-101 (Figure 26). The resulting solid was used as a heterogeneous catalyst for the liquid-phase allylic oxidation of cyclohexene and α -pinene and epoxidation of caryophyllene (Scheme 32).²²⁷ α -Pinene and caryophyllene oxidized prod-

ucts can be used as food and cosmetic stabilizers and as flavoring substances.²²⁸ Depending on the nature of the transition metal present in the polyoxometalate, H_2O_2 or O_2 was used as the oxidizing reagent for $(\text{PW}_{11}\text{TiO}_{40})^{5-}$ or $(\text{PW}_{11}\text{CoO}_{39})^{5-}$, respectively. Incorporation of titanium and cobalt heteropolyanions inside MIL-101 was simply achieved by contacting acetonitrile solutions of these polyoxometalates and the MOF for 24 h at 298 K.²²⁷ Subsequent desorption experiments of the resulting MIL-101 incorporated polyoxoanions showed that about 10 and 7 wt % of the titanium and cobalt heteropolyanions, respectively, remain irreversibly adsorbed in the MOF. These loadings correspond approximately to 1 polyoxometalate anion per supercage. It was shown that the interactions that maintain adsorption of the polyoxometalate to MIL-101 are strong Coulombic forces, since reextraction can be efficiently performed using a 1 M solution of Bu_4NClO_4 in acetonitrile.

As observed in similar host–guest systems based on MOFs, while the position and width of the XRD pattern characteristic of MIL-101 remains unaltered, the relative intensity of the peaks changes upon adsorption of the heteropolyanions. Isothermal gas adsorption showed a pore volume reduction due to the incorporation of polyoxometalates.

Controls with MIL-101 showed that this MOF exhibits a low activity for the oxidation of cyclohexene and α -pinene and gives 40% conversion for caryophyllene epoxidation using H_2O_2 as oxidizing reagent. When MIL-101 contains titanium and cobalt heteropolyanions, the catalytic activity for these oxidation reactions increases and the TOF approaches that measured for the corresponding free transition metal heteropolyoxoanions in the homogeneous phase. Thus, adsorption inside porous MIL-101 is not detrimental with respect to the intrinsic activity of these Keggin polyoxometalates.^{218,219,227} On the contrary, MIL-supported polyoxometalates exhibit some selectivity improvement toward the primary oxidation products, reducing their undesirable over-oxidation. Comparison of MIL-supported and silica-supported polyoxometalate selectivity indicates that the higher selectivity observed for MIL-101 must be originated by confinement within the cavities of the microporous MOF. In the case of cyclohexene and caryophyllene oxidations, formation of cyclic 1,2-diols arising from hydrolytic ring

Scheme 32. Oxidation of Three Alkenes by H_2O_2 or O_2 Catalyzed by MIL-101 Containing Titanium or Cobalt Heteropolyoxoanion

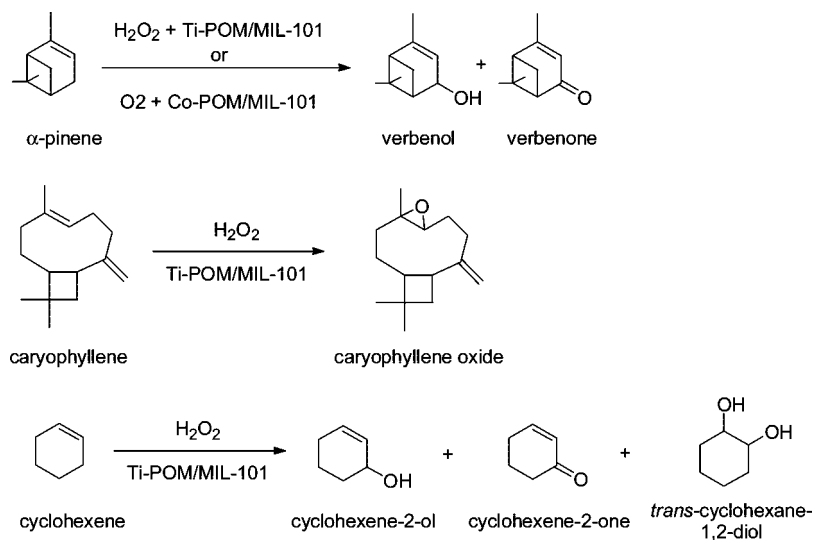
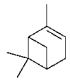
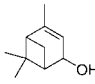
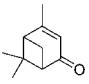
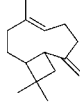
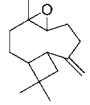
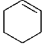
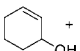
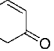
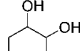


Table 8. Results of Alkene Oxidation with H₂O₂ and O₂ in the Presence of MIL-101 Supported Heteropolyanions; Data Taken from Ref 227

Catalyst	Oxidant	Conversion (%)	Selectivity (%)		
					
--		15	33	27	
MIL-101		14	14	7	
(PW ₁₁ CoO ₃₉) ⁵⁻	O ₂	45	36	24	
(PW ₁₁ CoO ₃₉) ⁵⁻ /MIL-101		45	29	27	
--		16	7	7	
MIL-101		18	8	7	
(PW ₁₁ TiO ₄₀) ⁵⁻	H ₂ O ₂	42	25	18	
(PW ₁₁ TiO ₄₀) ⁵⁻ /MIL101		40	32	30	
					
--		13	23		
MIL-101		40	41		
(PW ₁₁ TiO ₄₀) ⁵⁻	H ₂ O ₂	60	52		
(PW ₁₁ TiO ₄₀) ⁵⁻ /MIL101		71	80		
			 + 		
MIL-101		8	60	10	
(PW ₁₁ TiO ₄₀) ⁵⁻	H ₂ O ₂	7	7	32	
(PW ₁₁ TiO ₄₀) ⁵⁻ /MIL101		39	32	46	

aperture of the epoxides was minimized in MIL-101 supported (PW₁₁TiO₄₀)⁵⁻ compared to the homogeneous phase catalysis due to the steric protection of the confined reaction cavity. Table 8 summarizes the results reported. No leaching from the solid to the liquid phase was observed since filtration of the solid stops the reaction, and no titanium was detected by chemical analyses of the liquid phase.

The (PW₁₁CoO₃₉)⁵⁻/MIL-101 catalyst used at 0.4 mol % in Co with respect to α -pinene maintained its activity for five reuses for the oxidation of α -pinene with oxygen, and this reused catalyst showed the same XRD and IR spectrum as the fresh one with a 20% decrease in surface area due to the presence of hardly removable byproduct. In contrast to the behavior of (PW₁₁CoO₃₉)⁵⁻/MIL-101 using oxygen as oxidant, a study showed that the stability of (PW₁₁TiO₄₀)⁵⁻/MIL-101 toward H₂O₂ is highly dependent on the concentration of H₂O₂ and reaction temperature. At H₂O₂ concentrations higher than 0.4 M, the MIL-101 matrix was unstable and this lack of complete stability explains the poor reusability of (PW₁₁TiO₄₀)⁵⁻/MIL-101 (Ti/substrate mol ratio 0.6%) for the oxidation of 0.1 M cyclohexene with 0.12 M H₂O₂ at 343 K in which an abrupt change in conversion due to the massive leaching of the heteropolyanion was observed at the third reuse.

Liu, Su, and co-workers have used the acid polyoxometalates embedded within a copper trimesate MOF and used

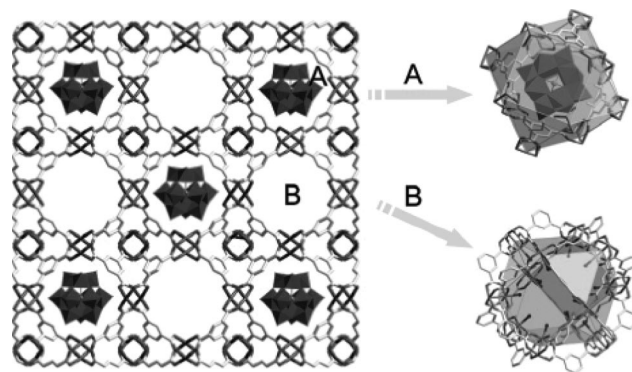


Figure 27. View along the (001) plane of a model of the Keggin polyoxometalates located at the A cages of the copper trimesate framework. Reproduced with permission from ref 229. Copyright 2009 American Chemical Society.

the resulting host–guest material as heterogeneous catalyst for the hydrolysis of carboxylic esters.²²⁹ The encapsulation of a series of six acid polyoxometalates including H₄SiW₁₂O₄₀·nH₂O, H₄SiMo₁₂O₄₀·nH₂O, H₄GeW₁₂O₄₀·nH₂O, H₃AsMo₁₂O₄₀·nH₂O, H₃PW₁₂O₄₀·nH₂O, and H₃PMo₁₂O₄₀·nH₂O inside the copper trimesate MOF was performed in a one-step process simultaneously with the synthesis of this MOF from Cu(NO₃)₂ and H₃btc. The loading level ranges from 36 to 45%, and the crystallinity of the materials obtained is high. The structure of the host MOF is defined by a face-centered cubic lattice having an alternation of cuboctahedral “A” (1.3 nm diameter, 1.1 nm opening) connected to cuboctahedral “B” (1.0 nm diameter, 0.93 nm opening) cages through the six open squares (Figure 27). Polyoxometalate molecules occupy the A cavities while the smaller B cavities of the MOF accommodate water and (CH₃)₄N⁺ molecules. The materials were found to be stable to most organic solvents (methanol, ethanol, acetonitrile, acetone, chloroform, and dmf) at 353 K for 10 h as well as moderate acid and basic aqueous solutions.

The fact that the polyoxometalate incorporated inside the MOF is fully protonated was inferred indirectly by the fact that the copper trimesate framework is neutral, and elemental analysis determines that the POM@MOF composite should contain only two (CH₃)₄N⁺ cations. Therefore, protonation of the Keggin anion is necessary for charge compensation. The site of protonation could not be determined by XRD or bond valence analyses due to anion disordering, but this failure to detect protons is a common fact in heteropolyacids. What is remarkable and would deserve a further study is how and when the protons are generated on the polyoxometalate. Because the synthesis of the material is performed under strong basic conditions using (CH₃)₄NOH at 453 K and considering that heteropolyacids are strong Brønsted acids, it is necessary to address when the basic medium is converted into a strongly acidic one.

The POM@MOF composite material was stable for 10 h at 353 K in 0.02 M NaOH or 0.02 M HCl and for 3 months in deionized water. Incorporation of heteropolyacids inside the micropores of the MOF framework reduces the surface area from 1116 m² g⁻¹ for the original host to 460 m² g⁻¹ when containing H₃PW₁₂O₄₀. This data is consistent with the incorporation of the phosphotungstate but indicates that the host still retains some free porosity, which is important to allow accessibility of the acid sites.²²⁹

Thermal treatment at 473 K for 12 h of the MOF containing H₃PW₁₂O₄₀ shows a weight loss of 13.4%; this

Table 9. Catalyst Activity for Hydrolysis of Ethyl Acetate in Water Excess^a

catalyst	acid amount (mmol g ⁻¹)	turnover number (mmol mmol _{H⁺} ⁻¹ min ⁻¹)
solid oxides		
H ₃ PW ₁₂ O ₄₀ @MOF dehydrated	0.57	313.8
H ₃ PW ₁₂ O ₄₀ @MOF hydrated	0.18	273.9
H ₃ PW ₁₂ O ₄₀ /SBA-15	0.09	275.0
C _{52.5} H _{0.5} PW ₁₂ O ₄₀	0.15	200.6
Cs ₃ PW ₁₂ O ₄₀	0	
SO ₄ ²⁻ /ZrO ₂	0.20	127.5
Nb ₂ O ₅	0.31	12.9
HZSM-5	0.39	70.8
HY	2.60	
organic resins		
Nafion H	0.80	202.3
Amberlyst-15	4.70	41.2
liquid acids		
H ₂ SO ₄	19.8	46.1

^a Reaction conditions: temperature 333 K, 30 mL of aqueous solution of ethyl acetate (16.9 mmol), catalyst weight 0.20 g. Data taken from reference 229.

experimental value matches with the calculated weight loss for the desorption of 37 water molecules plus 2 tetramethylammonium ions. The evacuation of (CH₃)₄N⁺ was confirmed by IR. It was assumed that removal of (CH₃)₄N⁺ should leave protons to maintain the electroneutrality of the solid. Titration of the solid with NaOH indicates an acid site density of 5.7 × 10⁻⁴ mol g⁻¹ as compared to a value of 1.8 × 10⁻⁴ mol g⁻¹ for the untreated H₃PW₁₂O₄₀@MOF sample. These values of acid sites correspond to three and one proton per polyoxotungstate, respectively. This matches with the theoretical values according to the formula.

Dehydrated H₃PW₁₂O₄₀@MOF was found to exhibit a catalytic activity per acid site 3–7 times higher than H₂SO₄, H₃PW₁₂O₄₀, and SO₄²⁻/ZrO₂ for the hydrolysis of ethyl acetate. A mechanical mixture of H₃PW₁₂O₄₀@MOF or hydrated H₃PW₁₂O₄₀@MOF exhibits low activity. Table 9 shows a summary of the performance of H₃PW₁₂O₄₀@MOF with respect to other acids.²²⁹

H₃PW₁₂O₄₀@MOF was found to be a heterogeneous catalyst since no leaching of H₃PW₁₂O₄₀ was observed and the hydrolysis stops when the solid is filtered from the medium. In addition, H₃PW₁₂O₄₀@MOF recovered by filtration, washed with MeOH, and dried at 473 K was reused for 15 cycles without losing activity. It has been claimed that hydrophobicity of the internal MOF surface, protecting the heteropolyacid from undergoing deactivation by the excess of water employed, is the reason for this increased catalytic performance together with high heteropolyacid loading and dispersion.²²⁹ It has been proposed that the catalytic activity of H₃PW₁₂O₄₀@MOF depends on the size and accessibility of the substrates. Substrates with smaller sizes and hydrophobicity such as methyl and ethyl acetate undergo hydrolysis at the same rate and faster than methyl and ethyl benzoate or 4-methylphenyl propionate. However, considering the differences in the structure of the carbonyl

groups, data showing the relative reactivity of these esters under homogeneous catalysis should have been presented to support this claim.

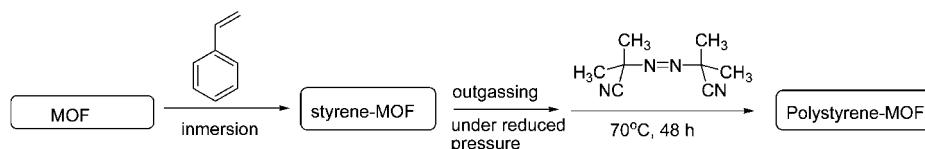
2.4.4. MOFs as Nanometric Reaction Cavities

The influence of the medium in terms of polarity, hydrogen bond interactions, hydrophilicity/hydrophobicity, viscosity, etc. on the chemical reactivity, although poorly understood in general, is a very well documented fact. At the molecular level, the surroundings experienced by a chemical compound undergoing transformation have been defined as the reaction cavity.²³⁰ This reaction cavity can be flexible and dynamic, like when the reaction is carried out in a solvent, or can be rigid with defined electrostatic potentials like in micro/mesoporous solids. The specific properties of the zeolite pores influencing the reactivity in the ground and excited states of substrates have been the subject of considerable interest.^{231–234} In addition, when the molecular size of a substrate has similar dimensions to the host matrix in which it is contained, distortion of the molecular orbital geometry and energy can take place, giving rise to the so-called *electronic confinement* effect.^{234–236} In this context, it will be of interest to delineate which are the particularities of MOFs as reaction cavities and what is the strength of force potentials and electrostatic fields inside the empty spaces defined by the framework.

Most of the host–guest inclusion complexes in zeolites have been prepared by adsorption of the molecule or species from the exterior to the interior of the zeolite micropores, or in some cases by introducing them as organic structure-directing agents.^{237,238} Polymers, being macromolecules of large kinetic diameter, cannot diffuse inside the zeolite micropores. For this reason, there are numerous studies showing different methodologies to prepare composites in which the organic polymer is hosted inside the zeolite voids. The majority of them are based on the adsorption of a suitable monomer that, in a subsequent step, undergoes polymerization inside the channels.^{238–248}

One example of performing a reaction inside the MOFs pores is styrene polymerization.²⁴⁹ This process has been attempted in two different MOFs, namely, [M₂(bdc)₂(teda)] (M = Zn²⁺ or Cu²⁺, teda = triethylenediamine) and [Cu(pzdc)₂(4,4'-bpy)] (pzdc = pirazine-2,3-dicarboxylate, 4,4'-bpy = 4,4'-bipyridine). Both MOFs have regular and continuous one-dimensional nanochannels with cross sections of 0.75 × 0.75 nm² and 0.82 × 0.60 nm², respectively. The process followed to effect polymerization is indicated in Scheme 33.

In spite of achieving similar styrene loadings (2.7 styrene molecules per nm³), styrene could not be polymerized in [Cu(pzdc)₂(4,4'-bpy)] even at 373 K. On the basis of ²H NMR spectroscopy, this failure to polymerize styrene inside the pyrazine MOF has been ascribed to the restricted mobility of styrene inside this MOF even at 343 K (very broad NMR signal) that contrasts with the high mobility with fast rotation around the C1–C4 axis of styrene ring when this molecule

Scheme 33. Styrene Radical Polymerization Procedure Inside MOFs

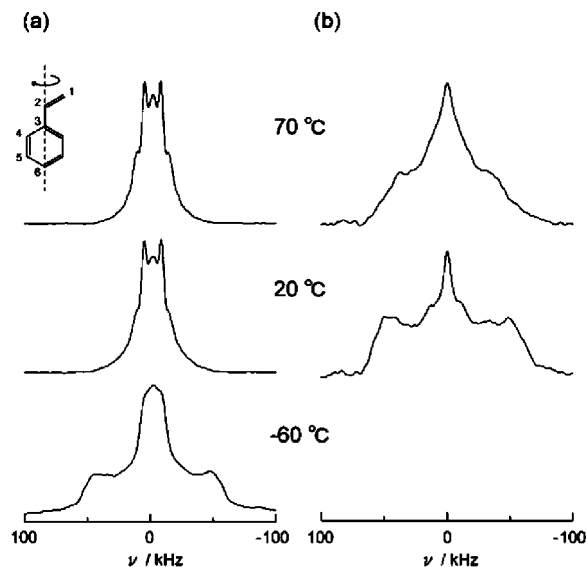


Figure 28. Solid-state ^2H NMR spectra recorded for perdeuterated styrene incorporated inside $[\text{Zn}_2(1,4\text{-bdc})_2(\text{teda})]$ (a) and $[\text{Cu}(\text{pzdc})_2(4,4'\text{-bpy})]$ (b). Reproduced with permission from ref 249. Copyright 2005 Royal Society of Chemistry.

is inside the benzenedicarboxylate MOF. Figure 28 shows the solid-state ^2D NMR spectra of perdeuterated styrene incorporated inside the benzenedicarboxylate and pyrazine MOFs recorded at three different temperatures. This lack of rotational mobility has been attributed to the strong confinement of styrene due to the intense potential inside the channels of pyrazine MOF.²⁴⁹ Note that, as we have commented in section 2.3, $[\text{Cu}(\text{pzdc})_2(4,4'\text{-bpy})]$ was found to be active for the anionic polymerization of methyl propiolate, due to the marked Lewis basicity of the carboxylate oxygen atoms.¹⁷⁶ On the contrary, in the case of styrene polymerization, we are dealing with a radical polymerization initiated by azodiisobutyronitrile (AIBN).

Radical polymerization of styrene was successful with $[\text{M}_2(\text{bdc})_2(\text{teda})]$ (polymerization yield about 70%), and no difference due to the nature of the Zn^{2+} or Cu^{2+} metal was observed.²⁴⁹ Quantitative recovery of the resulting polystyrene accommodated inside MOF was performed by dissolving the host matrix with 0.1 N NaOH. It was observed that the resulting polymers exhibit an average molecular weight, \bar{M}_w , around 56 000 with a remarkably low polydispersity

(1.66). Analogous polymerization procedure in the absence of MOF leads to a polydispersity of 4.68. EPR spectroscopy during the polymerization of styrene inside MOFs showed an intense signal assigned to the propagating radical. The signal did not disappear even after storing the sample for one week at 343 K. This remarkable fact of having a living radical inside MOF contrasts with the EPR spectra in homogeneous phase and was attributed to the suppression of termination reaction and radical transfer inside the MOFs channels.²⁴⁹

A detailed study by the group of Kitagawa has specifically addressed the chain conformation and dynamics of single polystyrene chains hosted inside the channels of monodirectional $[\text{Zn}_2(\text{bdc})_2(\text{teda})]$.²⁵⁰ The channel dimensions of this MOF ($0.75 \times 0.75 \text{ nm}^2$) do not allow accommodation of more than one polystyrene chain ($0.44 \times 0.68 \text{ nm}^2$), and therefore, it was assumed that the polymer chains are independent and surrounded by the MOF framework. Two-dimensional heteronuclear ^1H – ^{13}C solid-state NMR spectra at 5 ms contact time reveal dipole–dipole interactions and magnetization transfer between the hydrogen atoms of the main polystyrene chain and the carboxylate and aromatic carbons of the benzenedicarboxylate moiety as well as the triethylenediamine carbons.²⁵⁰ In turn, the hydrogen atoms of the triethylenediamine building block shows interactions with the carbon atoms of the main polystyrene chains. Figure 29 presents some exemplary two-dimensional heteronuclear ^1H – ^{13}C NMR spectra showing the host–guest interactions. These interactions between MOF and the polymeric chain reveal the degree of intimacy and contact in the host–guest composite.²⁵⁰

Isolation of polystyrene chains inside MOF nanochannels provides a unique opportunity to study the dynamics of a single chain. The bulk polymer exhibits a dominant low-frequency ($k_1 = <10^5 \text{ s}^{-1}$) 180° flip of the phenyl rings around the C1–C4 axis, together with less probable rapid phenyl rotation ($k_2 = <10^8 \text{ s}^{-1}$) with librational motion ($k_3 = 10^{10} \text{ s}^{-1}$). Using a polystyrene with perdeuterated aromatic rings, the solid-state ^2H NMR spectrum of the composite indicates that the component associated to the 180° flip of the phenyl ring is even further favored upon encapsulation, with its probability increasing up to 97% at 313 K and exhibiting a quasi single-type phenyl flipping motion with a low activation energy estimated as 8.8 kJ mol^{-1} . In the case of bulk polystyrene, the energy barrier can range from 38 to

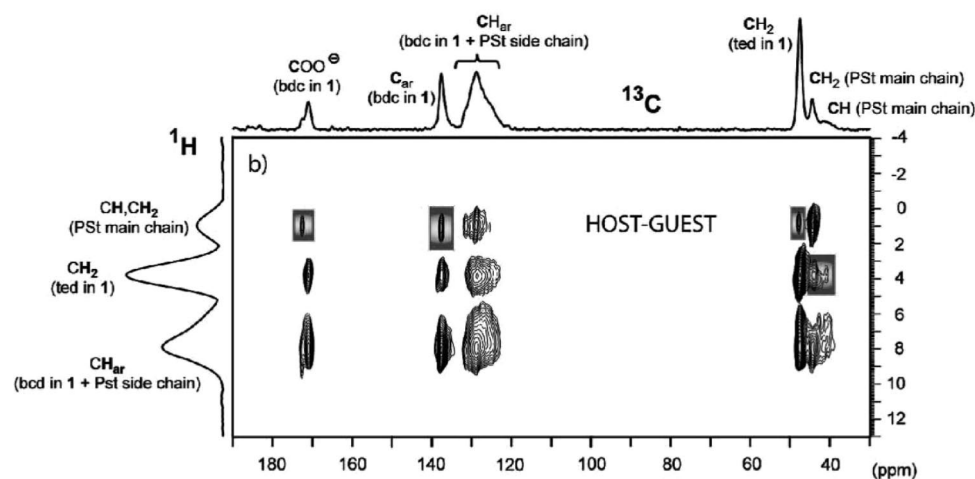
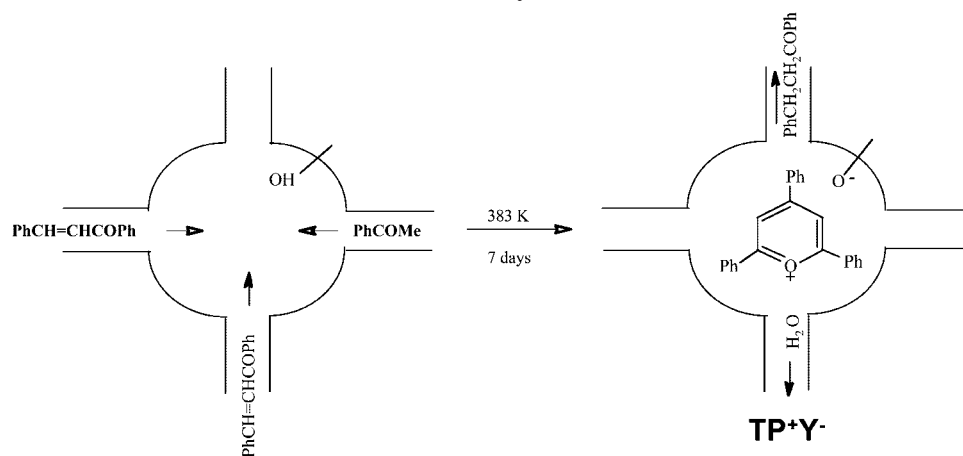


Figure 29. Two-dimensional heteronuclear ^1H – ^{13}C NMR spectrum recorded for polystyrene hosted inside the nanochannels of $[\text{Zn}_2(\text{bdc})_2(\text{teda})]$ MOF. Reproduced with permission from ref 250. Copyright 2008 American Chemical Society.

Scheme 34. Ship-in-a-Bottle Synthesis of 2,4,6-Triphenylpyrylium Ion Inside the Cages of Tridirectional, Large-Pore Y Zeolite to Form a Host–Guest Material (TP⁺Y⁻) That Acts As Photocatalyst



240 kJ mol⁻¹. This low and uniform activation energy for conformational change has been attributed to the low steric hindrance for the phenyl ring motion confined inside the larger flat and smooth MOF nanochannels.²⁵⁰

Tridirectional microporous solids in which the empty pore system defines cages and cavities interconnected by windows of smaller dimensions are suitable materials to perform chemical transformations generally denoted as ship-in-a-bottle.²¹² In these processes, small precursors that can diffuse through the micropore system of the host material react to form species that can be accommodated inside the cages, but they are too large to diffuse through the small window. Regarding the guest, the structural condition for a ship-in-a-bottle synthesis is that the molecular dimensions of the compound formed have to be smaller than the size of the cages, but larger than the window openings. In this way, after ship-in-a-bottle synthesis from the small precursors, the resulting species will remain permanently immobilized inside the micropores of the host matrix.²¹² This immobilization has been coined as mechanical immobilization to indicate that it does not result from the existence of covalent bonds between the host and the guest, but is rather due to a physical entrapment.²⁵¹ Scheme 34 illustrates the concept of ship-in-a-bottle synthesis with the reported formation of 2,4,6-triphenylpyrylium by condensation of chalcone and acetophenone inside the cages of zeolite Y.²³³

The preparation of supramolecular host–guest entities based on the formation of a guest inside the micropores of tridirectional, large-pore zeolites has been a subject of interest since the 1990s, and their characterization, particularly with respect to the internal location of the encapsulated guest, was challenging.^{212,233,252} Thus, considering the parallelism between zeolites and MOFs, it could be anticipated that tridirectional MOFs having appropriate micropore geometry would also attract interest as hosts to perform ship-in-a-bottle synthesis. In principle, MOFs would offer the advantage with respect to zeolites of an easy guest recovery by dissolution of the framework under mild conditions.

In a pioneering work in this field, Pan et al.²⁵³ have used a MOF having Co(4,4'-bphdc) building blocks as a recyclable nanoporous material suitable for ship-in-a-bottle synthesis. The key point of the system is the reversible conversion of Co(4,4'-bphdc) from nonporous one-directional structure when the MOF is immersed in water, [Co(4,4'-bphdc)-(H₂O)₂], into a microporous three-directional solid (super-cages of 0.5 × 1.1 × 1.1 nm³ connected by windows of

0.80 nm of maximum dimension) by performing solvothermal reaction in the presence of 4,4'-bpy to yield [Co₃(4,4'-bphdc)₃(4,4'-bpy)].²⁵³ Figure 30 presents a view showing the windows of the MOF structure as determined by single-crystal XRD. This MOF was notably hydrophobic as concluded from the 1 wt % of water adsorption at 15 torr and 303 K. In contrast, [Co₃(4,4'-bphdc)₃(4,4'-bpy)] MOF adsorbs almost the same amount of cyclohexane as zeolite Y in spite of the smaller pore volume of MOF (0.25 cm³ g⁻¹) as compared to zeolite Y (0.32 cm³ g⁻¹).²⁵³ The heat of *n*-hexane adsorption of [Co₃(4,4'-bphdc)₃(4,4'-bpy)] MOF (66 kJ mol⁻¹) is also considerably higher than that for zeolite Y (45.5 kJ mol⁻¹). From the rate of cyclohexane adsorption (kinetic diameter ≈ 0.6 nm) and the adsorption of mesitylene and triisopropylbenzene, it was estimated that the windows of the MOF should have an effective diameter of about 0.8 nm.

[Co₃(4,4'-bphdc)₃(4,4'-bpy)] was examined for its ability as host for photochemical reactions.²⁵³ For this purpose, *o*-methyl dibenzyl ketone was selected as a probe. The photochemistry of asymmetrically substituted dibenzyl ke-

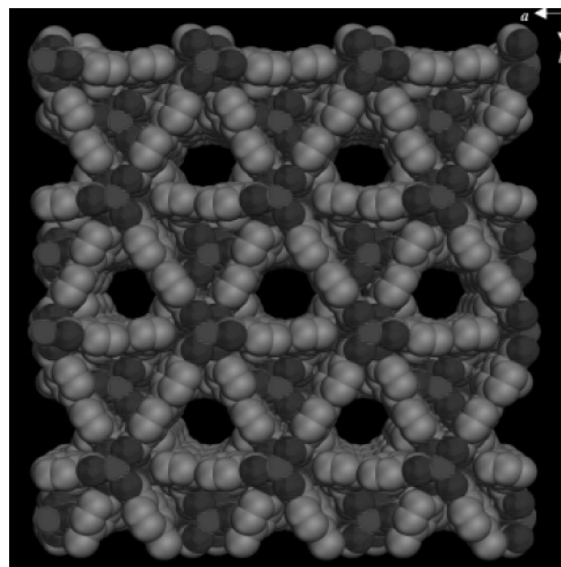
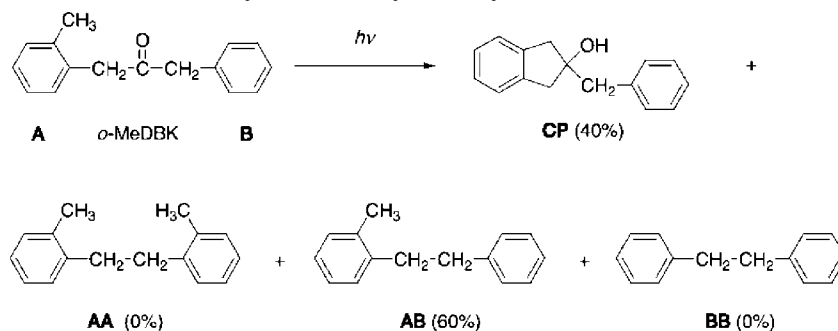
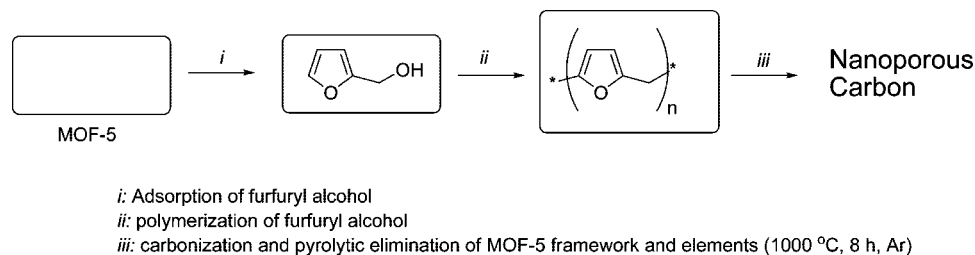


Figure 30. Top view (001) of the channels showing the window openings of a tridirectional MOF based on Co(bphdc). This MOF is unstable in water and collapses, giving chains of Co(biphenyl-dicarboxylate). Reproduced with permission from ref 253. Copyright 2003 Wiley-VCH Verlag GmbH & Co. KGaA.

Scheme 35. Product Distribution in the Photolysis of *o*-Methyl Dibenzyl Ketone

Scheme 36. Formation of Nanoporous Carbon by Carbonization of Poly(Furfuryl Alcohol) Inside MOF-5



tones has been extensively studied in many solids and confined spaces including zeolites, since the resulting product distribution can serve to determine the cage effect and the mobility of the free radicals in the medium.^{254,255} Asymmetric dibenzyl ketones can undergo homolytic cleavage in the α -position of the CO to give two differently substituted benzyl radicals that can recombine to give three possible diarylethanes. In solution, benzyl radicals can diffuse out of the solvent cage before reacting and the product distribution arises from the random coupling of the two benzyl radicals, giving 25, 50, and 25% of the three possible A–A, A–B, and B–B diarylethanes, respectively. When diffusion is restricted due to a cage effect, then the product distribution changes, favoring the asymmetric A–B diarylethane arising from recombination of the geminate radical pair. Following this, it was observed that, when performing the photolysis of *o*-dibenzyl ketone inside [Co₃(4,4'-bphdc)₃(4,4'-bpy)] MOF, asymmetric *o*-tolyl phenyl ethane was formed with a 60% yield and 100% selectivity accompanied with 40% of intramolecular hydrogen abstraction (Scheme 35).²⁵³ The lack of formation of ditolyl and diphenyl ethane indicates that [Co₃(4,4'-bphdc)₃(4,4'-bpy)] MOF as host exerts 100% cage effect, exclusively allowing recombination of the geminate benzyl radicals. To put this value into context, photolysis of the same compound in NaX gives 78% cage effect.²⁵⁴ Moreover, although the product mass balance by extraction was only 50%, complete recovery of the products could be achieved by immersing the MOF in water, destroying the porous structure, before extraction of the organic material. It should be mentioned that the mass balance of the same reaction in NaX is only 70%, thus showing the advantages of using MOFs as compared to zeolites for photochemical reactions.

On the other hand, zeolites and mesoporous silicas have been used as templates for the preparation of micro- and mesoporous carbons that constitute the *replica* of the rigid silica framework. The process generally involves two steps, i.e., adsorption of a carbon precursor and the subsequent carbonization of the organic compound. A similar strategy has been recently used to obtain nanoporous carbon from MOF-5.²⁵⁶ As carbon precursor, furfuryl alcohol was used.

The process is presented in Scheme 36. As can be seen there, after prior activation of MOF at 473 K for 24 h to empty its micropores, there is a step consisting of the adsorption of furfuryl alcohol and simultaneous polymerization of furfuryl alcohol by treating the sample at 423 K for 48 h under furfuryl alcohol atmosphere. The carbonation was carried out at 1273 K for 8 h under Ar atmosphere.²⁵⁶ Interestingly, MOF-5 is completely degraded and its residues are evaporated in the carbonization process. When the system is pyrolyzed at 1073 K, the presence of ZnO is observed by XRD of the resulting material. It has been proposed that, at higher temperature and in the presence of carbon, zinc oxide is reduced to zinc metal, which melts and evaporates (zinc metal boiling point 1181 K), and for this reason, no inorganic residue is contaminating the nanoporous carbon.

Isothermal nitrogen adsorption indicates that the nanoporous carbon exhibits micro-, meso-, and macroporosity with average pore diameters of 1.0, 15, and 50 nm, respectively. The specific BET surface area is 2 872 m² g⁻¹, and the pore volume is 2.06 cm³ g⁻¹. These values even compare favorably with the original MOF-5 used as template. Also, the hydrogen uptake at -160 °C and 760 torr of the nanoporous carbon is 2.6 wt %, which is also higher than that corresponding to MOF-5 (1.5 wt %).²⁵⁶ The resulting nanoporous carbon also exhibits outstanding electrochemical properties. A capacitor prepared with two electrodes of nanoporous carbon and sulfuric acid as electrolyte is able to store 204 F g⁻¹, cycling from -0.5 to 0.5 V at a speed of 5 mV s⁻¹. This value is significantly higher than the 102–163 F g⁻¹ range reported for the mesoporous carbon replica of SBA-15.²⁵⁷ Figure 31 shows the cyclic voltamperograms recorded at different scan rates for electrodes based on nanoporous carbon using MOF-5 as template, from which the capacitance data can be deduced.

This behavior of MOF-5 as clean template for the preparation of nanoporous carbon replicas represents an advantage with respect to silicas that require an extra step of silica dissolution, normally by attack in hydrofluoric acid. It would be of interest to expand this use of MOFs as templates and particularly to show that the pore system of

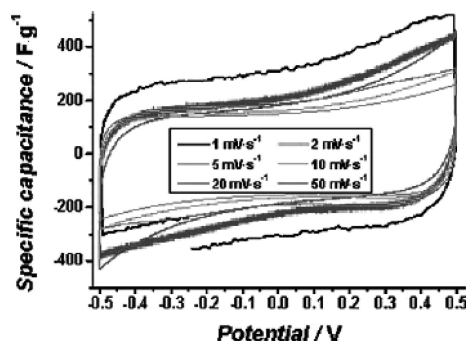


Figure 31. Cyclic voltammograms at different scan rates showing the Faraday capacitance of electrodes prepared with nanoporous carbon obtained using MOF-5 as template. Reproduced with permission from ref 256. Copyright 2008 American Chemical Society.

the resulting carbon constitutes a good replica of the porous system of the template.

3. Conclusions and Future Possibilities

One can safely say that catalytic studies with MOFs are in their infancy. Up to now only the “easier” and most direct potential applications have been attempted. We believe that it should be possible to go into more sophisticated materials in which the ligands between the metals will be formed by transition metal complexes (TMC) with one or two metals at a controlled distance. Such types of materials will allow for generation not only of heterogeneous catalysts fully based on transition metal complexes but also the combination of uni- or multimetallic sites in the TMC with molecular confinement in the pores. Such a design may approximate these materials to the catalytic behavior observed with enzymes.

The possibility to generate the metal component of the MOF with a large variety of transition metals could be largely exploited for Lewis acid catalysis, provided that the metal is able to accept electrons from the reactant. In addition, the organic component of the MOF can support acid, base, or acid–base pairs that, by themselves or in combination with the above-described possibilities, will allow one to perform cascade reactions.^{258,259}

There is a certain interest in the chemical industry in exploiting MOFs as heterogeneous catalysts. The main reason for this interest is that currently industry is using transition metal carboxylates in some processes mostly as Lewis acids and oxidation catalysts. Examples include epoxide ring aperture with alcohols by zinc carboxylates and alkylaromatic oxidation using cobalt salts in acetic acid.

Also, MOFs offer great promise as enantioselective catalysts, a topic that has not been possible to develop using zeolites. Asymmetric syntheses are routinely practiced in the synthesis of drugs, and these reactions are almost completely performed using expensive homogeneous catalysts. By using chiral ligands, a vast number of new MOFs would be available to be tested in this field. Considering the simplicity of the synthesis of MOFs and their affordability, it will be important to know if MOFs can outperform in large-scale or asymmetric reactions, advantageously replacing the homogeneous processes. There is no doubt that, as in the case of zeolites, gradual introduction of MOFs as industrial catalysts will give relevance to this area and will trigger further research in this area.

We believe that MOFs will not be able to substitute zeolites and zeotypes; this should not be the objective. We hope that MOFs, if properly engineered, can complement the inorganic molecular sieves, as catalysts in the field of chemicals and fine chemicals production. To achieve this objective, stability of MOFs has to be demonstrated and the productivity of these catalysts has to be determined and checked for viability.

Finally, there is a need for theoretical studies in this new field, assisting the design of MOFs and providing insight into the interaction of the substrates and MOFs. Clarifying the reaction mechanism, the geometry of the transition states, and the controlling step in the reaction mechanisms will serve to develop extremely efficient MOFs in which each of the components plays the expected role, resembling the catalytic sites of natural enzymes.

4. List of Acronyms and Abbreviations Used

ata	2-aminoterephthalate
bdc	1,4-benzenedicarboxylate (terephthalate)
bpb	1,4-bis(4'-pyrazolyl) benzene
bphdc	4,4'-biphenyldicarboxylate
bpydc	2,2'-bipyridine-4,4'-dicarboxylate
2,2'-bpy	2,2'-bipyridine
4,4'-bpy	4,4'-bipyridine
4-btapa	1,3,5-benzene tricarboxylic acid tris[<i>N</i> -(4-pyridyl)-amide]
btec	1,2,4,5-benzenetetracarboxylate
btc	1,3,5-benzenetricarboxylate (trimesate)
btt	1,3,5-benzenetristetrazolate
bzim	benzimidazole
1,4-chdc	<i>trans</i> -1,4-cyclohexanedicarboxylate
COF	covalent organic framework
CP	coordination polymer
CPO	coordination polymer of Oslo
def	diethyl formamide
1,4-dicb	1,4-diisocyanobenzene
4,4'-dicbp	4,4'-diisocyanobiphenyl
dmf	<i>N,N</i> -dimethylformamide
DTBP	2,6-di- <i>tert</i> -butyl phenol
2-eim	2-ethylimidazole
HDS	hydrodesulfurization
H ₂ hfipbb	4,4'-(hexafluoroisopropylidene)bis(benzoic acid)
[H ₂ tmpyp] ⁴⁺	5,10,15,20-tetrakis(1-methyl-4-pyridinio)porphyrin
HKUST	Hong Kong University of Science and Technology
4,5-icd	4,5-imidazolecarboxylate
im	imidazole
ITQMOF	Instituto de Tecnología Química metal organic framework
L-Lact	L-lactic acid
LCCT	ligand-to-cluster charge transfer transition
LMCT	ligand-to-metal charge transfer transition
MAO	methylaluminoxane
MB	methyl blue
mesoMOF	mesoporous metal organic framework
MIL	Matériaux de l'Institut Lavoisier
2-mim	2-methylimidazole
5-mipt	5-methylisophthalate
MOCP–H/ MOCP–H'	metal organic coordination polymer; H and H' stand for high surface area
MOF	metal organic framework compound
MPF	metal peptide framework
oba	4,4'-oxybis(benzoate)
OG	Orange G
P	phenol
phen	1,10-phenanthroline

PIZA	Porphyritic Illinois Zeolite Analogue
2,3-pyda	pyridine-2,3-dicarboxylate
2,4-pyda	pyridine-2,4-dicarboxylate
2-pymo	2-hydroxypyrimidinolate
pz	pyrazine
pzdc	pyrazine-2,3-dicarboxylate
RBBR	Remazol brilliant blue R
RhB	Rhodamine B
RPF	rare-earth polymeric framework
salenMn	(<i>R,R</i>)-(–)-1,2-cyclohexanediamino- <i>N,N'</i> -bis(3- <i>tert</i> -butyl-5-(4-pyridyl)salicyli-dene)MnCl
salphdc	<i>N,N'</i> -phenylenebis(salicylideneimine)dicarboxylate
^t BuOOH	<i>tert</i> -butylhydroperoxide
teda	triethylenediamine
T–H	tetralin
thf	tetrahydrofuran
T=O	α-tetralone
T–OH	α-tetralol
TOF	turnover frequency
T–OOH	α-tetralinhydroperoxide
tpcpp	tetra(<i>p</i> -carboxyphenyl)porphyrin
UHP	urea hydroperoxide
ZIF	zeolitic imidazolate framework
ZMOF	zeolite-like metal organic framework

5. Acknowledgments

The authors thank the Dirección General de Investigación Científica y Técnica of Spain (project MAT2006-14274-C02-01), Consolider-Ingenio 2010, and the UPV (project PAID-06-06-4726) for funding. The Ministerio de Educación y Ciencia of Spain is gratefully acknowledged for a “Ramón y Cajal” research contract to FXLX.

6. References

- Corma, A. *Chem. Rev.* **1995**, *95*, 559.
- Corma, A. *Chem. Rev.* **1997**, *97*, 2373.
- Boronat, M.; Corma, A.; Renz, M.; Viruela, P. M. *Chem.—Eur. J.* **2006**, *12*, 7067.
- Corma, A.; Davis, M. E. *ChemPhysChem* **2004**, *5*, 304.
- Sun, J. L.; Bonneau, C.; Cantin, A.; Corma, A.; Diaz-Cabanas, M. J.; Moliner, M.; Zhang, D. L.; Li, M. R.; Zou, X. D. *Nature* **2009**, *458*, 1154.
- Alvaro, M.; Carbonell, E.; Esplá, M.; Garcia, H. *Appl. Catal., B* **2005**, *57*, 37.
- Kinoshita, Y.; Matsubara, I.; Higuchi, T.; Saito, Y. *Bull. Chem. Soc. Jpn.* **1959**, *32*, 1221.
- Berlin, A. A.; Matveeva, N. G. *Russ. Chem. Rev.* **1960**, *29*, 119.
- (a) Sowerby, D. B.; Audrieth, L. F. *J. Chem. Educ.* **1960**, *37*, 134.
(b) Tomic, E. A. *J. Appl. Polym. Sci.* **1965**, *9*, 3745.
- (a) Hoskins, B. F.; Robson, R. *J. Am. Chem. Soc.* **1990**, *112*, 1546.
(b) Batten, S. R.; Hoskins, B. F.; Robson, R. *J. Am. Chem. Soc.* **1995**, *117*, 5385.
- Yaghi, O. M.; Li, H. L. *J. Am. Chem. Soc.* **1995**, *117*, 10401.
- Li, H.; Eddaoudi, M.; O’Keeffe, M.; Yaghi, O. M. *Nature* **1999**, *402*, 276.
- Rowsell, J. L. C.; Yaghi, O. M. *Microporous Mesoporous Mater.* **2004**, *73*, 3.
- These type of compounds would be more properly referred to as supramolecular architectures.
- Strictly speaking, the mechanism of adsorption in microporous materials (pores < 2 nm) is pore filling as opposed to mono/multilayer adsorption occurring in mesoporous materials. Therefore, the values of specific surface area extracted for a microporous material by using the Langmuir or the BET methods cannot be considered as their “true” surface area, but they have rather to be taken as “apparent” or “equivalent” surface areas.
- Ferey, G.; Mellot-Drazniaks, C.; Serre, C.; Millange, F.; Dutour, J.; Surble, S.; Margiolaki, I. *Science* **2005**, *309*, 2040.
- Rowsell, J. L. C.; Yaghi, O. M. *Angew. Chem., Int. Ed.* **2005**, *44*, 4670.
- Rosi, N. L.; Eckert, J.; Eddaoudi, M.; Vodak, D. T.; Kim, J.; O’Keeffe, M.; Yaghi, O. M. *Science* **2003**, *300*, 1127.
- Latroche, M.; Surble, S.; Serre, C.; Mellot-Drazniaks, C.; Llewellyn, P. L.; Lee, J. H.; Chang, J. S.; Jung, S. H.; Ferey, G. *Angew. Chem., Int. Ed.* **2006**, *45*, 8227.
- Ni, Z.; Jerrell, J. P.; Cadwallader, K. R.; Masel, R. I. *Anal. Chem.* **2007**, *79*, 1290.
- Xiong, R. C.; Fern, J. T.; Keffer, D. J.; Fuentes-Cabrera, M.; Nicholson, D. M. *Mol. Simul.* **2009**, *35*, 910.
- Kitagawa, S.; Kondo, M. *Bull. Chem. Soc. Jpn.* **1998**, *71*, 1739.
- Kitagawa, S.; Kitaura, R.; Noro, S. *Angew. Chem., Int. Ed.* **2004**, *43*, 2334.
- Serre, C.; Bourrelly, S.; Vimont, A.; Ramsahye, N. A.; Maurin, G.; Llewellyn, P. L.; Daturi, M.; Filinchuk, Y.; Leynaud, O.; Barnes, P.; Ferey, G. *Adv. Mater.* **2007**, *19*, 2246.
- Serre, C.; Mellot-Drazniaks, C.; Surble, S.; Audebrand, N.; Filinchuk, Y.; Ferey, G. *Science* **2007**, *315*, 1828.
- Mellot-Drazniaks, C.; Serre, C.; Surble, S.; Audebrand, N.; Ferey, G. *J. Am. Chem. Soc.* **2005**, *127*, 16273.
- Maspoch, D.; Ruiz-Molina, D.; Wurst, K.; Domingo, N.; Cavallini, M.; Biscarini, F.; Tejada, J.; Rovira, C.; Veciana, J. *Nat. Mater.* **2003**, *2*, 190.
- Meier, W. M.; Olson, D. H.; Baerlocher, C. *Zeolites* **1996**, *17*, 1.
- Eddaoudi, M.; Li, H. L.; Yaghi, O. M. *J. Am. Chem. Soc.* **2000**, *122*, 1391.
- Cote, A. P.; Benin, A. I.; Ockwig, N. W.; O’Keeffe, M.; Matzger, A. J.; Yaghi, O. M. *Science* **2005**, *310*, 1166.
- Gandara, F.; de Andres, A.; Gomez-Lor, B.; Gutierrez-Puebla, E.; Iglesias, M.; Monge, M. A.; Proserpio, D. M.; Snejko, N. *Cryst. Growth Des.* **2008**, *8*, 378.
- Manton, A.; Massuger, L.; Rabu, P.; Palivan, C.; McCusker, L. B.; Taubert, A. *J. Am. Chem. Soc.* **2008**, *130*, 2517.
- Liu, Y. L.; Kravtsov, V. C.; Larsen, R.; Eddaoudi, M. *Chem. Commun.* **2006**, 1488.
- Park, K. S.; Ni, Z.; Cote, A. P.; Choi, J. Y.; Huang, R. D.; Uribe-Romo, F. J.; Chae, H. K.; O’Keeffe, M.; Yaghi, O. M. *Proc. Natl. Acad. Sci.* **2006**, *103*, 10186.
- Wang, X. S.; Ma, S. Q.; Sun, D. F.; Parkin, S.; Zhou, H. C. *J. Am. Chem. Soc.* **2006**, *128*, 16474.
- Chui, S. S. Y.; Lo, S. M. F.; Charmant, J. P. H.; Orpen, A. G.; Williams, I. D. *Science* **1999**, *283*, 1148.
- Kongshaug, K. O.; Fjellvag, H. *Solid State Sci.* **2002**, *4*, 443.
- Harbuzaru, B. V.; Corma, A.; Rey, F.; Atienzar, P.; Jorda, J. L.; Garcia, H.; Ananias, D.; Carlos, L. D.; Rocha, J. *Angew. Chem., Int. Ed.* **2008**, *47*, 1080.
- Harbuzaru, B. V.; Corma, A.; Rey, F.; Jorda, J. L.; Ananias, D.; Carlos, L. D.; Rocha, J. *Angew. Chem., Int. Ed.* **2009**, *48*, 6476.
- O’Keeffe, M.; Peskov, M. A.; Ramsden, S. J.; Yaghi, O. M. *Acc. Chem. Res.* **2008**, *41*, 1782.
- Ockwig, N. W.; Delgado-Friedrichs, O.; O’Keeffe, M.; Yaghi, O. M. *Acc. Chem. Res.* **2005**, *38*, 176.
- Reticular Chemistry Structure Resource, <http://rcsr.anu.edu.au/home>.
- Hawxwell, S. M.; Espallargas, G. M.; Bradshaw, D.; Rosseinsky, M. J.; Prior, T. J.; Florence, A. J.; van de Streek, J.; Brammer, L. *Chem. Commun.* **2007**, 1532.
- Black, C. A.; Hanton, L. R.; Spicer, M. D. *Chem. Commun.* **2007**, 3171.
- Ren, P.; Liu, M. L.; Zhang, J.; Shi, W.; Cheng, P.; Liao, D. Z.; Yan, S. P. *Dalton Trans.* **2008**, 4711.
- Tian, Y. Q.; Zhao, Y. M.; Chen, Z. X.; Zhang, G. N.; Weng, L. H.; Zhao, D. Y. *Chem.—Eur. J.* **2007**, *13*, 4146.
- Lehnert, R.; Seel, F. Z. *Anorg. Allg. Chem.* **1980**, *464*, 187.
- Huang, L. M.; Wang, H. T.; Chen, J. X.; Wang, Z. B.; Sun, J. Y.; Zhao, D. Y.; Yan, Y. S. *Microporous Mesoporous Mater.* **2003**, *58*, 105.
- Huang, X. C.; Lin, Y. Y.; Zhang, J. P.; Chen, X. M. *Angew. Chem., Int. Ed.* **2006**, *45*, 1557.
- Zhang, J. P.; Chen, X. M. *Chem. Commun.* **2006**, 1689.
- Li, H.; Eddaoudi, M.; Groy, T. L.; Yaghi, O. M. *J. Am. Chem. Soc.* **1998**, *120*, 8571.
- Li, H. L.; Davis, C. E.; Groy, T. L.; Kelley, D. G.; Yaghi, O. M. *J. Am. Chem. Soc.* **1998**, *120*, 2186.
- Loiseau, T.; Muguerra, H.; Ferey, G.; Haouas, M.; Taulelle, F. J. *Solid State Chem.* **2005**, *178*, 621.
- Guilera, G.; Steed, J. W. *Chem. Commun.* **1999**, 1563.
- Yang, S. Y.; Long, L. S.; Huang, R. B.; Zheng, L. S. *Main Group Metal Chem.* **2002**, *25*, 329.
- Yang, S. Y.; Sun, Z. G.; Long, L. S.; Huang, R. B.; Zheng, L. S. *Main Group Metal Chem.* **2002**, *25*, 579.
- Estermann, M.; McCusker, L. B.; Baerlocher, C.; Merrouche, A.; Kessler, H. *Nature* **1991**, *352*, 320.
- Strohmaier, K. G.; Vaughan, D. E. W. *J. Am. Chem. Soc.* **2003**, *125*, 16035.
- Corma, A.; Diaz-Cabanas, M. J.; Jorda, J. L.; Martinez, C.; Moliner, M. *Nature* **2006**, *443*, 842.
- Corma, A. *J. Catal.* **2003**, *216*, 298.
- Llabrés i Xamena, F. X.; Abad, A.; Corma, A.; Garcia, H. *J. Catal.* **2007**, *250*, 294.

- (62) Llabrés i Xamena, F. X.; Corma, A.; Garcia, H. *J. Phys. Chem. C* **2007**, *111*, 80.
- (63) Alaerts, L.; Seguin, E.; Poelman, H.; Thibault-Starzyk, F.; Jacobs, P. A.; De Vos, D. E. *Chem.—Eur. J.* **2006**, *12*, 7353.
- (64) Prestipino, C.; Regli, L.; Vitillo, J. G.; Bonino, F.; Damin, A.; Lamberti, C.; Zecchina, A.; Solari, P. L.; Kongshaug, K. O.; Bordiga, S. *Chem. Mater.* **2006**, *18*, 1337.
- (65) Dinca, M.; Dailly, A.; Liu, Y.; Brown, C. M.; Neumann, D. A.; Long, J. R. *J. Am. Chem. Soc.* **2006**, *128*, 16876.
- (66) Chen, B. L.; Ockwig, N. W.; Millward, A. R.; Contreras, D. S.; Yaghi, O. M. *Angew. Chem., Int. Ed.* **2005**, *44*, 4745.
- (67) Dietzel, P. D. C.; Panella, B.; Hirscher, M.; Blom, R.; Fjellvag, H. *Chem. Commun.* **2006**, 959.
- (68) Dinca, M.; Long, J. R. *J. Am. Chem. Soc.* **2007**, *129*, 11172.
- (69) Vitillo, J. G.; Regli, L.; Chavan, S.; Ricchiardi, G.; Spoto, G.; Dietzel, P. D. C.; Bordiga, S.; Zecchina, A. *J. Am. Chem. Soc.* **2008**, *130*, 8386.
- (70) Dinca, M.; Long, J. R. *Angew. Chem., Int. Ed.* **2008**, *47*, 6766.
- (71) Schlichte, K.; Kratzke, T.; Kaskel, S. *Microporous Mesoporous Mater.* **2004**, *73*, 81.
- (72) Xiao, B.; Wheatley, P. S.; Zhao, X. B.; Fletcher, A. J.; Fox, S.; Rossi, A. G.; Megson, I. L.; Bordiga, S.; Regli, L.; Thomas, K. M.; Morris, R. E. *J. Am. Chem. Soc.* **2007**, *129*, 1203.
- (73) Noro, S.; Kitagawa, S.; Yamashita, M.; Wada, T. *Chem. Commun.* **2002**, 222.
- (74) Kitagawa, S.; Noro, S.; Nakamura, T. *Chem. Commun.* **2006**, 701.
- (75) Kitaura, R.; Onoyama, G.; Sakamoto, H.; Matsuda, R.; Noro, S.; Kitagawa, S. *Angew. Chem., Int. Ed.* **2004**, *43*, 2684.
- (76) Wu, C. D.; Hu, A.; Zhang, L.; Lin, W. B. *J. Am. Chem. Soc.* **2005**, *127*, 8940.
- (77) Szeto, K. C.; Prestipino, C.; Lamberti, C.; Zecchina, A.; Bordiga, S.; Bjorgen, M.; Tilset, M.; Lillerud, K. P. *Chem. Mater.* **2007**, *19*, 211.
- (78) Szeto, K. C.; Lillerud, K. P.; Tilset, M.; Bjorgen, M.; Prestipino, C.; Zecchina, A.; Lamberti, C.; Bordiga, S. *J. Phys. Chem. B* **2006**, *110*, 21509.
- (79) Llabrés i Xamena, F. X.; Casanova, O.; Galiasso Tailleur, R.; Garcia, H.; Corma, A. *J. Catal.* **2008**, *255*, 220.
- (80) Navarro, J. A. R.; Barea, E.; Salas, J. M.; Masciocchi, N.; Galli, S.; Sironi, A.; Ania, C. O.; Parra, J. B. *Inorg. Chem.* **2006**, *45*, 2397.
- (81) Tabares, L. C.; Navarro, J. A. R.; Salas, J. M. *J. Am. Chem. Soc.* **2001**, *123*, 383.
- (82) Louis, B.; Detoni, C.; Carvalho, N. M. F.; Duarte, C. D.; Antunes, O. A. C. *Appl. Catal., A* **2009**, *360*, 218.
- (83) Wang, Z. Q.; Cohen, S. M. *J. Am. Chem. Soc.* **2007**, *129*, 12368.
- (84) Tanabe, K. K.; Wang, Z. Q.; Cohen, S. M. *J. Am. Chem. Soc.* **2008**, *130*, 8508.
- (85) Wang, Z. Q.; Cohen, S. M. *Angew. Chem., Int. Ed.* **2008**, *47*, 4699.
- (86) Dugan, E.; Wang, Z. Q.; Okamura, M.; Medina, A.; Cohen, S. M. *Chem. Commun.* **2008**, 3366.
- (87) Wang, Z. Q.; Cohen, S. M. *Chem. Soc. Rev.* **2009**, *38*, 1315.
- (88) Eddaoudi, M.; Kim, J.; Rosi, N.; Vodak, D.; Wachter, J.; O'Keeffe, M.; Yaghi, O. M. *Science* **2002**, *295*, 469.
- (89) Costa, J. S.; Gamez, P.; Black, C. A.; Roubeau, O.; Teat, S. J.; Reedijk, J. *Eur. J. Inorg. Chem.* **2008**, 1551.
- (90) Goto, Y.; Sato, H.; Shinkai, S.; Sada, K. *J. Am. Chem. Soc.* **2008**, *130*, 14354.
- (91) Ingleson, M. J.; Barrio, J. P.; Bacsá, J.; Dickinson, C.; Park, H.; Rosseinsky, M. J. *Chem. Commun.* **2008**, 1287.
- (92) Ingleson, M. J.; Barrio, J. P.; Guilbaud, J. B.; Khimyak, Y. Z.; Rosseinsky, M. J. *Chem. Commun.* **2008**, 2680.
- (93) Zhang, X.; Llabrés i Xamena, F. X.; Corma, A. *J. Catal.* **2009**, *265*, 155.
- (94) Hwang, Y. K.; Hong, D. Y.; Chang, J. S.; Jhung, S. H.; Seo, Y. K.; Kim, J.; Vimont, A.; Daturi, M.; Serre, C.; Ferey, G. *Angew. Chem., Int. Ed.* **2008**, *47*, 4144.
- (95) Banerjee, M.; Das, S.; Yoon, M.; Choi, H. J.; Hyun, M. H.; Park, S. M.; Geo, G.; Kim, K. *J. Am. Chem. Soc.* **2009**, *131*, 7524.
- (96) Demessence, A.; D'Alessandro, D. M.; Foo, M. L.; Long, J. R. *J. Am. Chem. Soc.* **2009**, *131*, 8784.
- (97) Das, S.; Kim, H.; Kim, K. *J. Am. Chem. Soc.* **2009**, *131*, 3814.
- (98) Dhakshinamoorthy, A.; Alvaro, M.; Garcia, H. *J. Catal.* **2009**, *267*, 1.
- (99) Greathouse, J. A.; Allendorf, M. D. *J. Am. Chem. Soc.* **2006**, *128*, 10678.
- (100) Tachikawa, T.; Choi, J. R.; Fujitsuka, M.; Majima, T. *J. Phys. Chem. C* **2008**, *112*, 14090.
- (101) Gomez Silva, C.; Corma, A.; Garcia, H. *J. Mater. Chem.* in press.
- (102) Corma, A.; Fornes, V.; Martinaranda, R. M.; Garcia, H.; Primo, J. *Appl. Catal.* **1990**, *59*, 237.
- (103) Corma, A.; Fornes, V.; Martín-Aranda, R. M.; Rey, F. *J. Catal.* **1992**, *134*, 58.
- (104) Tranchemontagne, D. J.; Mendoza-Cortés, J. L.; O'Keeffe, M.; Yaghi, O. M. *Chem. Soc. Rev.* **2009**, *38*, 1257.
- (105) Seo, J. S.; Whang, D.; Lee, H.; Jun, S. I.; Oh, J.; Jeon, Y. J.; Kim, K. *Nature* **2000**, *404*, 982.
- (106) Dybtsev, D. N.; Nuzhdin, A. L.; Chun, H.; Bryliakov, K. P.; Talsi, E. P.; Fedin, V. P.; Kim, K. *Angew. Chem., Int. Ed.* **2006**, *45*, 916.
- (107) Gomez-Lor, B.; Gutierrez-Puebla, E.; Iglesias, M.; Monge, M. A.; Ruiz-Valero, C.; Snejko, N. *Inorg. Chem.* **2002**, *41*, 2429.
- (108) Barthelet, K.; Adil, K.; Millange, F.; Serre, C.; Riou, D.; Ferey, G. *J. Mater. Chem.* **2003**, *13*, 2208.
- (109) Efraty, A.; Feinstein, I. *Inorg. Chem.* **1982**, *21*, 3115.
- (110) Jaffe, I.; Segal, M.; Efraty, A. *J. Organomet. Chem.* **1985**, *294*, C17.
- (111) Feinstein-Jaffe, I.; Efraty, A. *J. Mol. Catal.* **1986**, *35*, 285.
- (112) Feinstein-Jaffe, I.; Efraty, A. *J. Mol. Catal.* **1987**, *40*, 1.
- (113) Tannenbaum, R. *Chem. Mater.* **1994**, *6*, 550.
- (114) Tannenbaum, R. *J. Mol. Catal. A: Chem.* **1996**, *107*, 207.
- (115) Fujita, M.; Kwon, Y. J.; Washizu, S.; Ogura, K. *J. Am. Chem. Soc.* **1994**, *116*, 1151.
- (116) Ohmori, O.; Fujita, M. *Chem. Commun.* **2004**, 1586.
- (117) Tanski, J. M.; Wolczanski, P. T. *Inorg. Chem.* **2001**, *40*, 2026.
- (118) Evans, O. R.; Ngo, H. L.; Lin, W. B. *J. Am. Chem. Soc.* **2001**, *123*, 10395.
- (119) Chang, J. S.; Hwang, J. S.; Jhung, S. H.; Park, S. E.; Ferey, G.; Cheetham, A. K. *Angew. Chem., Int. Ed.* **2004**, *43*, 2819.
- (120) Guzman, J.; Carrettin, S.; Corma, A. *J. Am. Chem. Soc.* **2005**, *127*, 3286.
- (121) Concepcion, P.; Carrettin, S.; Corma, A. *Appl. Catal., A* **2006**, *307*, 42.
- (122) (a) Zhang, X.; Shi, H.; Xu, B.-Q. *Angew. Chem., Int. Ed. Engl.* **2005**, *44*, 7132. (b) Zhang, X.; Corma, A. *Angew. Chem., Int. Ed.* **2008**, *47*, 4358.
- (123) Llabrés i Xamena, F. X. unpublished results, 2008.
- (124) Hermes, S.; Schroter, M. K.; Schmid, R.; Khodeir, L.; Muhler, M.; Tissler, A.; Fischer, R. W.; Fischer, R. A. *Angew. Chem., Int. Ed.* **2005**, *44*, 6237.
- (125) Sabo, M.; Henschel, A.; Froede, H.; Klemm, E.; Kaskel, S. *J. Mater. Chem.* **2007**, *17*, 3827.
- (126) Opelt, S.; Turk, S.; Dietzsch, E.; Henschel, A.; Kaskel, S.; Klemm, E. *Catal. Commun.* **2008**, *9*, 1286.
- (127) Henschel, A.; Gedrich, K.; Kraehnert, R.; Kaskel, S. *Chem. Commun.* **2008**, 4192.
- (128) Dhakshinamoorthy, A.; Alvaro, M.; Garcia, H. *Adv. Synth. Catal.* **2009**, *351*, 2271.
- (129) Suslick, K. S.; Bhyrappa, P.; Chou, J. H.; Kosal, M. E.; Nakagaki, S.; Smithenry, D. W.; Wilson, S. R. *Acc. Chem. Res.* **2005**, *38*, 283.
- (130) Kim, J.; Bhattacherjee, S.; Jeong, K.-E.; Jeong, S.-Y.; Ahn, W.-S. *Chem. Commun.* **2009**, 3904.
- (131) Hwang, Y. K.; Hong, D. Y.; Chang, J. S.; Seo, H.; Yoon, M.; Kim, J.; Jhung, S. H.; Serre, C.; Ferey, G. *Appl. Catal., A* **2009**, *358*, 249.
- (132) Cho, S. H.; Ma, B. Q.; Nguyen, S. T.; Hupp, J. T.; Albrecht-Schmitt, T. E. *Chem. Commun.* **2006**, 2563.
- (133) Sabater, M. J.; Corma, A.; Domenech, A.; Fornes, V.; Garcia, H. *Chem. Commun.* **1997**, 1285.
- (134) Baleizao, C.; Garcia, H. *Chem. Rev.* **2006**, *106*, 3987.
- (135) Lu, Y.; Tonigold, M.; Bredenkotter, B.; Volkmer, D.; Hitzbleck, J.; Langstein, G. Z. *Anorg. Allg. Chem.* **2008**, *634*, 2411.
- (136) Balkus, J.; Kenneth, J.; Pisklak, T. J.; Huang, R. *ACS Symp. Ser.* **2008**, *986*, 76.
- (137) Kato, C. N.; Hasegawa, M.; Sato, T.; Yoshizawa, A.; Inoue, T.; Mori, W. *J. Catal.* **2005**, *230*, 226.
- (138) Seki, K.; Takamizawa, S.; Mori, W. *Chem. Lett.* **2001**, 122.
- (139) Abad, A.; Almela, C.; Corma, A.; Garcia, H. *Chem. Commun.* **2006**, 3178.
- (140) Abad, A.; Concepcion, P.; Corma, A.; Garcia, H. *Angew. Chem., Int. Ed.* **2005**, *44*, 4066.
- (141) Hill, C. L.; Anderson, T. M.; Han, J. W.; Hillesheim, D. A.; Geletii, Y. V.; Okun, N. M.; Cao, R.; Botar, B.; Musaev, D. G.; Morokuma, K. *J. Mol. Catal. A: Chem.* **2006**, *251*, 234.
- (142) Han, J. W.; Hill, C. L. *J. Am. Chem. Soc.* **2007**, *129*, 15094.
- (143) Gandara, F.; de Andres, A.; Gomez-Lor, B.; Gutierrez-Puebla, E.; Iglesias, M.; Monge, M. A.; Proserpio, D. M.; Snejko, N. *Cryst. Growth Des.* **2008**, *8*, 378.
- (144) Bernini, M. C.; Gandara, F.; Iglesias, M.; Snejko, N.; Gutierrez-Puebla, E.; Brusau, E. V.; Narda, G. E.; Monge, M. A. *Chem.—Eur. J.* **2009**, *15*, 4896.
- (145) Nuzhdin, A. L.; Dybtsev, D. N.; Bryliakov, K. P.; Talsi, E. P.; Fedin, V. P. *J. Am. Chem. Soc.* **2007**, *129*, 12958.
- (146) Korotkikh, O.; Farrauto, R. *Catal. Today* **2000**, *62*, 249.
- (147) Zou, R. Q.; Sakurai, H.; Xu, Q. *Angew. Chem., Int. Ed.* **2006**, *45*, 2542.
- (148) Zou, R. Q.; Sakurai, H.; Han, S.; Zhong, R. Q.; Xu, Q. *J. Am. Chem. Soc.* **2007**, *129*, 8402.

- (149) Yu, Z. T.; Liao, Z. L.; Jiang, Y. S.; Li, G. H.; Li, G. D.; Chen, J. S. *Chem. Commun.* **2004**, 1814.
- (150) Bakac, A.; Espenson, J. H. *Inorg. Chem.* **1995**, *34*, 1730.
- (151) Yu, Z. T.; Liao, Z. L.; Jiang, Y. S.; Li, G. H.; Chen, J. S. *Chem.—Eur. J.* **2005**, *11*, 2642.
- (152) Mahata, P.; Madras, G.; Natarajan, S. *J. Phys. Chem. B* **2006**, *110*, 13759.
- (153) Alvaro, M.; Carbonell, E.; Ferrer, B.; Llabrés i Xamena, F. X.; Garcia, H. *Chem.—Eur. J.* **2007**, *13*, 5106.
- (154) Bordiga, S.; Lamberti, C.; Ricchiardi, G.; Regli, L.; Bonino, F.; Damin, A.; Lillerud, K. P.; Bjorgen, M.; Zecchina, A. *Chem. Commun.* **2004**, 2300.
- (155) Llabrés i Xamena, F. X.; Calza, P.; Lamberti, C.; Prestipino, C.; Damin, A.; Bordiga, S.; Pelizzetti, E.; Zecchina, A. *J. Am. Chem. Soc.* **2003**, *125*, 2264.
- (156) Calza, P.; Paze, C.; Pelizzetti, E.; Zecchina, A. *Chem. Commun.* **2001**, 2130.
- (157) Fuentes-Cabrera, M.; Nicholson, D. M.; Sumpter, B. G.; Widom, M. *J. Chem. Phys.* **2005**, *123*, 124713.
- (158) Choi, J. H.; Choi, Y. J.; Lee, J. W.; Shin, W. H.; Kang, J. K. *Phys. Chem. Chem. Phys.* **2009**, *11*, 628.
- (159) Civalieri, B.; Napoli, F.; Noel, Y.; Roetti, C.; Dovesi, R. *CrystEngComm* **2006**, *8*, 364.
- (160) Civalieri, B. personal communication, 2009.
- (161) Biswas, S.; Tonigold, M.; Volkmer, D. *Z. Anorg. Allg. Chem.* **2008**, *634*, 2532.
- (162) Gascon, J.; Hernandez-Alonso, M. D.; Almeida, A. R.; van Klink, G. P. M.; Kapteijn, F.; Mul, G. *ChemSusChem* **2008**, *1*, 981.
- (163) North, M.; Usanov, D. L.; Young, C. *Chem. Rev.* **2008**, *108*, 5146.
- (164) Kesanli, B.; Lin, W. *Coord. Chem. Rev.* **2003**, *246*, 305.
- (165) Chen, B.; Zhao, X.; Putkham, A.; Hong, K.; Lobkovsky, E. B.; Hurtado, E. J.; Fletcher, A. J.; Thomas, K. M. *J. Am. Chem. Soc.* **2008**, *130*, 6411.
- (166) Horike, S.; Dinca, M.; Tamaki, K.; Long, J. R. *J. Am. Chem. Soc.* **2008**, *130*, 5854.
- (167) Gandara, F.; Gutierrez-Puebla, E.; Iglesias, M.; Proserpio, D. M.; Snejko, N.; Monge, M. A. *Chem. Mater.* **2009**, *21*, 655.
- (168) Ngo, H. L.; Hu, A.; Lin, W. *J. Mol. Catal. A: Chem.* **2004**, *215*, 177.
- (169) Wu, C. D.; Lin, W. *Angew. Chem., Int. Ed.* **2007**, *46*, 1075.
- (170) Horcajada, P.; Surlle, S.; Serre, C.; Hong, D. Y.; Seo, Y. K.; Chang, J. S.; Grenèche, J. M.; Margiolaki, I.; Ferey, G. *Chem. Commun.* **2007**, 2820.
- (171) Ferey, G.; Serre, C.; Mellot-Draznieks, C.; Millange, F.; Surlle, S.; Dutour, J.; Margiolaki, I. *Angew. Chem., Int. Ed.* **2004**, *43*, 6296.
- (172) Dupont, J.; Consorti, C. S.; Spencer, J. *Chem. Rev.* **2005**, *105*, 2527.
- (173) Ravon, U.; Domine, M. E.; Gaudillere, C.; Desmartin-Chomel, A.; Farrasseng, D. *New J. Chem.* **2008**, *32*, 937.
- (174) Gonzalez-Arellano, C.; Corma, A.; Iglesias, M.; Sanchez, F. *Chem. Commun.* **2005**, 1990.
- (175) Matsuda, R.; Kitaura, R.; Kitagawa, S.; Kubota, Y.; Belosludov, R. V.; Kobayashi, T. C.; Sakamoto, H.; Chiba, T.; Takata, M.; Kawazoe, Y.; Mita, Y. *Nature* **2005**, *436*, 238.
- (176) Uemura, T.; Kitaura, R.; Ohta, Y.; Nagaoka, M.; Kitagawa, S. *Angew. Chem., Int. Ed.* **2006**, *45*, 4112.
- (177) Hasegawa, S.; Horike, S.; Matsuda, R.; Furukawa, S.; Mochizuki, K.; Kinoshita, Y.; Kitagawa, S. *J. Am. Chem. Soc.* **2007**, *129*, 2607.
- (178) Loiseau, T.; Serre, C.; Huguencard, C.; Fink, G.; Taulelle, F.; Henry, M.; Bataille, T.; Ferey, G. *Chem.—Eur. J.* **2004**, *10*, 1373.
- (179) Gascon, J.; Aktay, U.; Hernandez-Alonso, M. D.; van Klink, G. P. M.; Kapteijn, F. *J. Catal.* **2009**, *261*, 75.
- (180) Arstad, B.; Fjellvag, H.; Kongshaug, K. O.; Swang, O.; Blom, R. *Adsorption* **2008**, *14*, 755.
- (181) Hermes, S.; Schroder, F.; Amirjalayer, S.; Schmid, R.; Fischer, R. A. *J. Mater. Chem.* **2006**, *16*, 2464.
- (182) Muller, M.; Hermes, S.; Kaehler, K.; van den Berg, M. W. E.; Muhler, M.; Fischer, R. A. *Chem. Mater.* **2008**, *20*, 4576.
- (183) Kim, H.; Chun, H.; Kim, G. H.; Lee, H. S.; Kim, K. *Chem. Commun.* **2006**, 2759.
- (184) Houk, R. J. T.; Jacobs, B. W.; El Gabaly, F.; Chang, N. N.; Talln, A. A.; Graham, D. D.; House, S. D.; Robertson, I. M.; Allendorf, M. D. *Nano Lett.* **2009**, *9*, 3413.
- (185) Schroeder, F.; Esken, D.; Kokoja, M.; van den Berg, M. W. E.; Lebedev, O. I.; van Tendeloo, G.; Walaszek, B.; Buntkowsky, G.; Limbach, H. H.; Chaudret, B.; Fischer, R. A. *J. Am. Chem. Soc.* **2008**, *130*, 6119.
- (186) Yamaguchi, K.; Mizuno, N. *Chem.—Eur. J.* **2003**, *9*, 4353.
- (187) Yamaguchi, K.; Mizuno, N. *Angew. Chem., Int. Ed.* **2002**, *41*, 4538.
- (188) Zhan, B. Z.; White, M. A.; Sham, T. K.; Pincock, J. A.; Doucet, R. J.; Rao, K. V. R.; Robertson, K. N.; Cameron, T. S. *J. Am. Chem. Soc.* **2003**, *125*, 2195.
- (189) Zhan, B. Z.; White, M. A.; Pincock, J. A.; Robertson, K. N.; Cameron, T. S.; Sham, T. K. *Can. J. Chem.* **2003**, *81*, 764.
- (190) Greathouse, J. A.; Allendorf, M. D. *J. Am. Chem. Soc.* **2006**, *128*, 10678.
- (191) Turner, S.; Lebedev, O. I.; Schroder, F.; Esken, D.; Fischer, R. A.; Van Tendeloo, G. *Chem. Mater.* **2008**, *20*, 5622.
- (192) Besson, S.; Gacoin, T.; Ricolleau, C.; Boilot, J. P. *Chem. Commun.* **2003**, 360.
- (193) Moon, H. R.; Kim, J. H.; Suh, M. P. *Angew. Chem., Int. Ed.* **2005**, *44*, 1261.
- (194) Lee, E. Y.; Suh, M. P. *Angew. Chem., Int. Ed.* **2004**, *43*, 2798.
- (195) Suh, M. P.; Moon, H. R.; Lee, E. Y.; Jang, S. Y. *J. Am. Chem. Soc.* **2006**, *128*, 4710.
- (196) Uemura, T.; Hiramatsu, D.; Yoshida, K.; Isoda, S.; Kitagawa, S. *J. Am. Chem. Soc.* **2008**, *130*, 9216.
- (197) Hoffmann, M. R.; Martin, S. T.; Choi, W.; Bahnemann, D. W. *Chem. Rev.* **1995**, *95*, 69.
- (198) Anpo, M. *Catal. Surv. Jpn.* **1997**, *1*, 169.
- (199) Aprile, C.; Corma, A.; Garcia, H. *Phys. Chem. Chem. Phys.* **2008**, *10*, 769.
- (200) Hanley, T.; Krisnandi, Y.; Eldewik, A.; Luca, V.; Howe, R. *Ionics* **2001**, *7*, 319.
- (201) Persaud, L.; Bard, A. J.; Champion, A.; Fox, M. A.; Mallouk, T. E.; Webber, S. E.; White, J. M. *J. Am. Chem. Soc.* **1987**, *109*, 7309.
- (202) Liu, X.; Iu, K. K.; Thomas, J. K. *J. Chem. Soc., Faraday Trans.* **1993**, *89*, 1861.
- (203) Kim, Y. I.; Keller, S. W.; Krueger, J. S.; Yonemoto, E. H.; Saupé, G. B.; Mallouk, T. E. *J. Phys. Chem. B* **1997**, *101*, 2491.
- (204) Cosa, G.; Galletero, M. S.; Fernández, L.; Márquez, F.; García, H.; Scaiano, J. C. *New J. Chem.* **2002**, *26*, 1448.
- (205) Cosa, G.; Chretien, M. N.; Galletero, M. S.; Fornes, V.; Garcia, H.; Scaiano, J. C. *J. Phys. Chem. B* **2002**, *106*, 2460.
- (206) Bossmann, S. H.; Shahin, N.; Le Thanh, H.; Bonfill, A.; Worner, M.; Braun, A. M. *ChemPhysChem* **2002**, *3*, 401.
- (207) Bossmann, S. H.; Jockusch, S.; Schwarz, P.; Baumeister, B.; Goeb, S.; Schnabel, C.; Payawan, L., Jr.; Pokhrel, M. R.; Woerner, M.; Braun, A. M.; Turro, N. J. *Photochem. Photobiol. Sci.* **2003**, *2*, 477.
- (208) Muller, M.; Zhang, X. N.; Wang, Y. M.; Fischer, R. A. *Chem. Commun.* **2009**, 119.
- (209) Corrent, S.; Cosa, G.; Scaiano, J. C.; Galletero, M. S.; Alvaro, M.; García, H. *Chem. Mater.* **2001**, *13*, 715.
- (210) Hansen, P. L.; Wagner, J. B.; Helveg, S.; Rostrup-Nielsen, J. R.; Clausen, B. S.; Topsøe, H. *Science* **2002**, *295*, 2053.
- (211) Kasatkin, I.; Kurr, P.; Knip, B.; Trunschke, A.; Schlogl, R. *Angew. Chem., Int. Ed.* **2007**, *46*, 7324.
- (212) Corma, A.; Garcia, H. *Eur. J. Inorg. Chem.* **2004**, 1143.
- (213) Alkordi, M. H.; Liu, Y. L.; Larsen, R. W.; Eubank, J. F.; Eddaoudi, M. *J. Am. Chem. Soc.* **2008**, *130*, 12639.
- (214) Młodnicka, T. *J. Mol. Catal.* **1986**, *36*, 205.
- (215) De Vos, D. E.; Sels, B. F.; Jacobs, P. A. *Adv. Catal.* **2001**, *46*, 1.
- (216) Simonneaux, G.; Tagliatesta, P. *J. Porphyrins Phthalocyanines* **2004**, *8*, 1166.
- (217) Griffith, W. P. *Transition Met. Chem.* **1991**, *16*, 548.
- (218) Maksimchuk, N. V.; Meigunov, M. S.; Chesalov, Y. A.; Mrowiec-Bialon, J.; Jarzebski, A. B.; Kholdeeva, O. A. *J. Catal.* **2007**, *246*, 241.
- (219) Maksimchuk, N. V.; Melgunov, M. S.; Mrowiec-Bialon, J.; Jarzebski, A. B.; Kholdeeva, O. A. *J. Catal.* **2005**, *235*, 175.
- (220) Coronado, E.; Gomez-Garcia, C. *J. Chem. Rev.* **1998**, *98*, 273.
- (221) Hagrman, D.; Hagrman, P. J.; Zubieta, J. *Angew. Chem., Int. Ed.* **1999**, *38*, 3165.
- (222) Zheng, L. M.; Wang, Y. S.; Wang, X. Q.; Korp, J. D.; Jacobson, A. J. *Inorg. Chem.* **2001**, *40*, 1380.
- (223) Inman, C.; Knaust, J. M.; Keller, S. W. *Chem. Commun.* **2002**, 156.
- (224) Yang, L.; Naruke, H.; Yamase, T. *Inorg. Chem. Commun.* **2003**, *6*, 1020.
- (225) Wei, M. L.; He, C.; Hua, W. J.; Duan, C. Y.; Li, S. H.; Meng, Q. J. *J. Am. Chem. Soc.* **2006**, *128*, 13318.
- (226) Zhao, X. Y.; Liang, D. D.; Liu, S. X.; Sun, C. Y.; Cao, R. G.; Gao, C. Y.; Ren, Y. H.; Su, Z. M. *Inorg. Chem.* **2008**, *47*, 7133.
- (227) Maksimchuk, N. V.; Timofeeva, M. N.; Melgunov, M. S.; Shmakov, A. N.; Chesalov, Y. A.; Dybtsev, D. N.; Fedin, V. P.; Kholdeeva, O. A. *J. Catal.* **2008**, *257*, 315.
- (228) Bauer, K.; Garbe, D.; Surburg, H. *Common Fragrance and Flavor Materials*; Wiley-VCH: New York, 1997.
- (229) Sun, C.-Y.; Liu, S.-X.; Liang, D.-D.; Shao, K.-Z.; Ren, Y.-H.; Su, Z.-M. *J. Am. Chem. Soc.* **2009**, *131*, 1883.
- (230) Weiss, R. G.; Ramamurthy, V.; Hammond, G. S. *Acc. Chem. Res.* **1993**, *26*, 530.
- (231) Ramamurthy, V.; Eaton, D. F.; Caspar, J. V. *Acc. Chem. Res.* **1992**, *25*, 299.
- (232) Garcia, H.; Roth, H. D. *Chem. Rev.* **2002**, *102*, 3947.
- (233) Corma, A.; Garcia, H. *Chem. Commun.* **2004**, 1443.
- (234) Marquez, F.; Zicovich-Wilson, C. M.; Corma, A.; Palomares, E.; Garcia, H. *J. Phys. Chem. B* **2001**, *105*, 9973.

- (235) Marquez, F.; Garcia, H.; Palomares, E.; Fernandez, L.; Corma, A. *J. Am. Chem. Soc.* **2000**, *122*, 6520.
- (236) Marquez, F.; Zicovich-Wilson, C. M.; Corma, A.; Palomares, E.; Garcia, H. *J. Phys. Chem. B* **2001**, *105*, 9973.
- (237) Balkus, K. J.; Gabrielov, A. G.; Bell, S. L.; Bedioui, F.; Roue, L.; Devynck, J. *Inorg. Chem.* **1994**, *33*, 67.
- (238) Atienzar, P.; Diaz-Cabanas, M. J.; Moliner, M.; Peris, E.; Corma, A.; Garcia, H. *Chem.—Eur. J.* **2007**, *13*, 8733.
- (239) Zecchina, A.; Llabrés i Xamena, F. X.; Paze, C.; Turnes Palomino, G.; Bordiga, S.; Otero Arean, C. *Phys. Chem. Chem. Phys.* **2001**, *3*, 1228.
- (240) Zecchina, A.; Paze, C.; Otero Arean, C.; Turnes Palomino, G.; Llabrés i Xamena, F. X.; Bordiga, S. *Stud. Surf. Sci. Catal.* **2001**, *135*, 274.
- (241) Cardin, D. J.; Constantine, S. P.; Gilbert, A.; Lay, A. K.; Alvaro, M.; Galletero, M. S.; Garcia, H.; Marquez, F. *J. Am. Chem. Soc.* **2001**, *123*, 3141.
- (242) Alvaro, M.; Corma, A.; Ferrer, B.; Galletero, M. S.; Garcia, H.; Peris, E. *Chem. Mater.* **2004**, *16*, 2142.
- (243) Alvaro, M.; Cardin, D. J.; Colquhoun, H. M.; Garcia, H.; Gilbert, A.; Lay, A. K.; Thorpe, J. H. *Chem. Mater.* **2005**, *17*, 2546.
- (244) Fornes, V.; Garcia, H.; Gomez-Garcia, C. J.; Peris, E. *Chem. Phys. Lett.* **2005**, *416*, 271.
- (245) Domenech, A.; Galletero, M. S.; Garcia, H.; Peris, E. *Electrochem. Commun.* **2006**, *8*, 1335.
- (246) Alvaro, M.; Ferrer, B.; Garcia, H.; Peris, E. *J. Phys. Chem. B* **2006**, *110*, 16887.
- (247) Alvaro, M.; Cabeza, J. F.; Corma, A.; Garcia, H.; Peris, E. *J. Am. Chem. Soc.* **2007**, *129*, 8074.
- (248) Peris, E.; Hernando, J.; Llabrés i Xamena, F. X.; van Hulst, N. F.; Bourdelande, J. L.; Garcia, H. *J. Phys. Chem. C* **2008**, *112*, 4104.
- (249) Uemura, T.; Kitagawa, K.; Horike, S.; Kawamura, T.; Kitagawa, S.; Mizuno, M.; Endo, K. *Chem. Commun.* **2005**, 5968.
- (250) Uemura, T.; Horike, S.; Kitagawa, K.; Mizuno, M.; Endo, K.; Bracco, S.; Comotti, A.; Sozzani, P.; Nagaoka, M.; Kitagawa, S. *J. Am. Chem. Soc.* **2008**, *130*, 6781.
- (251) Raymo, F. M.; Stoddart, J. F. *Chem. Rev.* **1999**, *99*, 1643.
- (252) Schulz-Ekloff, G.; Wöhrle, D.; van Duffel, B.; Schoonheydt, R. A. *Microporous Mesoporous Mater.* **2002**, *51*, 91.
- (253) Pan, L.; Liu, H.; Lei, X.; Huang, X.; Olson, D. H.; Turro, N. J.; Li, J. *Angew. Chem., Int. Ed.* **2003**, *42*, 542.
- (254) Turro, N. J. *Acc. Chem. Res.* **2000**, *33*, 637.
- (255) *Photochemistry in Organized and Constrained Media*; Ramamurthy, V., Ed.; VCH: New York, 1991.
- (256) Liu, B.; Shioyama, H.; Akita, T.; Xu, Q. *J. Am. Chem. Soc.* **2008**, *130*, 5390.
- (257) Wang, D.-W.; Li, F.; Liu, M.; Cheng, H.-M. *New Carbon Mater.* **2007**, *22*, 307.
- (258) Climent, M. J.; Corma, A.; Iborra, S. *ChemSusChem* **2009**, *2*, 500.
- (259) Climent, M. J.; Corma, A.; Iborra, S.; Santos, L. *Chem.—Eur. J.* **2009**, *15*, 8834.

CR9003924